Theoretical Studies on Polyester Polycondensation Catalyst

（ポリエステル重合触媒の理論的研究）

Isamu Shigemoto

Department of Chemistry,
Graduate School of Science,
Osaka University

2013

Acknowledgement

The present doctoral thesis is described on the basis of the author's study at Osaka University from April 2010 to March 2013 under the supervision of Professor Mitsutaka Okumura. The author would like to express sincere gratitude to him for his many valuable discussions, suggestions and continued encouragement. The author is grateful to Dr. Shusuke Yamanaka, Dr. Takashi Kawakami and Dr. Yasutaka Kitagawa for their kind advices and assistances. Sincerely acknowledgement is also made to Dr. Toshihide Inoue, Dr. Tetsuya Goto, Dr. Tetsuya Tsunekawa, Dr. Yoshiki Makabe and Dr. Koji Yamauchi (Toray Industries, Inc.) for their continuous encouragement, suggestions, and helpful advice.

The author gratefully acknowledges Mr. Masatoshi Aoyama, Mr. Jun Sakamoto and Mr. Yoichiro Tanaka (Toray Industries, Inc.) for their sincere collaboration and valuable discussions based on the experimental facts. The author is heavily indebted to his colleagues at Toray Industries, Inc., especially to Mr. Hiroshi Taiko, Mr. Tomonori Kawakami and Mr. Masahiro Kitabata for their valuable suggestions, kind assistance and continued encouragement throughout the present study.

Many thanks are also given to all members and secretaries of the laboratory of Professor Mitsutaka Okumura, especially to Dr. Kazuyuki Okazaki, Dr. Toru Matsui, Dr. Yasuyuki Nakanishi, Dr. Yusuke Kataoka, Dr. Toru Saito, Mr. Keiji Kinoshita, Mr. Keita Kanda, Mr. Akira, Ito, Mr. Kohei Sakata, Mr. Kohei Tada, Mr. Hiroshi Hatake, Ms. Natsumi Yasuda, Ms. Yuka Iwasaki, Mr. Koki Ueda, Mr. Sachio Hayashi, Ms. Mizuho Miki, Mr. Shohei Yoshimura, Mr. Takumi Kawashima, Mr. Kyouhei Komi, Ms. Saaya Tamura, Mr. Ryo Nakajima, Mr. Hiroyuki Nakano and Ms. Eriko Kambayashi.

Finally, the author would like to express his sincere thanks to his family, especially his wife Yukie and his daughter Natsumi for their continuous support and heavy encouragement.

Isamu Shigemoto

March, 2013

Contents

Chapter 1.

Introduction to This Thesis: Manufacture and Properties of Polyesters

Chapter 1.

Introduction to This Thesis:

Manufacture and Properties of Polyesters

1.1. Outline of manufacture of polyesters [1,2]

In 1946, Whinfield and Dickson discovered poly(ethylene terephthalate) (PET), which was the first linear polyester which had high melting point (265 °C) and good hydrolytic stability. [3] Subsequently many other aromatic polyesters have been synthesized and studied. Among these polyesters, PET and poly(butylene terephthalate) (PBT) have been produced commercially for more than 50 years. Poly(trimethylene terephthalate) (PTT) was commercialized very recently. PET is used worldwide for the production of synthetic fibers, films, beverage bottles, and molded plastic parts, because of its good physical properties and moderate costs. Molecular formulae of these polyesters are shown in scheme 1.1.

PET is manufactured from ethylene glycol (EG) and terephthalic acid (TPA) or dimethyl terephthalate (DMT). The polymerization proceeds in two steps: the esterification and condensation reactions. Usually during the polymerization reaction there are some side reactions, including thermal degradation, hydrolysis, cyclization, and diethylene glycol (DEG) formation. These side reactions influence physical properties of the polymer.

In this chapter, details of the synthetic methods are described as an introduction to this thesis. In addition, some important physical properties of polyesters are also mentioned.

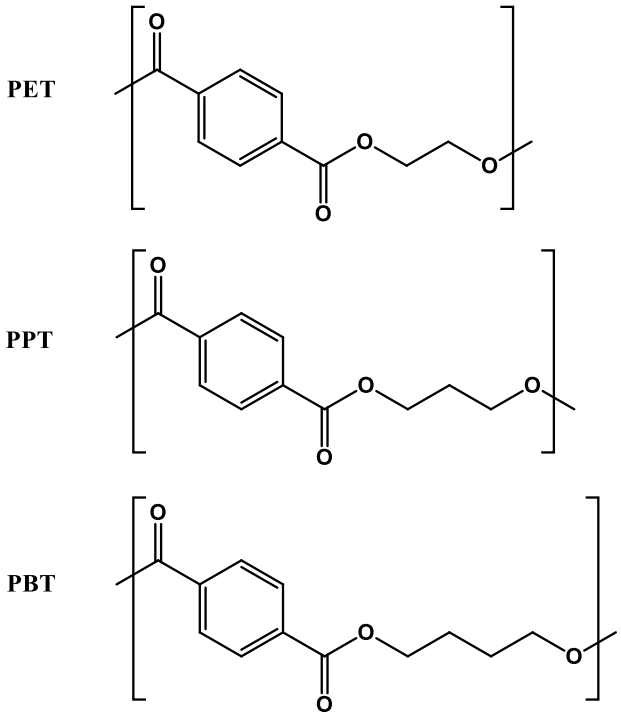

Scheme 1.1. Molecular formulae of poly(ethylene terephthalate) (PET), poly(propylene terephthalate) (PPT), and poly(butylene terephthalate) (PBT).

1.2. Synthetic methods [1]

Polyesters, especially PET were manufactured as industrial products by ICI (UK, 1949) and Du Pont (USA, 1953) soon after the technology of manufacturing was developed by Whinfield and Dickson. [3] Polyester is typically manufactured by two routes: transesterification of dimethylester with diol to form an intermediate diester and oligomers, followed by polycondensation to form the polymer; or direct esterification of the diacid with the diol, followed by polycondensation. In this section, the conventional methods for the manufacture of PET will be described.

1.2.1. Raw materials

Raw materials for PET manufacture are terephthalic acid (TPA) or dimethyl terephthalate (DMT) and ethylene glycol (EG). DMT was widely used in the early years of PET manufacture because it can be easily purified by distillation. Recently, pure TPA has replaced DMT as the preferred raw material after the development of purified TPA by Amoco. [3] Crude TPA is produced by the air oxidation of p-xylene in

acetic acid. 4-carboxybenzaldehyde (4-CBA), which acts as a chain terminator in the PET polymerization, is one of the main impurities present in the crude form. Because this contaminant has a very similar structure to that of TPA, it is difficult to remove 4-CBA from TPA. In the Amoco process, TPA can be purified by dissolution in water and hydrogenation with Pd/C catalyst. [3]

1.2.2. Polymerization methods

PET is prepared in two steps: the first step, prepolymerization forming bis-(2-hydroxyethyl) terephthalate (BHET), the precursor for the second step, melt polycondensation. Scheme 1.2 shows the schemes for these reactions.

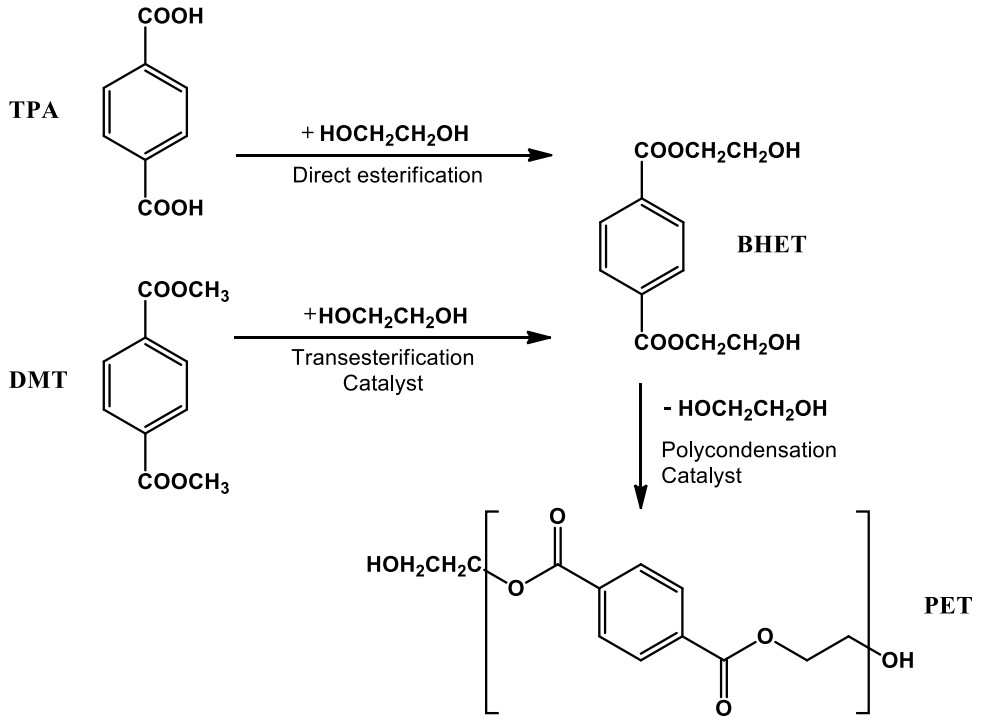

Scheme 1.2. Schemes for the PET polymerization process. [1]

First step: prepolymerization There are two processes in prepolymerization: one produces BHET from DMT and EG, and the other uses TPA and EG.

(a) Transesterification: The monomers for the transesterification reaction are DMT and EG. A reactor is charged with DMT and EG with a 1:2.1–2.3 molar ratio and catalysts. A slow stream of nitrogen is passed through the apparatus. The reaction temperature

should be 170–210 °C. During this reaction, methanol is collected into a graduated receiver as a by-product to allow estimation of the extent of conversion. When the distillation of methanol ceases, the reaction is completed and bis-(2-hydroxyethyl) terephthalate (BHET) is obtained in the first step.

(b) Direct esterification: This reaction is a heterogeneous reaction with monomers of TPA and EG. The mixture of monomers should be charged as a slurry, because TPA is hard to dissolve in EG. The TPA:EG molar ratio used is 1:1.5–3, and the reaction temperature is usually 240–260 °C. Generally, catalysts are not used for this reaction, since the acid functional groups of TPA can catalyze the reaction. Water formed during the reaction as a by-product should be collected for the estimation of the reaction conversion. In the commercial reaction, some PET prepolymer (BHET) is added in order to shorten the reaction time.

Second step: polycondensation BHET produced from the transesterification or direct esterification reaction is gradually heated to 280–290 °C. The reactor is evacuated to low pressure (below 1mmHg), while maintaining the temperature. In this step, EG is collected as a by-product. The final degree of polymerization is raised to about 100. Molecular weight in the melt polymerization step is limited, eigher because the melt viscosity would be too high or degradation reactions would overtake the polycondensation reactions. [2] When it is necessary to make polymer of higher molecular weight, solid-state polymerization is commonly used (see subsection 1.2.5 for detail). The overall reaction time, including the esterification and the polycondensation processes, is long and usually varies from 5 to 10 h.

1.2.3. Polymerization kinetics under various reaction conditions

Tomita reported stirring speed and reaction temperature effects on the polycondensation kinetics. [4] Higher intrinsic viscosity (IV) was obtained at faster stirring speeds, and the reaction time was shortened at higher reaction temperatures. Chegolya *et al*. [5] used TPA as an additive during the polycondensation process of the prepolymer produced by the direct esterification method. The polycondensation process proceeded two to three times faster with the introduction of certain amounts of TPA into the prepolymer. They suggested that the carboxylic acid group of TPA formed an ion pair by autoprotolysis and the proton catalyzed the reaction. [5]

1.2.4. Catalysts and additives

Many researchers have studied the effects of various catalysts for both reactions: transesterification and polycondensation. The mechanism of catalysis in the both reactions is, however, not fully understood. So clarification of the mechanism is one of the major subjects of interest in the present study.

Tomita *et al*. [6] investigated the rate of transesterification of DMT with EG and the effect of catalysts. They used various concentrations of zinc acetate and manganese acetate as the catalysts. While it requires about 2 h reaction time to obtain high conversion with the zinc acetate catalytic system, high conversion is obtained in 20 min with the manganese catalytic system, using optimum concentrations for each. The optimum concentrations of zinc acetate and manganese acetate are 1×10^{-3} and 5×10^{-3} mol/mol DMT, respectively. The electrophilic mechanism for metallic catalysis (the metal center of the catalyst acts as electrophilic Lewis acid) [6,7] is illustrated in scheme 1.3.

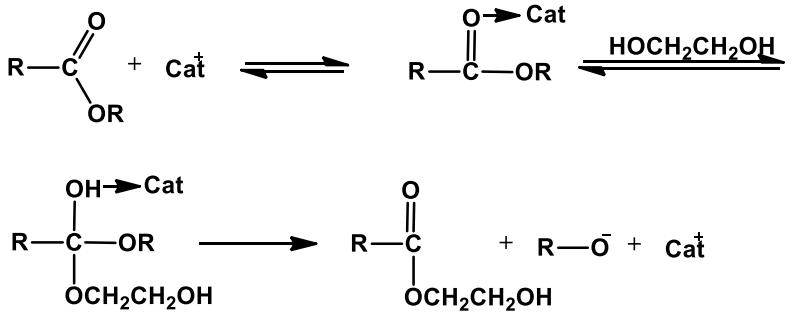

Scheme 1.3. The electrophilic (Lewis acid) mechanism for metallic catalysis. [1]

Shah *et al*. investigated the effect of various metallic catalysts on the polycondensation reaction of BHET [7]. They polymerized PET with different concentrations of catalysts and reaction temperatures and compared their intrinsic viscosities. The results show that titanium-based catalyst is the most active and antimony- and tin-based catalysts are less active. The activity of the polycondensation catalysts increases in the order Ti > Sn > Sb > Mn > Pb. [7] However, titanium-based catalysts have the disadvantage of imparting a yellow color to the polymer. [2] The optimum concentration for titanium-based catalyst ($KTiO_x$), tin-based catalyst ($SnO(But)_2$), and antimony-based catalyst (Sb_2O_3) are 1.5×10^{-4}, 2×10^{-4}, and 2.4×10^{-4} mol/mol BHET,

respectively. [7] In the presence of excess catalyst, the intrinsic viscosity of the resultant PET falls, because there is a competition for catalyst between the sites responsible for the polymerization reaction like chain end groups and internal sites on the formed polymer, like ester oxygens. [7] The intrinsic viscosity increased with an increase in the reaction temperature in the range of 270-295 °C. [7]

MacDonald studied several catalysts for polycondensation in his review. [2] Germanium oxide is also used; although it is a more active catalyst than antimony oxide, its high cost precludes common use for commercial PET production. [2] Titanium-based catalysts are also very active relative to antimony, but they are prone to hydrolysis to form oxoalkoxides, which have reduced activity and make the polymer hazy. Karayannidis *et al*. [8] studied the effect of catalysts in the synthesis of PTT. They synthesized PTT from TPA and 1,3-propanediol (PDO) in the presence of various catalytic systems using the direct technique used for PET. They obtained high molecular weight PTT polymer when titanium tetrabutoxide (TBOT) was used as catalyst for both esterification and polycondensation steps. Although PET becomes yellow when titanium compounds are used for its production, in Shah's study [7], TBOT did not show such effects for the PTT polymer. [8] Antimony oxide historically emerged as the catalyst of choice because it demonstrates a good balance between catalytic activity in the presence of the phosphorous-based stabilizer, color, and cost. [2] However, recently antimony-containing compounds have become subject to discussion due to their potential hazard to health and environment. Glycol residues from PET have to be burnt in special furnaces or be disposed off as hazardous waste, leading to higher disposal costs. [2,9,10] In some PET final products, such as food package or soft-drink bottles, release some antimony compounds, impacting public health. [2,9,10] So PET manufacturers are now focusing on potential alternative to antimony catalyst.

Two different catalytic mechanisms were proposed by Ravindranath [11] (Figure 1.1a) and Parshall and Ittel [12] (Figure 1.1b). Although the catalytic mechanism is still poorly understood, the "Ravindranath mechanism" involves a hexacoordinated metal catalyst molecule. In the primary step, the metal ion coordinates to the ester carbonyl bond. The coordination of the ester carbonyl bond lowers the electron density of the carbonyl carbon atom and facilitates nucleophilic attack. Then the reaction proceeds via the activation of the hydroxyl endgroup of a different incoming polymer chain, which attacks the positively polarized carbonyl carbon, generating a new

ester bond and metal glycolate species through intramolecular rearrangement (Figure 1.1a). The other mechanism proposed by Parshall and Ittel involves a pentacoordinated metal center. In this mechanism the hydroxyl end-groups of two different incoming polymer chain ends coordinate to the metal center in the form of alkoxide ligands. Intramolecular rearrangement within the coordination sphere then results in the formation of a new ester linkage, which couples the two growing polymer chains, thereby generating new metal glycolate species (Figure 1.1b).

In the present study, it is the primary purpose to investigate the catalytic mechanism on the polycondensation reaction, as will be discussed in detail in Chapter 3.

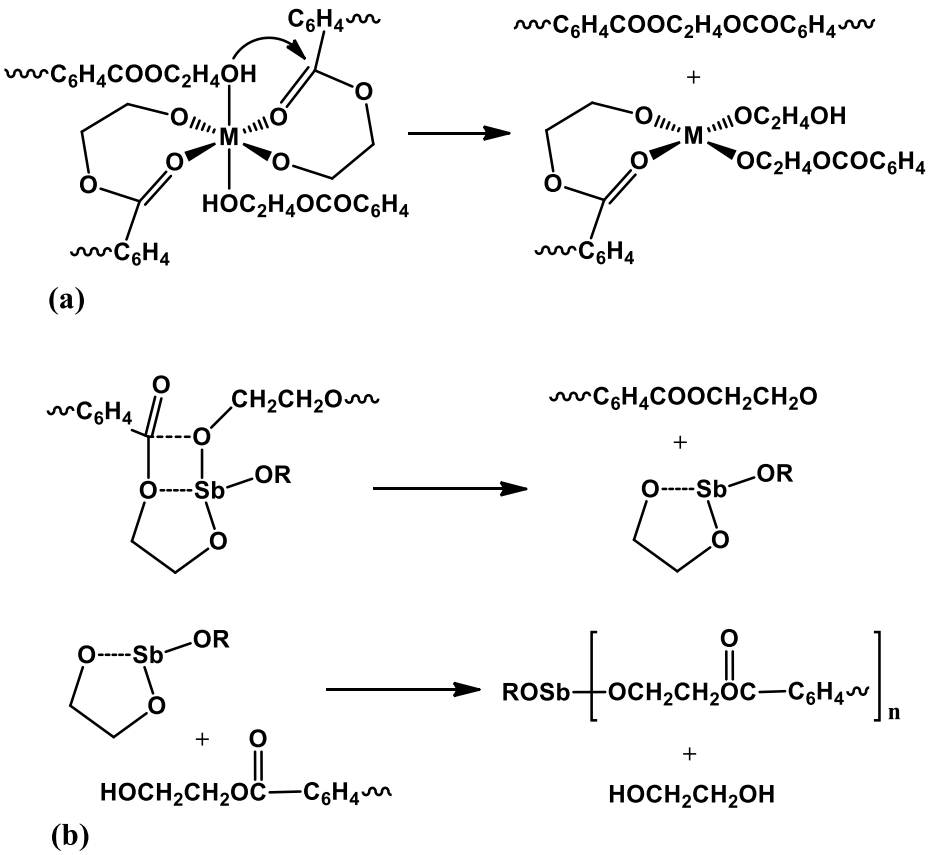

Figure 1.1. Mechanisms of catalysis in polycondensation reaction. (a) "Ravindranath" mechanism [11], (b) "Parshall and Ittel" mechanism [12].

A phosphorous-based stabilizer is commonly added with the catalysts to prevent color-forming degradation reactions during the polycondensation process and subsequent polymer processing. Trimethylphosphate (TMP), triethylphosphate (TEP), triphenylphosphate (TPP), and phosphoric acid (H_3PO_4) are widely used as thermal stabilizers.

1.2.5. Solid-state polymerization

Condensation polymers undergo further polycondensation in the solid state at temperatures between their glass transition temperature and their crystalline melting temperature. This phenomenon has been widely used to produce very high molecular weight (430,000 g/mol number average molecular weight) PET for injection or blow molding applications, because a number average molecular weight of only 15,000–25,000 g/mol can be achieved in the common melt polymerization process. The solid-state polymerization of PET is carried out at around 220–230 °C for 10–30 h. [13-15] The polymer chip from the polycondensation reaction is first crystallized to prevent sintering and then heated at a temperature roughly 20 °C below the melt temperature either in a vacuum or in a hot inert gas in a device that agitates the solid.

1.2.6. Copolymerization

Copolymerization is one of the most attractive techniques to differentiate the properties of PET and to overcome some of its undesirable properties, such as pilling, low moisture regain, static charging, poor dyeability and adhesion to metals, due to high glass transition temperature, and poor processability, due to high melting temperature. A large variety of copolyesters can be obtained from the combination of different monomers. For example, 1,3-propanediol, 1,4-butanediol and isophthalic acid can be added to improve dyeability of PET because PTT, poly(butylene isophthalate) (PBI) and poly(ethylene isophthalate) (PEI) have a lower glass transition temperature and crystallinity, so they absorb dye more easily. In addition, films of PET copolymers with 1,4-butanediol or isophthalic acid have improved adhesion to metal plates and gave excellent shock resistance and barrier properties against corrosive compounds. Also, it has been reported that PET copolymer with poly(ethylene naphthalate) or poly(ethylene isophthalate) can be used to increase the gas barrier properties of PET.

Copolymers of PET have gained significant commercial interest, since the addition of

some other polyesters, such as PEN and PEI into PET tend to improve gas barrier properties. Loss of CO_2 from carbonated beverage packages and O_2 ingress from the atmosphere into packages containing oxygen-sensitive products can limit shelf life, so improved gas barrier properties can increase package performance.

1.3. Physical properties [1]

The useful properties of PET have spurred numerous studies of other ring-containing polyesters. The characteristics of polyesters depend on their structures, symmetries, and conformational features.

Thermal properties Table 1.1 shows melting temperatures of some aromatic phenylene ring-containing polyesters. The terephthalate polyesters are tough, colorless, semi-crystalline solids. [17] Their glass transition temperatures (Tg), a thermal property of the amorphous phase, fall steadily with increasing alkylene group length. The members with x = 3, 4, 6, or higher even numbers crystallize rapidly from the melt, whereas with x = 2, 5, and 7 they crystallize slowly. [18] At ambient temperature, the lower members dissolve in relatively few solvents; phenols, phenol-chlorohydrocarbon mixtures, hexafluoroisopropanol, and trihalogenoacetic acids.

Crystallinity Usually crystallization in high polymers with regular repeating units can be achieved by heating the polymer to a temperature above Tg or dissolving the polymer and evaporating the solvent. The densities vary with crystallinity, but are in the range of 1.2–1.4 g/cm^3. [19]

Gas barrier properties Another important feature of polyesters is their gas barrier properties. PET film is widely used as a packaging material for food, pharmaceuticals, electronics and medical products, because of its good mechanical properties and low cost. However, there is a continuing practical need to improve barrier properties of PET. Crystallization and orientation are two approaches used to obtain barrier enhancement. It can also be improved by coating with poly(vinylidene chloride) or through vacuum metallization. Copolymerization with other aromatic polyesters with meta- or ortho-phenylene linkages, instead of para-linkages, is another approach.

Brolly *et al*. [20] carried out sorption and diffusion tests with CO_2 and PET and PEN

films. The results showed that PEN is less permeable than PET, and both polymers become less permeable to CO_2 when they are oriented. [20] The orientation, achieved through drawing or stretching of an amorphous polymer film, leads to reorientation and closer chain packing, and restriction of chain mobility. Since sorption and diffusion occur in the amorphous regions, these processes can be altered due to changes in the spatial distribution of the amorphous phase during drawing. When polymers are stretched, their gas barrier properties improve substantially. This is due to changes in shape, extent, and perfection of the non-permeable crystalline regions, as well as a result of the chain ordering effects imparted in the amorphous regions.

Table 1.1. Transition temperatures of ring-containing polyesters. [16]

Series	Structural type	Repeating-unit formula	*T*m (°C) for repeating unit with *x* methylene units									
			1	2	3	4	5	6	7	8	9	10
	Poly(alkylene terephthalate)	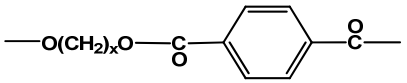	269	265	233	232	134	154	85	132	95	125
1	*T*g[a]			115	95	80	45	45		45	35	25
	*T*g[b]		101	69	35	22	10	-9	3		-3	-5
2	Poly(alkylene isophthalate)	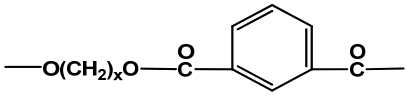		240	132	152		140				
3	Poly(alkylene 4,4'-bibenzoate)	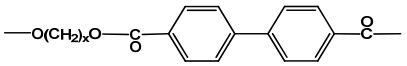		350	280	328	217	240	150	193	128	164
4	Poly(alkylene 2,6-naphthalane-dicarboxylate)	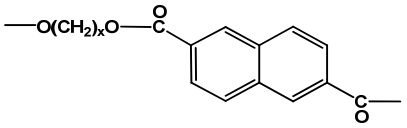	340	266	199	241	135	211	130	185	124	144

a Values reported by dynamic mechanical testing methods.
b Values reported by thermal analysis methods.

1.4. References

[1] Pang K, Kotek R, Tonelli A. Review of conventional and novel polymerization processes for polyesters. Prog. Polym. Sci. 2006; 31: 1009-1037.

[2] MacDonald WA. New advances in poly(ethylene terephthalate) polymerization and degradation. Polym. Int. 2002; 51(10): 923-930.

[3] Paul D. Encyclopedia of Polymer Science and Engineering, vol. 12, 2nd ed. New York: Wiley; 1985. p. 118–256.

[4] Tomita K. Studies on the formation of poly(ethylene terephthalate): 1. Propagation and degradation reactions in the polycondensation of bis(2-hydroxyethyl) terephthalate. Polymer 1973; 14: 50–54.

[5] Chegolya AS, Shevchenko VV, Mikhailov GD. The formation of polyethylene terephthalate in the presence of dicarboxylic acids. J. Polym. Sci: Part A Polym. Chem. 1979; 17: 889–904.

[6] Tomita K, Ida H. Studies on the formation of poly (ethylene terephthalate): 2. Rate of transesterification of dimethyl terephthalate with ethylene glycol. Polymer 1973; 14: 55–60.

[7] Shah TH, Bhatty JI, Gamlen GA. Aspects of the chemistry of poly(ethylene terephthalate): 5. Polymerization of bis-(2-hydroxyethyl) terephthalate by various metallic catalysts. Polymer 1984; 25: 1333–1336.

[8] Karayannidis GP, Roupakias CP, Bikiaris DN, Achilias DS. Study of various catalysts in the synthesis of poly(propylene terephthalate) and mathematical modeling of the esterification reaction. Polymer 2003; 44: 931–42.

[9] Thiele UK. Quo vadis polyester catalyst. Chem. Fibers. Int. 2004; 54(June): 162–163.

[10] Finelli L, Lorenzetti C, Messori M, Sisti L, Vannini M. Comparison between titanium tetrabutoxide and a new commercial titanium dioxide based catalyst used for the synthesis of poly(ethylene terephthalate). J. Appl. Polym. Sci. 2004; 92: 1887–1892.

[11] Ravindranath K, Mashelkar RA. In: Whelan A, Craft JL, editors. Developments in Plastic Technology, vol. 2. London: Elsevier Applied Science Publishers, 1985. Chapter 1.

[12] Parshall GW, Ittel S. Homogeneous Catalysis, 2nd ed. New York: Wiley-Interscience, 1992. Chapter 11.

[13] Duh B. Effect of antimony catalyst on solid-state polycondensation of poly(ethylene terephthalate). Polymer 2002; 43: 3147–3154.

[14] Duh B. Reaction kinetics for solid-state polymerization of poly(ethylene terephthalate). J. Appl. Polym. Sci. 2001; 81: 1748–1761.

[15] Zhi-Lian T, Gao Q, Nan-Zun H, Sironi C. Solid-state polycondensation of poly(ethylene terephthalate): kinetics and mechanism. J. Appl. Polym. Sci. 1995; 57: 473–485.

[16] Paul D. Encyclopedia of Polymer Science and Engineering, vol. 12, 2nd ed. New York: Wiley; 1985. p. 10–11.

[17] Michaels AS, Vieth WR, Barrie JA. Solution of gases in polyethylene terephthalate. J. Appl. Phys. 1963; 34: 1–12.

[18] Polyakova A, Liu RYF, Schiraldi A, Hiltner A, Baer E. Oxygen-barrier properties of copolymers based on ethylene terephthalate. J. Polym. Sci.: Part B Polym. Phys. 2001; 39: 1889–1899.

[19] Kint DPR, Ilarduya AMD, Munoz-Guerra S. Poly(ethylene terephthalate) copolymers containing 5-tert-butyl isophthalic units. J. Polym. Sci.: Part A Polym. Chem. 2001; 39: 1994–2004.

[20] Brolly JB, Bower DI, Ward IM. Diffusion and sorption of CO_2 in poly(ethylene terephthalate) and poly(ethylene naphthalate). J. Polym. Sci.: Part B Polym. Phys. 1996; 34: 769–780.

Chapter 2.

Theoretical Backgrounds

Chapter 2.

Theoretical Backgrounds

In the present study, quantum chemical calculation methods are employed to investigate chemical reactions and catalytic mechanism of polyesters. In this chapter, rough pictures of the methods: density functional theory, basis sets and electron population analysis, potential energy surface, and principal component analysis are provided.

2.1. Density functional theory [1,2,18]

2.1.1. The Kohn-Sham equation

The Schrödinger equation that describes the quantum nature of matter is

$$\hat{H}\Psi = E\Psi \tag{2.1.1}$$

where the Hamiltonian, $\hat{H}$, for a Coulombic system is given by

$$\hat{H} = -\sum_i \frac{1}{2}\nabla_i^2 - \sum_{iA} \frac{Z_A}{|\mathbf{r}_i - \mathbf{r}_A|} + \sum_{i>j} \frac{1}{r_{ij}} \tag{2.1.2}$$

with a specified set of nuclei with charges Z_A and positions $\mathbf{r}_A$ and number of electrons N. The task is to simply minimize the energy over all possible antisymmetric wave functions, $\Psi(\mathbf{x}_1, \mathbf{x}_2, \mathbf{x}_3 \cdots \mathbf{x}_N)$, where $\mathbf{x}_i$ contains the spatial coordinate $\mathbf{r}_i$ and spin coordinate σ_i. This enables us to find the minimizing Ψ and hence the ground state energy, E. The problem is that "application of these laws leads to equations that are too complex to be solved" (P. A. M. Dirac).

In the density functional theory (DFT), the problem is reformulated in a philosophically and computationally different manner. The basic foundation of DFT is the Hohenberg-Kohn theorem, [3] which states that the external potential is a functional of the ground-state electron density. In other words, the density (an observable in 3D space) is used to describe the complicated physics behind the interactions between electrons and, therefore, determines everything about the system. In Kohn-Sham (KS)

theory, [4] this is formulated as a simple expression for the ground state energy

$$\begin{aligned} E[\rho] &= \sum_i \left\langle \phi_i \left| -\frac{1}{2}\nabla^2 \right| \phi_i \right\rangle - \sum_A \int \frac{Z_A}{|\mathbf{r}-\mathbf{R}_A|}\rho(\mathbf{r})\,d\mathbf{r} + \frac{1}{2}\iint \frac{\rho(\mathbf{r})\rho(\mathbf{r}')}{|\mathbf{r}-\mathbf{r}'|}\,d\mathbf{r}\,d\mathbf{r}' + E_{\mathrm{xc}}[\rho] \\ &= T_{\mathrm{S}}[\rho] + V_{\mathrm{ne}}[\rho] + J[\rho] + E_{\mathrm{xc}}[\rho] \end{aligned} \tag{2.1.3}$$

where the forms of some of the functionals are explicitly known. The kinetic energy for the KS non-interacting reference system is

$$T_{\mathrm{S}}[\rho] = \sum_i \left\langle \phi_i \left| -\frac{1}{2}\nabla^2 \right| \phi_i \right\rangle \tag{2.1.4}$$

in terms of $\{\phi_i\}$, the set of one electron KS orbitals. The electron density of the KS reference system is given by

$$\rho(\mathbf{r}) = \sum_i |\phi_i(\mathbf{r})|^2 \tag{2.1.5}$$

The other two known energy components are the nucleus electron potential energy, expressed in terms of the external potential due to the nuclei, $v(\mathbf{r}) = -\Sigma_A(Z_A / |\mathbf{r} - \mathbf{R}_A|)$

$$V_{\mathrm{ne}}[\rho] = \int \rho(\mathbf{r})v(\mathbf{r})\,d\mathbf{r} \tag{2.1.6}$$

and the classical electron-electron repulsion energy is

$$J[\rho] = \frac{1}{2}\int\int \frac{\rho(\mathbf{r})\rho(\mathbf{r}')}{|\mathbf{r}-\mathbf{r}'|}\,d\mathbf{r}\,d\mathbf{r}' \tag{2.1.7}$$

Much is known about the key remaining term, the exchange-correlation functional, $E_{\mathrm{xc}}[\rho]$, although no explicit form is available. It can be expressed in the constrained search formulation for density functionals [5]

$$\begin{aligned} E_{\mathrm{xc}}[\rho] &= \min_{\Psi\to\rho} \left\langle \Psi \left| T + V_{\mathrm{ee}} \right| \Psi \right\rangle - T_{\mathrm{S}}[\rho] - J[\rho] \\ &= (T[\rho] - T_{\mathrm{S}}[\rho]) + (V_{\mathrm{ee}}[\rho] - J[\rho]) \end{aligned} \tag{2.1.8}$$

It can also be expressed elegantly through the adiabatic connection [6,7]

$$E_{\mathrm{xc}}[\rho] = \int_0^1 \left\langle \Psi_\lambda \left| V_{\mathrm{ee}} \right| \Psi_\lambda \right\rangle d\lambda - J[\rho] \tag{2.1.9}$$

The Kohn-Sham orbitals are determined by solving the Kohn-Sham equations. These can be derived by applying the variational principle to the electronic energy $E[\rho]$, with the charge density given by (2.1.5).

$$\hat{h}\phi_i(\mathbf{r}) = \varepsilon_i\phi_i(\mathbf{r}) \tag{2.1.10}$$

where $\hat{h}$ represents the Kohn-Sham Hamiltonian and ε_i is the Kohn-Sham orbital energy associated. The Kohn-Sham Hamiltonian can be written as

$$\hat{h} = -\frac{1}{2}\nabla^2 - \sum_A \frac{Z_A}{|\mathbf{r}-\mathbf{R}_A|} + \int \frac{\rho(\mathbf{r}')}{|\mathbf{r}-\mathbf{r}'|}d\mathbf{r}' + V_{\text{xc}}(\mathbf{r}) \tag{2.1.11}$$

In (2.1.11), V_{xc} is the functional derivative of the exchange-correlation energy, given by

$$V_{\text{xc}}[\rho] = \frac{\delta E_{\text{xc}}[\rho]}{\delta\rho} \tag{2.1.12}$$

Once E_{xc} is known, V_{xc} can be readily obtained.

Many density functional approximations (DFA) have been developed for practical applications. DFT applications have increased enormously in many areas of chemistry due to the excellent performance of these approximate functionals. However, it is important for DFT to fully connect to its roots as an exact theory rather than rest on its laurels as the "best semi-empirical" method, where the parameters are so successful because they are not system dependent. The approach is computationally very different from the direct solution of the Schrödinger equation, where the time is spent in a search over the whole of Hilbert space to find the wave function. In DFT, with a given form for E_{xc}, the search is only to find the three-dimensional density, which is a comparatively trivial problem.

2.1.2. Exchange-correlation functionals

LDA (local density approximation) The form of exchange for the uniform electron gas proposed by Dirac is known to be [8]

$$E_{\text{x}}^{\text{LDA}}[\rho] = -\frac{3}{4}\left(\frac{3}{\pi}\right)^{1/3}\int \rho^{4/3}\,d\mathbf{r} \tag{2.1.13}$$

The functional for correlation was not derived from first principles, instead Monte Carlo simulations of the uniform gas were used to parameterize interpolations between the known forms in the high- and low-density limits. There exist widely used LDA correlation functionals developed by Vosko *et al.* [9] and Perdew. [10]

GGA (generalized gradient approximation) The uniform electron gas has an incredibly different density to those found in atomic or molecular systems. In

chemistry, knowledge of the gradient of the density $\nabla\rho$ is needed at the most fundamental level. The gradient expansion for the slowly varying uniform electron gas is carried out in terms of the dimensionless reduced gradient $x = |\nabla\rho| / \rho^{4/3}$ [or similarly $2(3\pi^2)^{1/3} s = x$] and has the form

$$E_{\mathrm{x}}^{\mathrm{GEA}} = -\int \rho^{4/3} \left[\frac{3}{4} \left(\frac{3}{\pi} \right)^{1/3} + \frac{7}{432\pi(3\pi^2)^{1/3}} x^2 + \cdots \right] d\mathbf{r} \tag{2.1.14}$$

However, this idea gives rise to major problems when applied directly to atoms and molecules, because their densities are anything but slowly varying. This is not due to the nuclei, where x is well-defined, but rather to the atomic tails, as for any exponentially decaying density $x \to \infty$. Here the solution was the development of the generalized gradient approximation (GGA), which takes the simple form for exchange:

$$E_{\mathrm{x}}^{\mathrm{GGA}}[\rho, x] = -\int \rho^{4/3} F(x)\, d\mathbf{r} \tag{2.1.15}$$

where $F(x)$ can be chosen to obey the gradient expansion (2.1.14) in the low x limit. There are now many exchange functionals of the GGA type and the two most commonly used are B88 [11]

$$E_{\mathrm{x}}^{\mathrm{B88}} = -\sum_{\sigma=\alpha,\beta} \int \rho_\sigma^{4/3} \left[\frac{3}{4} \left(\frac{6}{\pi} \right)^{1/3} + \frac{\beta x_\sigma^2}{1 + 6\beta x_\sigma \sinh^{-1} x_\sigma} \right] d\mathbf{r} \tag{2.1.16}$$

and PBE [12]

$$E_{\mathrm{x}}^{\mathrm{PBE}} = -\int \rho^{4/3} \left[\frac{3}{4} \left(\frac{3}{\pi} \right)^{1/3} + \frac{\mu s^2}{1 + \mu s^2 / \kappa} \right] d\mathbf{r} \tag{2.1.17}$$

As with LDA, the development of functionals for correlation has been more complex and taken longer to develop. Currently, there are two main functionals that are well-established, LYP [13] and PBE. [12] Many other GGA functionals have been developed and described in many literatures.

Hybrid functionals Probably the last clear advance in the development of exchange-correlation functionals came in 1993, with the inclusion of some Hartree-Fock (HF) exchange into the functional.

$$E_{\mathrm{x}}^{\mathrm{HF}} = -\frac{1}{2}\sum_{ij\sigma}\iint \frac{\phi_{i\sigma}^{*}(\mathbf{r})\phi_{j\sigma}(\mathbf{r})\phi_{j\sigma}^{*}(\mathbf{r}')\phi_{i\sigma}(\mathbf{r}')}{\left|\mathbf{r}-\mathbf{r}'\right|} d\mathbf{r}\, d\mathbf{r}' \tag{2.1.18}$$

The original idea came from Becke, who used the adiabatic connection to argue that the functional should contain some $E_{\mathrm{x}}^{\mathrm{HF}}$ and proposed a linear model that mixes it with some local DFA exchange and correlation type functionals.

$$E_{\mathrm{xc}}^{\mathrm{BHH}} = \frac{1}{2}E_{\mathrm{x}}^{\mathrm{HF}} + \frac{1}{2}E_{\mathrm{xc}}^{\mathrm{LDA}} \tag{2.1.19}$$

This gave rise to functionals, such as BHLYP, [14] which did not perform uniformly better than GGA functionals. However, the next step that quickly followed was to introduce a little bit of experimental data to refine the idea, [15] giving rise to

$$E_{\mathrm{xc}}^{\mathrm{B3}} = aE_{\mathrm{x}}^{\mathrm{HF}} + (1-a)E_{\mathrm{x}}^{\mathrm{LDA}} + b\Delta E_{\mathrm{x}}^{\mathrm{B88}} + cE_{\mathrm{c}}^{\mathrm{GGA}} + (1-c)E_{\mathrm{c}}^{\mathrm{LDA}} \tag{2.1.20}$$

where the parameters *a*, *b*, and *c* were fitted to a set of experimental data, the G1 data set of Pople and co-workers. This was implemented into the Gaussian package [16] by

$$E_{\mathrm{xc}}^{\mathrm{B3LYP}} = 0.2E_{\mathrm{x}}^{\mathrm{HF}} + 0.8E_{\mathrm{x}}^{\mathrm{LDA}} + 0.72\Delta E_{\mathrm{x}}^{\mathrm{B88}} + 0.81E_{\mathrm{c}}^{\mathrm{LYP}} + 0.19E_{\mathrm{c}}^{\mathrm{VWN}} \tag{2.1.21}$$

using the LYP functional and also VWN [with some confusion over which parameterization (III or V) to use]. This functional has been incredibly successful and extremely widely used, to the extent that in many circles the term DFT is almost synonymous with running a B3LYP calculation. B3LYP has possibly outperformed all expectations, which is excellent for the field of chemistry as it has enabled numerous supporting and illuminating calculations to be carried out. However, B3LYP is successful as a result of some cancellation of errors, which creates a tremendous challenge for the development of new and better exchange-correlation functionals. There is also a large variety of other hybrid functionals.

2.1.3. Time-dependent density functional theory

Time-dependent density functional response theory (TDDFT) was first proposed by Runge and Gross in 1984. [17] More recently, the theory has been reformulated by Stratmann *et al*. [18] and built into Gaussian quantum chemistry program package. [19] From that time, TDDFT has been applied to a number of different atoms and molecules.

The time-dependent Kohn-Sham equation

$$\left[-\frac{1}{2}\nabla^2 + V_{\mathit{eff}}(\mathbf{r},t)\right]\phi(\mathbf{r},t) = i\frac{\partial}{\partial t}\phi(\mathbf{r},t) \tag{2.1.22}$$

can be derived assuming the existence of a potential $V_{\mathrm{eff}}(\mathbf{r},t)$, for an independent particle

system, whose orbitals $\phi(\mathbf{r},t)$ yield the same charge density $\rho(\mathbf{r},t)$ as for the interacting system. This potential has the form

$$V_{\text{eff}}(\mathbf{r},t) = V(t) + V_{\text{SCF}}(\mathbf{r},t) \tag{2.1.23}$$

where $V(t)$ is an applied field (perturbation) turned on slowly in the distant past. The self-consistent field V_{SCF} is defined as

$$V_{\text{SCF}}(\mathbf{r},t) = \int \frac{\rho(\mathbf{r},t)}{|\mathbf{r}-\mathbf{r}'|} d\mathbf{r}' + V_{\text{xc}}(\mathbf{r},t) \tag{2.1.24}$$

where the exchange-correlation potential is given as the functional derivative of the exchange-correlation action A_{xc}, represented by

$$V_{\text{xc}}[\rho](\mathbf{r},t) = \frac{\delta A_{\text{xc}}[\rho]}{\delta\rho(\mathbf{r},t)} \approx \frac{\delta E_{\text{xc}}[\rho_t]}{\delta\rho_t(\mathbf{r})} = V_{\text{xc}}[\rho_t](\mathbf{r}) \tag{2.1.25}$$

Here the unknown functional A_{xc} of ρ over both space and time is approximated by E_{xc} (the exchange-correlation functional of time-independent Kohn-Sham theory) which is a function ρ_t of space at fixed t. This local approximation in time is commonly referred to as the adiabatic approximation and appears to work best for low-lying excited states of clear valence type when used in conjunction with standard functionals.

Linear response of the density matrix For a system initially in the ground state, the effect of a perturbation introduced into the Kohn-Sham (or the HF) Hamiltonian by turning on an applied field $\delta V(t)$ is, to first order

$$\delta V_{\text{eff}}(\mathbf{r},t) = \delta V(t) + \delta V_{\text{SCF}}(\mathbf{r},t) \tag{2.1.26}$$

where $\delta V_{\text{SCF}}(\mathbf{r},t)$ is the linear response of the self-consistent field arising from the change in the charge density given by (transforming to the frequency representation)

$$\delta\rho(\mathbf{r},\omega) = \sum_{ai} \delta P_{ai}(\omega)\phi_a(\mathbf{r})\phi_i^*(\mathbf{r}) + \sum_{ia} \delta P_{ia}(\omega)\phi_i(\mathbf{r})\phi_a^*(\mathbf{r}) \tag{2.1.27}$$

where $\delta P_{st}(\omega)$ is the linear response of the KS/HF density matrix in the basis of the unperturbed molecular orbitals. It is convenient to divide δP into hole-particle (δP_{ai}) and particle-hole (δP_{ia}) parts, which are related by complex conjugation, as these are the only nonzero terms. We use the usual convention in labeling the MOs (i.e., i, j for occupied; a,b for virtual; s,t,u,v for general orbitals). Using elementary results from time-dependent perturbation theory, one can write down the linear response of the KS/HF density matrix to the applied field as

$$\delta P_{st}(\omega) = \frac{\Delta n_{st}}{(\varepsilon_s - \varepsilon_t) - \omega} \delta V_{st}^{\text{eff}}(\omega) \tag{2.1.28}$$

where Δn_{st} is the difference in occupation numbers and is 1 for $st = ai$ and is –1 for $st = ia$. This last equation is somewhat more complicated due to the fact that the potential δV_{SCF} depends on the response of the density matrix

$$\begin{aligned} \delta V_{st}^{\text{SCF}}(\omega) &= \sum_{uv} K_{st,uv}(\omega) \delta P_{uv}(\omega) \\ &= \sum_{bj} K_{st,bj}(\omega) \delta P_{bj}(\omega) + \sum_{jb} K_{st,jb}(\omega) \delta P_{jb}(\omega) \end{aligned} \tag{2.1.29}$$

where the coupling matrix **K** will be defined later. Substituting eqs. (2.1.26) and (2.1.29) into eq. (2.1.28) one obtains (after some algebra)

$$\left[\begin{pmatrix} \mathbf{A} & \mathbf{B} \\ \mathbf{B}^* & \mathbf{A}^* \end{pmatrix} - \omega \begin{pmatrix} 1 & 0 \\ 0 & -1 \end{pmatrix} \right] \begin{pmatrix} \delta P \\ \delta P^* \end{pmatrix} = \begin{pmatrix} -\delta V \\ -\delta V^* \end{pmatrix} \tag{2.1.30}$$

where the matrices **A** and **B** are defined as

$$A_{ai,bj} = \delta_{ab}\delta_{ij}(\varepsilon_a - \varepsilon_i) + K_{ai,bj} \tag{2.1.31}$$

and

$$B_{ai,bj} = K_{ai,jb} \tag{2.1.32}$$

It should be noted that the last two indices on the coupling matrix **K** are switched in the definitions of the **A** and **B** matrices.

Excitation energies in TDHF and TDDFT The coupling matrix given above for TDDFT is easily determined using the chain rule and making use of eqs. (2.1.24), (2.1.25) and (2.1.27). It is given by

$$\begin{aligned} K_{st\sigma,uv\tau} &= \frac{\partial V_{st}^{\text{SCF}}}{\partial P_{uv}} = \frac{\partial V_{st}^{\text{Coulomb}}}{\partial P_{uv}} + \frac{\partial V_{st}^{\text{xc}}}{\partial P_{uv}} \\ &= \left(\phi_{s\sigma}^*(\mathbf{r}) \phi_{t\sigma}(\mathbf{r}) \middle| \phi_{v\tau}^*(\mathbf{r}') \phi_{u\tau}(\mathbf{r}') \right) \\ &\quad + \int \phi_{s\sigma}^*(\mathbf{r}) \phi_{t\sigma}(\mathbf{r}) \frac{\delta^2 E_{\text{xc}}}{\delta\rho_\sigma(\mathbf{r})\delta\rho_\tau(\mathbf{r}')} \phi_{v\tau}^*(\mathbf{r}') \phi_{u\tau}(\mathbf{r}') d\mathbf{r} d\mathbf{r}' \end{aligned} \tag{2.1.33}$$

where σ and τ are spin indices.

Thus in the adiabatic approximation the coupling matrix is independent of ω (time and frequency independent) and is real when the molecular orbitals (MOs) or Kohn-Sham orbitals are real. The time-dependent Hartree-Fock (TDHF) equations, also known as the random phase approximation (RPA), can be derived along the same

lines as done here; the only difference with TDDFT is in this last equation which is

$$K_{st\sigma,uv\tau} = \left(\phi^*_{s\sigma}(\mathbf{r})\phi_{t\sigma}(\mathbf{r})\middle|\phi^*_{v\tau}(\mathbf{r}')\phi_{u\tau}(\mathbf{r}')\right) - \left(\phi^*_{s\sigma}(\mathbf{r})\phi_{u\sigma}(\mathbf{r})\middle|\phi^*_{v\tau}(\mathbf{r}')\phi_{t\tau}(\mathbf{r}')\right) \tag{2.1.34}$$

For RPA then, the **A** matrix is just the CIS (configuration interaction restricted to single excitations) Hamiltonian. In the notation used here, the interpretation of the B matrix is clear; it involves both excitation and de-excitation elements. Mathematically, this is also identical to computing matrix elements between doubly excited states and the ground state. Thus RPA includes higher order correlation effects through double excitations that are not being accounted for in the CIS method. TDDFT includes additional correlation effects through the exchange-correlation potential.

Working equations for TDHF and TDDFT In response theory, excitation energies are determined as poles of the response functions, leading to zero eigenvalues on the left hand side of (2.1.30). They can thus be determined as solutions to the non-Hermitian eigenvalue problem

$$\begin{bmatrix} \mathbf{A} & \mathbf{B} \\ \mathbf{B} & \mathbf{A} \end{bmatrix}\begin{bmatrix} \mathbf{X} \\ \mathbf{Y} \end{bmatrix} = \omega \begin{bmatrix} 1 & 0 \\ 0 & -1 \end{bmatrix}\begin{bmatrix} \mathbf{X} \\ \mathbf{Y} \end{bmatrix} \tag{2.1.35}$$

where the usual notation $X_{ai} = \delta P_{ai}(\omega)$ and $Y_{ai} = \delta P_{ia}(\omega)$ has been adopted. This eigenvalue problem, which is of dimension $2N$ (were $N = N_{\mathrm{Occ}}N_{\mathrm{Vir}}$), can be rewritten as a non-Hermitian problem of half the dimension (by means of a 2x2 unitary transformation)

$$(\mathbf{A}-\mathbf{B})(\mathbf{A}+\mathbf{B})\left|\mathbf{X}+\mathbf{Y}\right\rangle = \omega^2\left|\mathbf{X}+\mathbf{Y}\right\rangle \tag{2.1.36}$$

where $\mathbf{A}+\mathbf{B}$ and $\mathbf{A}-\mathbf{B}$ do not commute. If $(\mathbf{A}-\mathbf{B})$ is positive definite this last equation can be further transformed [multiplying both sides on the left by $(\mathbf{A}-\mathbf{B})^{-1/2}$]

$$(\mathbf{A}-\mathbf{B})^{1/2}(\mathbf{A}+\mathbf{B})(\mathbf{A}-\mathbf{B})^{1/2}\mathbf{T} = \omega^2\mathbf{T} \tag{2.1.37}$$

which is in the form of a Hermitian eigenvalue problem and where

$$\mathbf{T} = (\mathbf{A}-\mathbf{B})^{1/2})\left|\mathbf{X}+\mathbf{Y}\right\rangle \tag{2.1.38}$$

Note that in (2.1.36) and (2.1.37), the **A** and **B** matrices appear as linear combinations of each other. In this formulation, only matrix times vector products are of any interest, so the evaluation of these matrices times vector products can be done in a direct fashion (in the usual sense, so that the matrices are never constructed in memory).

2.2. Basis set expansion of one-electron orbitals [20]

2.2.1. Basis sets for quantum chemical calculations

To solve the quasi one-electron equation (2.1.10), basis set is introduced. Using a set of known basis functions, the differential equation could be converted to a set of algebraic equations and solved by standard matrix techniques.

Kohn-Sham orbitals $\{\phi_i\}$ are expanded by a set of K known basis functions $\{\chi_\mu(\mathbf{r}); \mu = 1,2,..., K\}$ in the linear expression

$$\phi_i = \sum_\mu C_{\mu i}\chi_\mu \tag{2.2.1}$$

If the set $\{\chi_\mu\}$ was complete, this expansion would be exact. Because of practical computational reasons, however, the expansion is always restricted to a finite set of K basis functions. Therefore, it is important to choose a basis will provide, as far as is possible, a reasonably accurate expansion for the exact one-electron orbitals $\{\phi_i\}$.

From (2.2.1), the problem of calculating the Kohn-Sham orbitals reduces to calculating the set of expansion coefficients $C_{\mu i}$. Matrix equation for the $C_{\mu i}$ is obtained by substituting (2.2.1) into the Kohn-Sham equation (2.1.10).

$$\hat{h}(\mathbf{r}_1)\sum_\nu C_{\nu i}\chi_\nu(\mathbf{r}_1) = \varepsilon_i \sum_\nu C_{\nu i}\chi_\nu(\mathbf{r}_1) \tag{2.2.2}$$

By multiplying by $\chi_\mu^*(\mathbf{r}_1)$ on the left and integrating,

$$\sum_\nu C_{\nu i}\int \chi_\mu^*(\mathbf{r}_1)\hat{h}(\mathbf{r}_1)\chi_\nu(\mathbf{r}_1)d\mathbf{r}_1 = \varepsilon_i \sum_\nu C_{\nu i}\int \chi_\mu^*(\mathbf{r}_1)\chi_\nu(\mathbf{r}_1)d\mathbf{r}_1 \tag{2.2.3}$$

It is convenient to define two matrices. The overlap matrix **S** has elements

$$S_{\mu\nu} = \int \chi_\mu^*(\mathbf{r}_1)\chi_\nu(\mathbf{r}_1)d\mathbf{r}_1 \tag{2.2.4}$$

and is a $K \times K$ Hermitian (usually real and symmetric) matrix. Since basis functions $\{\chi_\mu\}$ are not in general orthogonal, overlap each other with a magnitude $0 \le |S_{\mu\nu}| \le 1$, i.e., the diagonal elements of **S** are unity and the off-diagonal elements are less than one in magnitude ($\{\chi_\mu\}$ are assumed to be normalized). The other is a matrix form of one-electron operator $\hat{h}(\mathbf{r}_1)$ (called *Fock matrix* in the Hartree-Fock theory)

$$F_{\mu\nu} = \int \chi_\mu^*(\mathbf{r}_1)\hat{h}(\mathbf{r}_1)\chi_\nu(\mathbf{r}_1)d\mathbf{r}_1 \tag{2.2.5}$$

F is also a $K \times K$ Hermitian (usually real and symmetric) matrix.

With these definitions of **F** and **S**, integrated Kohn-Sham equation (2.2.3) can be

rewritten as

$$\sum_{\nu} F_{\mu\nu} C_{\nu i} = \varepsilon_i \sum_{\nu} S_{\mu\nu} C_{\nu i} \tag{2.2.6}$$

This can be written more compactly as the single matrix equation

$$\mathbf{FC} = \mathbf{SC}\varepsilon \tag{2.2.7}$$

2.2.2. Electron population analysis

The charge density for closed shell systems (2 electrons in 1 orbital)

$$\rho(\mathbf{r}) = 2\sum_{a} |\phi_a(\mathbf{r})|^2 = 2\sum_{a}\sum_{\mu}\sum_{\nu} C_{\mu a}\chi_{\mu}(\mathbf{r}) C^*_{\nu a}\chi^*_{\nu}(\mathbf{r}) = \sum_{\mu}\sum_{\nu} P_{\mu\nu}\chi_{\mu}(\mathbf{r})\chi^*_{\nu}(\mathbf{r}) \tag{2.2.8}$$

represents the probability of finding an electron in various regions of space where the density matrix is defined as

$$P_{\mu\nu} = 2\sum_{a}^{N/2} C_{\mu a} C^*_{\nu a} \tag{2.2.9}$$

There is no unique definition of the number of electrons to be associated with a given atom or nucleus in a molecule, but it is still sometimes useful to preform such population analyses. Since

$$N = 2\sum_{a}^{N/2} \int d\mathbf{r} |\phi_a(\mathbf{r})|^2 \tag{2.2.10}$$

divides the total number of electrons into two electrons per molecular orbital, by substituting the basis expansion of ϕ_a into (2.2.2), we have

$$N = \sum_{\mu}\sum_{\nu} P_{\mu\nu} S_{\nu\mu} = \sum_{\mu} (\mathbf{PS})_{\mu\mu} = \mathrm{tr}\mathbf{PS} \tag{2.2.11}$$

and it is possible to interpret $(\mathbf{PS})_{\mu\mu}$ as the number of electrons to be associated with χ_{μ}. This is called a *Mulliken population analysis*. Assuming the basis functions are centered on atomic nuclei, the corresponding number of electrons to be associated with a given atom in a molecule is obtained by summing over all basis functions centered on that atom. The net charge associated with an atom is then given by

$$q_A = Z_A - \sum_{\mu \in A} (\mathbf{PS})_{\mu\mu} \tag{2.2.12}$$

where Z_A is the charge of atomic nucleus A; the index of summation indicates that we only sum over the basis functions centered on A.

The definition (2.2.3) is by no means unique. Since tr**AB** = tr**BA**,

$$N = \sum_{\mu} (\mathbf{S}^{\alpha}\mathbf{P}\mathbf{S}^{1-\alpha})_{\mu\mu} \tag{2.2.13}$$

for any α. With $\alpha = 1/2$, we have

$$N = \sum_{\mu} (\mathbf{S}^{1/2}\mathbf{P}\mathbf{S}^{1/2})_{\mu\mu} = \sum_{\mu} \mathbf{P}'_{\mu\mu} \tag{2.2.14}$$

where we can show that **P'** is the density matrix in terms of a symmetrically orthogonalized basis set,

$$\rho(\mathbf{r}) = \sum_{\mu}\sum_{\nu} P'_{\mu\nu}\chi'_{\mu}(\mathbf{r})\chi'^{*}_{\nu}(\mathbf{r}) \tag{2.2.15}$$

$$\chi'_{\mu}(\mathbf{r}) = \sum_{\nu} (\mathbf{S}^{-1/2})_{\mu\nu}\chi_{\nu}(\mathbf{r}) \tag{2.2.16}$$

The diagonal elements of **P'** are commonly used for Löwdin population analysis

$$q_A = Z_A - \sum_{\mu\in A} (\mathbf{S}^{1/2}\mathbf{P}\mathbf{S}^{1/2})_{\mu\mu} \tag{2.2.17}$$

2.2.3. Gaussian type basis functions

Standard basis sets for molecular electronic structure calculations use linear combinations of Gaussian type functions as basis functions. The basis functions of this type are called contracted Gaussian functions (CGF).

$$\chi_{\mu}^{\mathrm{CGF}}(\mathbf{r} - \mathbf{R}_A) = \sum_{p=1}^{L} d_{p\mu} g_p(\alpha_{p\mu}, \mathbf{r} - \mathbf{R}_p) \tag{2.2.18}$$

where $\alpha_{p\mu}$ and $d_{p\mu}$ are the contraction exponents and coefficients and L is the length of the contraction. The normalized Gaussian primitive functions are of the 1*s*, 2*p*, 3*d*,... type,

$$g_{1s}(\alpha, \mathbf{r}) = (8\alpha^3/\pi^3)^{1/4}\exp[-\alpha r^2] \tag{2.2.19}$$

$$g_{2p_x}(\alpha, \mathbf{r}) = (128\alpha^5/\pi^3)^{1/4}\, x\exp[-\alpha r^2] \tag{2.2.20}$$

$$g_{3d_{xy}}(\alpha, \mathbf{r}) = (2048\alpha^7/\pi^3)^{1/4}\, xy\exp[-\alpha r^2] \tag{2.2.21}$$

The simplifications that occur for integral evaluation using these functions do not appear for the 2*s*, 3*p*, 4*d*,... Gaussians, and so any basis functions of *s* symmetry, for example a 2*s* or 3*s* function, is expanded in only 1*s* Gaussians, with similar restrictions on the other symmetry types.

In the present study, standard 6-31G** basis set proposed by Pople *et al*. [21,22] is

used for first- and second-row elements. The number "6" means six Gaussian primitive functions are used for basis functions for core orbitals. The notation "31" means *split valence* basis sets, which have two sizes of basis functions (one is constructed from three Gaussian primitives, while the other has only one primitive) for each valence orbital. The last symbol "*" indicates this basis set has polarization function. Split valence basis sets allow orbitals to change size, but not to change shape. To remove this limitation, orbitals with angular momentum (polarization function) are added to form polarized basis sets. For example, 6-31G** adds *d* functions to carbon atoms, *f* functions to transition metals, and *p* functions to hydrogen atoms.

2.3. Potential energy surface and chemical reaction [23,24]

From a computational point of view, many aspects of chemistry can be reduced to questions about potential energy surfaces (PES). A model surface of the energy as a function of the molecular geometry is shown in Figure 2.1 to illustrate some of the features. One can think of it as a hilly landscape, with valleys, mountain passes and peaks. Molecular structures correspond to the positions of the minima in the valleys on a PES. The energetics of reactions is easily calculated from the energies or altitudes of the minima for reactants and products. Reaction rates can be obtained from the height and profile of the mountain pass separating the valleys of the reactants and products. The shape of the valley around a minimum determines the vibrational spectrum. Each electronic state of a molecule has a separate PES, and the separation between these surfaces yields the electronic spectrum. Properties of molecules such as dipole moment, polarizability, NMR shielding, etc., depend on the response of the energy to applied electric and magnetic fields. Thus, the structure, properties, reactivity, and spectra of molecules can be readily understood in terms of PES. Except in very simple cases, the PES cannot be obtained from experiment. However, the field of computational chemistry has developed a wide array of methods for exploring PES. DFT is the most widely used in recent years among such calculation methods.

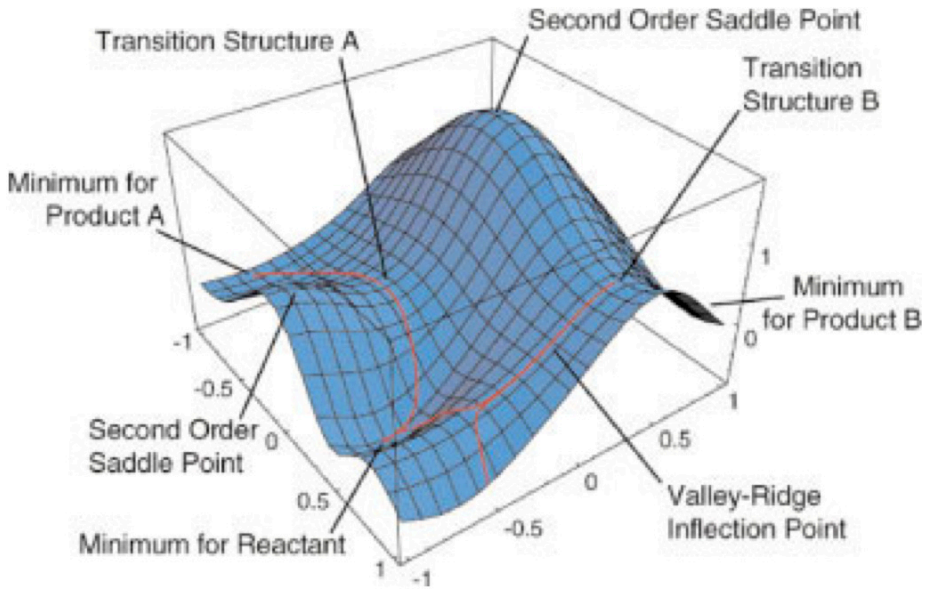

Figure 2.1. Model potential energy surface showing minima, transition states, a second-order saddle point, reaction paths, and a valley ridge inflection point. [23]

A PES arises naturally when the Born-Oppenheimer approximation is invoked in the solution of the Schrödinger equation for a molecular system. Essentially, this assumes that the electronic distribution of the molecule adjusts quickly to any movement of the nuclei. Except when PES for different states get too close to each other or cross, the Born-Oppenheimer approximation is usually quite good. Thus, the energy and behavior of a molecule can be expressed as a function of the positions of the nuclei, that is, a PES. The task for computational chemistry is to explore this PES with methods that are efficient and accurate enough to describe the chemistry of interest. Especially, equilibrium and transition state geometry optimization is the most interest from the point of view of chemical reactions.

2.3.1. Optimizing equilibrium geometries

In any optimization problem, the choice of coordinates can have an important influence on the efficiency of the optimization. Cartesian coordinates provide a simple and unambiguous representation for molecular geometries, and are used for calculating the molecular energy and its derivatives. However, the potential energy surface has very strong coupling between coordinates when represented in Cartesians. Bond lengths, valence angles, and torsions about bonds are more appropriate coordinates to describe the behavior of molecules. Because they express the natural connectivity of

chemical structures, there is much less coupling between these internal coordinates. Modern quantum chemistry program packages, such as Gaussian [19], automatically perform transformation of Cartesian coordinates, displacements, gradients (and Hessian, if necessary) to internals.

$$\Delta\mathbf{q} = \mathbf{B}\Delta\mathbf{x}, \quad \mathbf{g}_q = \mathbf{B}^{-1}\mathbf{g}_x, \quad \mathbf{H}_q = \mathbf{B}^{-T}\left(\mathbf{H}_x - \partial\mathbf{B}/\partial\mathbf{x}\mathbf{g}_q\right)\mathbf{B}^{-1} \tag{2.3.1}$$

where x are the Cartesian coordinates, q are the internal coordinates, $\mathbf{B} = \partial\mathbf{q}/\partial\mathbf{x}$ is the Wilson B matrix, $\mathbf{g}_x = dE/d\mathbf{x}$ is the Cartesian gradient, and $\mathbf{H}_x = d^2E/d\mathbf{x}^2$ is the Cartesian Hessian.

2.3.2. Finding transition states

A transition state is a stationary point on a potential energy surface that corresponds to a mountain pass (see Figure 2.1). It is a maximum in one and only one direction (along the transition vector, going from one valley to another) and a minimum in all other perpendicular directions (three $N_{\text{atoms}} - 7$ degrees of freedom). Transition states are often more difficult to find than equilibrium structures. In principle, a transition state could be found by minimizing the norm of the gradient, but this is usually not a good idea. Provided that the initial structure is close enough to the quadratic region of the transition state, general optimizing schemes (i.e., the quasi-Newton and GDIIS methods) can be adapted to find transition states. The initial Hessian must have the correct number of negative eigenvalues (one and only one), and the corresponding eigenvector must be a suitable approximation to the transition vector (i.e., pointing from one valley to the other).

Since the major problem in optimizing transition states is to get near enough to the quadratic region, quite a number of methods have been developed to get close to transition states. One approach is to approximate the potential energy surface for a reaction as the intersection surfaces for the reactants and products, modeled by molecular mechanics or valence bond methods. The lowest point on the seam of intersection can yield good estimates of the transition state geometry and Hessian (but molecular mechanics force fields may have to be modified to handle the larger distortions from equilibrium). A more general alternative is the coordinate driving or distinguished coordinate method (i.e., stepping a chosen variable (approximating a reaction coordinate) and optimizing the remaining ones). In present study, the author chose the distance between electrophilic and nucleophilic atoms as the “reaction

coordinate" and adopted the distinguished coordinate method to find initial guess of the transition state. Once the guess is located, the transition state geometry is refined by using general minimization schemes.

2.3.3. Following reaction paths

After a transition state has been located and a frequency calculation (a normal mode analysis) has verified that it has one and only one imaginary frequency, it is often necessary to confirm that it connects the desired reactants and products. The reaction path is also needed for calculating reaction rates by variational transition state theory or reaction path Hamiltonian methods. These provide more accurate treatments of reaction rates than simple transition state theory.

The steepest descent reaction path is defined by

$$d\mathbf{x}(s)/ds = -\mathbf{g}(s)/\left|\mathbf{g}(s)\right| \tag{2.3.2}$$

If mass weighted coordinates are used, the steepest descent path is the intrinsic reaction coordinate. [24] Methods for following the reaction path from the transition state down to the reactants and down to the products have been reviewed in a number of articles. The author adopted the algorithm proposed by Schlegel *et al.* [25,26] in the present study.

2.4. Principal component analysis [27]

Principal component analysis (PCA) in many ways forms the basis for multivariate data analysis. PCA provides an approximation of a data table, a data matrix **X** in terms of the product of two small matrices **T** and **P′**. These matrices, **T** and **P′**, capture the essential data patterns of **X**. Plotting the columns of **T** gives a picture of the dominant "object patterns" of **X** and, analogously, plotting the rows of **P′** shows the complementary "variable patterns".

As an example, consider a data matrix containing absorbances at $K = 100$ frequencies measured on $N = 10$ mixtures of two chemical constituent. This matrix is well approximated by a (10×2) matrix **T** times a (2×100) matrix **P′**, where **T** describes the concentrations of the constituents and **P** describes their spectra.

2.4.1. Problem definition for multivariate data

The starting point in all multivariate data analysis is a data matrix (a data table) denoted by **X**. The *N* rows in the table are termed "objects". These often correspond to chemical or geological samples. The *K* columns are termed "variables" and comprise the measurements made on the objects.

In general, almost any data matrix can be simplified by PCA. A large table of numbers is one of the more difficult things for the human mind to comprehend. PCA can be used together with a well selected set of objects and variables to build a model of how a physical or chemical system behaves, and this model can be used for prediction when new data are measured for the same system. PCA has also been used for unmixing constant sum mixtures. This branch is usually called curve resolution. PCA estimates the correlation structure of the variables. The importance of a variable in a PC model is indicated by the size of its residual variance. This is often used for variable selection.

Figure 2.2 shows a 3-space with a point swarm approximated by a one-component PC model: a straight line. A two-component PC model is a plane - defined by two orthogonal lines - and an *A*-components PC model is an *A*-dimensional hyperplane.

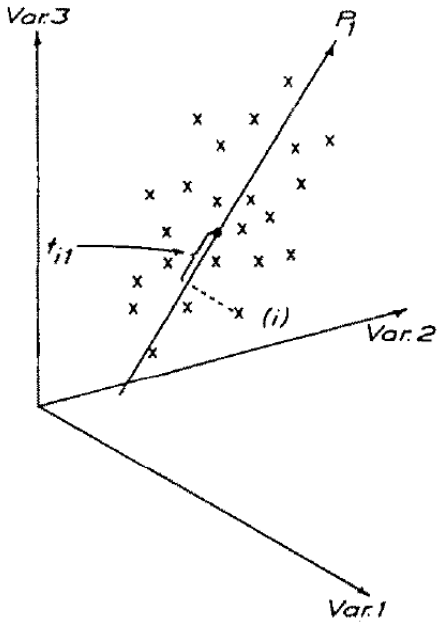

Figure 2.2. A data matrix **X** is represented as a swarm with *N* points in a K-dimensional space. This figure shows a 3-space with a straight line fitted to the points: a one-component PC model. The PC score of an object ($\boldsymbol{t}_i$) is its orthogonal projection on the PC line. The direction coefficients of the line from the loading vector $\boldsymbol{p}_k$. [27]

From Figure 2.2, it may be realized that the fitting of a principal component line to a number of data points is a least squares process. Lines, planes and hyperplanes can be seen as spaces with one, two and more dimensions. Hence, one can see PCA also as the projection of a point swarm in *M*-space down on a lower-dimensional subspace with *A* dimensions. Another way to think about PCA is to regard the subspaces as windows into *M*-space. The data are projected on to the window, which gives a picture of their configuration in *M*-space.

2.4.2. Mathematical definition of principal component analysis

The projection of $\mathbf{X}$ down on an *A*-dimensional subspace by means of the projection matrix $\mathbf{P}'$ gives the object coordinates in this plane, $\mathbf{T}$. The columns in $\mathbf{T}$ ($\boldsymbol{t}_a$) are called score vectors and the rows in $\mathbf{P}'$ ($\mathbf{p}_a'$) are called loading vectors. The latter comprise the direction coefficients of the PC (hyper) plane. The vectors $\mathbf{t}_a$ and $\mathbf{p}_a$ are orthogonal, i.e., $\mathbf{p}_i' \mathbf{p}_j = 0$ and $\mathbf{t}_i' \mathbf{t}_j = 0$ for $i \neq j$.

The deviations between projections and the original coordinates are termed the residuals. These are collected in the matrix $\mathbf{E}$. PCA in matrix form is the least squares model:

$$\mathbf{X} = \mathbf{1}\bar{\mathbf{x}} + \mathbf{T}\mathbf{P}' + \mathbf{E} \qquad (2.4.1)$$

Here the mean vector $\bar{\mathbf{x}}$ is explicitly included in the model formulation, but this is not mandatory. The data may be projected on a hyperplane passing through the origin.

The sizes of the vectors $\mathbf{t}_a$ and $\mathbf{p}_a$ in a PC dimension are undefined with respect to a multiplicative constant *c* as $\mathbf{tp} = (\mathbf{t}c)(\mathbf{p}/c)$, hence it is necessary to anchor the solution in some way. This is usually done by normalizing the vectors $\mathbf{p}_a$ to length 1.0 and choosing its largest element to be positive.

It is instructive to make a comparison with the singular value decomposition (SVD) formulation:

$$\mathbf{X} = \mathbf{1}\bar{\mathbf{x}} + \mathbf{U}\mathbf{D}\mathbf{V}' + \mathbf{E} \qquad (2.4.2)$$

In this instance, $\mathbf{V}'$ is identical with $\mathbf{P}'$. $\mathbf{U}$ contains the same column vectors as does $\mathbf{T}$, but normalized to length one. $\mathbf{D}$ is a diagonal matrix containing the lengths of the column vectors of $\mathbf{T}$. These diagonal elements of $\mathbf{D}$ are the square roots of the eigenvalues of $\mathbf{X}'\mathbf{X}$.

A basic assumption in the use of PCA is that the score and loading vectors corresponding to the largest eigenvalues contain the most useful information relating to

the specific problem, and that the remaining ones mainly comprise noise. Therefore, these vectors are usually written in order of descending eigenvalues.

Often the obtained PC model is rotated by the rotation matrix **R** to make the scores and loading easier to interpret. This is possible because of the equivalence

$$\mathbf{TP}' = \mathbf{TRR}^{-1}\mathbf{P}' = \mathbf{SQ}' \tag{2.4.3}$$

Once the PC model has been developed for a "training matrix", new objects or variables may be fitted to the model giving scores **t** for the new objects, or loadings **p** for the new variables, respectively. In addition, the variance of the residuals **e** is obtained for each fitted item, providing a measure of similarity between the item and the "training data". If this residual variance is larger than that found in the training stage, it can be concluded that the new object (or variable) does not belong to the training population. Hypothesis tests can be applied to this situation. The residuals may alternatively be interpreted as residual distances with respect to a pertinent PC model.

The formulae for a new object $\boldsymbol{x}$ are as follows: multiply by the loadings from the training stage of obtain the estimated scores **t**:

$$\mathbf{t} = \mathbf{xP} \tag{2.4.4}$$

x is projected into the A-dimensional space that was developed in the training stage. Calculated the residuals vector **e**:

$$\mathbf{e} = \mathbf{x} - \mathbf{tP}' \quad \text{or} \quad \mathbf{e} = \mathbf{x}(\mathbf{I} - \mathbf{PP}') \tag{2.4.5}$$

Here **I** is the identity matrix of size K. This calculation of the new scores $\mathbf{t}_a$ or loadings $\mathbf{p}_a$ is equivalent to linear regression because of the orthogonality of the vectors.

2.5. References

[1] Cohen AJ, Mori-Sánchez P, Yang W. Challenges for Density Functional Theory. Chem. Rev. 2012; 112: 289-320.

[2] Sousa SF, Fernandes PA, Ramos MJ. General Performance of Density Functionals. J. Phys. Chem. A 2007: 111; 10439-10452.

[3] Hohenberg P, Kohn W. Inhomogeneous Electron Gas. Phys. Rev. 1964; 136: B864-B871.

[4] Kohn W, Sham LJ. Self-Consistent Equations Including Exchange and Correlation Effects. Phys. Rev. 1965; 140: A1133-A1138.

[5] Levy M. Universal variational functionals of electron densities, first-order density matrices, and natural spin-orbitals and solution of the *v*-representability problem. Proc. Natl. Acad. Sci. U. S. A. 1979; 76: 6062-6065.

[6] Langreth DC, Perdew JP. Exchange-correlation energy of a metallic surface: Wave-vector analysis. II. Phys. Rev. B. 1982; 26: 2810-2818.

[7] Harris J, Jones RO. The surface energy of a bounded electron gas. J. Phys. F. 1974; 4: 1170-1186.

[8] Dirac PAM. Note on Exchange Phenomena in the Thomas Atom. Proc. Cambridge Philos. Soc. 1930; 26: 376-385.

[9] Vosko SH, Wilk L, Nusair M. Accurate spin-dependent electron liquid correlation energies for local spin density calculations: a critical analysis. Can. J. Phys. 1980; 58: 1200-1211.

[10] Perdew JP, Wang Y. Accurate and simple analytic representation of the electron-gas correlation energy. Phys. Rev. B. 1992; 45: 13244-13249.

[11] Becke AD. Density-functional exchange-energy approximation with correct asymptotic behavior. Phys. Rev. A. 1988; 38: 3098-3100.

[12] Perdew JP, Burke K, Ernzerhof M. Generalized Gradient Approximation Made Simple. Phys. Rev. Lett. 1996; 77: 3865-3868.

[13] Lee C, Yang W, Parr RG. Development of the Colle-Salvetti correlation-energy formula into a functional of the electron density. Phys. Rev. B. 1988; 37: 785-789.

[14] Becke AD. A new mixing of Hartree-Fock and local density-functional theories. J. Chem.

Phys. 1993; 98: 1372-1377.

[15] Becke AD. Density-functional thermochemistry. III. The role of exact exchange. J. Chem. Phys. 1993; 98: 5648-5652.

[16] Frisch MJ, Trucks GW, Schlegel HB, Gill PMW, Johnson BG, Wong MW, Foresman JB, Robb MA, Head-Gordon M, Replogle ES, Gomperts R, Andres JL, Raghavachari K, Binkley JS, Gonzalez C, Martin RL, Fox DJ, Defrees DJ, Baker J, Stewart JJP, Pople JA. *Gaussian 92/DFT*, Gaussian, Inc., Pittsburgh PA, 1993.

[17] Runge E, Gross EKU. Density-Functional Theory for Time-Dependent Systems. Phys. Rev. Lett. 1984; 52: 997-1000.

[18] Stratmann RE, Scuseria GE, Frisch MJ. An efficient implementation of time-dependent density-functional theory for the calculation of excitation energies of large molecules. J. Chem. Phys. 1998; 109: 8218-8224.

[19] *Gaussian* 98 (Revision A.1), Frisch MJ, Trucks GW, Scuseria GE, Robb MA, Cheeseman JR, Zakrzewski VG, Montgomery JA, Stratmann RE, Burant JC, Dapprich S, Millam JM, Daniels AD, Kudin KN, Strain MC, Farkas O, Tomasi J, Barone V, Cossi M, Cammi R, Mennucci B, Pomelli C, Adamo C, Clifford S, Ochterski J, Petersson GA, Ayala PY, Cui Q, Morokuma K, Malick DK, Rabuck AD, Raghavachari K, Foresman JB, Cioslowski J, Ortiz JV, Stefanov BB, Liu G, Liashenko A, Piskorz P, Komaromi I, Gomperts R, Martin RL, Fox DJ, Keith T, Al-Laham MA, Peng CY, Nanayakkara A, Gonzalez C, Challacombe M, Gill PMW, Johnson BG, Chen W, Wong MW, Andres JL, Head-Gordon M, Replogle ES, Pople JA, Gaussian, Inc., Pittsburgh, PA, 1998.

[20] Szabo A, Ostlund NS. Modern Quantum Chemistry – Introduction to Advanced Electronic Structure Theory –. Macmillan Publishing, 1982.

[21] Hehre WJ, Ditchfield R, Pople JA. Self-consistent molecular orbital methods. XII. Further extensions of Gaussian-type basis sets for use in molecular orbital studies of organic molecules. J. Chem. Phys. 1972; 56: 2257-2261.

[22] Francl MM, Pietro WJ, Hehre WJ, Binkley JS, Gordon MS, DeFrees DJ, Pople JA. Self-consistent molecular orbital methods. XIII. A polarization-type basis set for second-

row elements. J. Chem. Phys. 1982; 77: 3654-3665.

[23] Schlegel HB. Exploring Potential Energy Surfaces for Chemical Reactions: An Overview of Some Practical Methods. J. Comput. Chem. 2003; 24: 1514-1527.

[24] Fukui K. The Path of Chemical Reactions – The IRC Approach. Acc. Chem. Res. 1981; 14: 363-368.

[25] Gonzalez C, Schlegel HB. An improved algorithm for reaction path following. J. Chem. Phys. 1989; 90: 2154-2161.

[26] Gonzalez C, Schlegel HB. Reaction Path Following in Mass-Weighted Internal Coordinates. J. Phys. Chem. 1990; 94: 5523-5527.

[27] Wold S, Esbensen K, Geladi P. Principal Component Analysis. Chemometr. Intell. Lab. Syst. 1987; 2: 37-52.

Chapter 3.

The Mechanism of Catalysis in the Polycondensation Reaction of Polyesters

Chapter 3.

The Mechanism of Catalysis in the Polycondensation Reaction of Polyesters

3.1. Introduction

Poly(ethylene terephthalate) has become one of the most important thermoplastics because of its balance of excellent mechanical properties, good thermal properties and cost. It has assumed a role of primacy in the field of fibers, films and molding materials.

PET is made via a direct esterification route from terephthalic acid (TPA) and ethylene glycol (EG) followed by polycondensation stage or by an ester interchange process involving dimethyl ester of TPA and EG followed by polycondensation. [1-3] Among a large number of main group and transition metals that have been shown to have catalytic activity for the polycondensation of PET, [2-5] antimony trioxide is the most common polycondensation catalyst in commercial production. Although antimony has a good balance of catalytic activity, color and cost, more active catalyst is demanded to improve plant efficiencies. Furthermore, using antimony in the preparation of PET has come under increasing scrutiny in Europe and Asia. [1] This has led to PET manufacturers researching potential alternatives to antimony. Germanium oxide is a good catalyst; [1,2,4,5] although it demonstrates greater activity and better color than antimony, high cost prevents its common use in commercial production. [1]

The most promising candidate as an alternative to antimony is titanium. [1] Although titanium-based catalysts are very active relative to antimony, the first generation of titanium based catalysts, which were either alkoxides or simple chelates, were prone to hydrolysis to reduce activity and yielded polymers of poor color. Now several

companies are developing titanium-based catalysts and have patented in this area. [1] These latest catalysts are designed to be stable and have been formulated to give a balance of good activity and good color, however, more efficient and better color catalyst system is still demanded.

Despite the importance of catalysis to PET manufacture and a number of patents on this subject, the mechanism of catalysis in the polycondensation reaction is poorly understood; yet an increased understanding of how the metal center interacts with the polymerizing PET chain is important for facilitating further developments in catalyst design.

Three different mechanisms have been proposed; (i) the metal center acts as a Lewis acid, and activates carbonyl group to nucleophilic attack by the oxygen of an alcohol. [5] Other two mechanisms assume exchange reactions between the metal ligands with OH end-groups of oligomers; then (ii) the alkoxy oxygen atom of the ester coordinates to the metal atom, [6] or (iii) the carbonyl oxygen atom coordinates to the metal center, like the first mechanism, and the carbonyl carbon atom have an attack by the alkoxy oxygen atom of an ligand oligomer. [6] These three mechanisms are illustrated in Figure 3.1.

In this work, we carried out a theoretical study of the mechanism of catalysis in the PET polycondensation reaction, using the hybrid density functional theory (DFT) method at the B3LYP level of theory to determine the structures and energetics of the species involved in the reaction. Furthermore, the polarizable continuum model was utilized to account for the effect of the solvent. Diethylterephthalate (DET) molecule was employed as a model of PET oligomer, and antimony, germanium and titanium(IV) catalysts were modeled as ethoxides, with the formulae being $Sb(OEt)_3$, $Ge(OEt)_4$ and $Ti(OEt)_4$, respectively. Three mechanisms illustrated in Fig. 1.1 — Lewis acid (L), coordination of the ester alkoxy oxygen (E) and the carbonyl oxygen (C) — were considered and reaction pathways are investigated in detail. Methanol and ethanol were used as solvents to mimic polar environments in the polycondensation reactor.

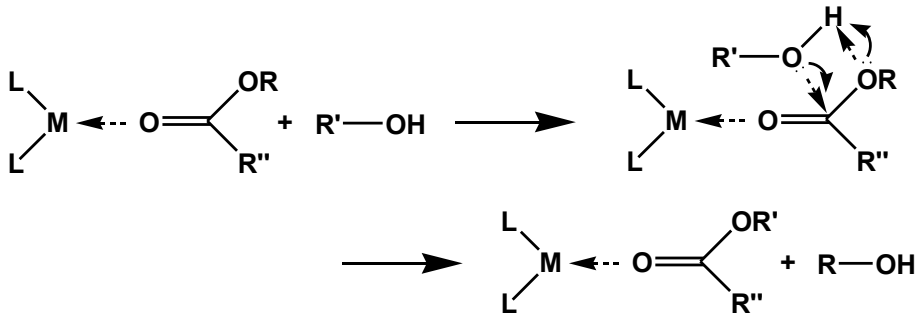

(i) Lewis acid mechanism (L)

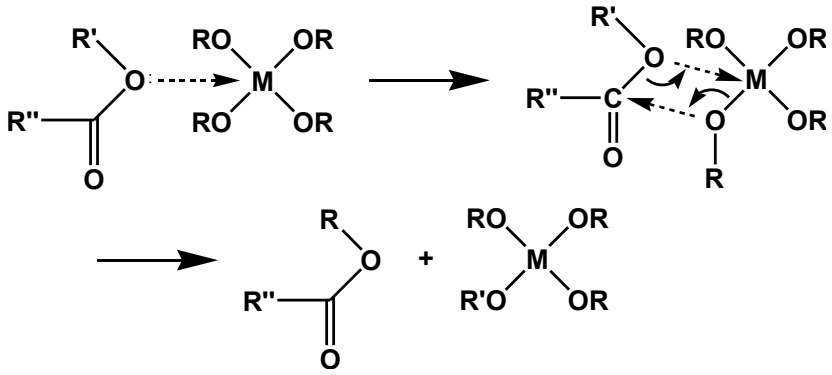

(ii) Coordination of the ester alkoxy oxygen atom mechanism (E)

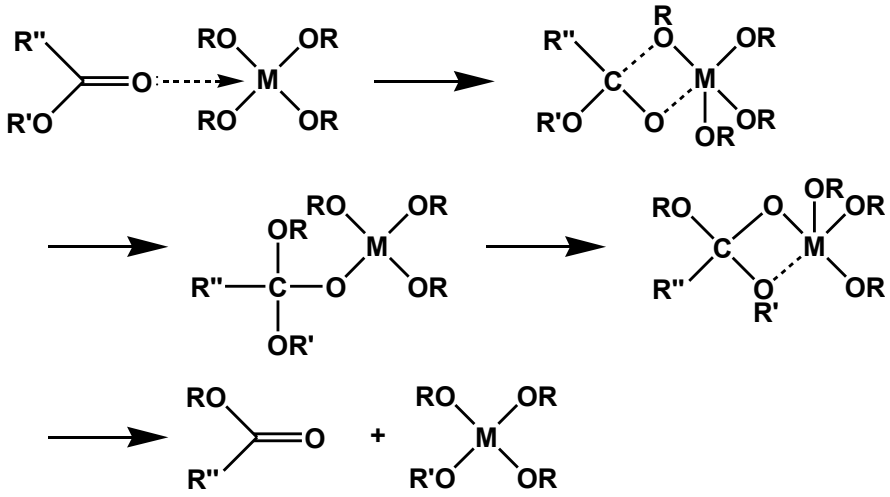

(iii) Coordination of the carboxy oxygen atom mechanism (C)

Figure 3.1. Proposed three mechanisms for polycondensation reaction of PET. (i) The metal center acts as a Lewis acid. (ii) The alkoxy oxygen atom of the ester coordinates to the metal atom. (iii) The carbonyl oxygen atom coordinates to the metal center and the alkoxy oxygen atom of an ligand oligomer attacks to the carbonyl carbon.

3.2. Computational procedure

All of the geometry optimizations were carried out in the gas phase using hybrid DFT (B3LYP) [7-9]. LanL2DZ effective core potentials and basis set [10-12] were used for metallic atoms (Ti, Sb, Ge and Zn) and 6-31G** basis set was adapted for non-metallic atoms (C, N, O and H) in model molecules. The harmonic vibrational frequencies of the reaction complexes were calculated at the same level of theory, and used first to determine whether the optimized structures are true minima or transition states (TSs). In order to verify that the transition states connect the reactants with the appropriate products, we followed the intrinsic reaction coordinates (IRC) using the algorithm developed by Gonzalez and Schlegel. [13,14] The charge densities of each atom were obtained using the standard Mulliken population analysis.

To account for the solvent effects, single point calculations were performed using the polarizable continuum model (PCM) developed by Tomasi and co-workers [15,16] on the optimized structures. The UAHF cavity model was applied in PCM calculations. Methanol and ethanol were chosen as solvents to represent polar environments, with the dielectric constants being 32.63 and 24.55, respectively. All calculations were performed with the Gaussian03 program package. [17]

3.3. Results and discussion

3.3.1. The polycondensation reaction without a catalyst

First of all, we had studied the transesterification reaction of DET with ethanol as a model system of a polycondensation reaction of PET without a catalyst. In this reaction, the oxygen atom of ethanol acts as a nucleophile and attacks to the carbonyl carbon atom of ester molecule, then four-centered cyclic TS is formed. The geometry of TS is illustrated in Figure 3.2. The activation energy in vacuo was calculated to be 45.4 kcal/mol; PCM corrected results were 46.1 and 46.1 kcal/mol for methanol and ethanol solvents, respectively (Table 3.1). These values are comparable to 40 kcal/mol reported by Yokoyama *et al.* [18] for uncatalyzed polycondensation experiments, but higher than 23 and 21 kcal/mol according to Challa [19] and Hovenkamp [20] respectively. PCM correction has only a little effect on activation energies.

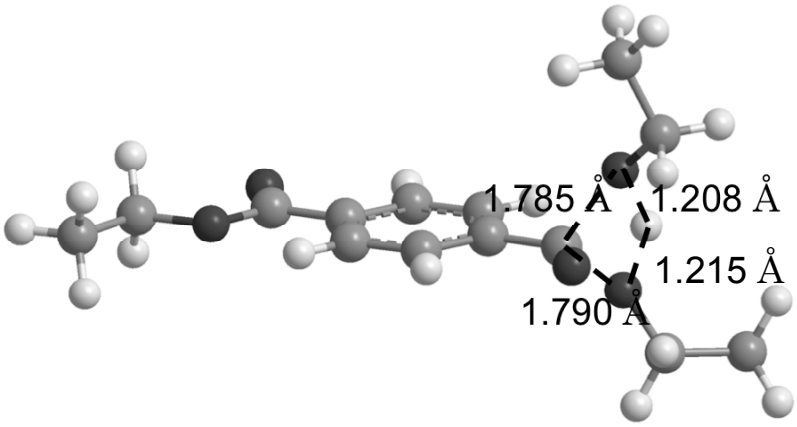

Figure 3.2. Optimized structure for the TS complex of transesterification reaction of DET with ethanol without catalyst. Reaction path with four-centered TS was assumed.

Table 3.1. Activation energies (kcal/mol) of the transesterification reaction of DET with ethanol.

Environment	In vacuo	Methanol	Ethanol
Activation energies	45.4	46.1	46.1

3.3.2. The molecular structures of model catalysts

To investigate the molecular structures of model catalysts, geometry optimization was performed for $Sb(OEt)_3$, $Ge(OEt)_4$ and $Ti(OEt)_4$ metal ethoxides. Optimized structures are illustrated in Figure 3.3, and metal-oxygen bond distances and Mulliken charge distribution are shown in Table 3.2. Because the ion radius of antimony(III) is larger than that of germanium(IV) or titanium(IV), the antimony-oxygen distances in $Sb(OEt)_3$, 1.96 Å, is longer than 1.75 Å in $Ge(OEt)_4$ or 1.80 Å in $Ti(OEt)_4$. On the other hand, $Sb(OEt)_3$ is similar to $Ge(OEt)_4$ with respect to Mulliken charge on oxygen atoms and $Ti(OEt)_4$ has different character from the other two alkoxides. It is anticipated that the charge value on oxygen is related to the activity as a polycondensation catalyst.

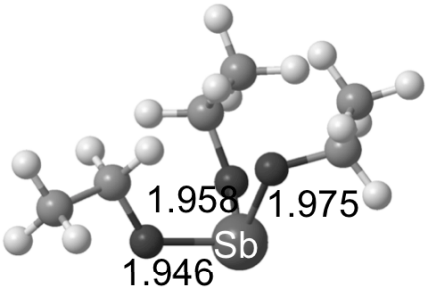

(a) $Sb(OEt)_3$

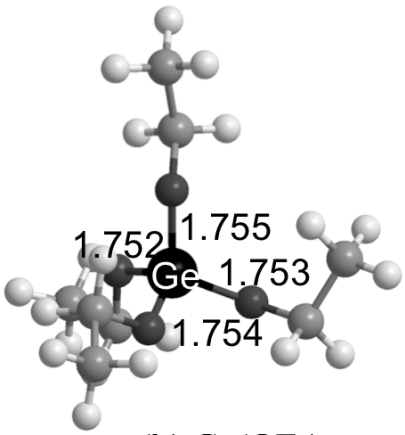

(b) $Ge(OEt)_4$

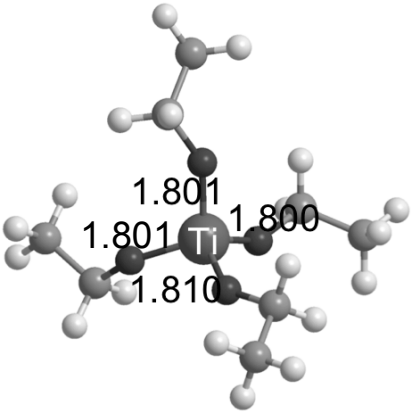

(c) $Ti(OEt)_4$

Figure 3.3. Optimized structure of $Sb(OEt)_3$, $Ge(OEt)_4$ and $Ti(OEt)_4$ model catalysts. Metal-oxygen bond lengths are shown in angstroms.

Table 3.2. Metal-oxygen bond distances and Mulliken charge distribution for model catalysts

		M-O distance	Mulliken charge	
		[Å]	M	O
Metal center	Antimony	1.946 - 1.975	1.444	–0.752 - –0.742
	Germanium	1.752 - 1.755	1.810	–0.752 - –0.743
	Titanium(IV)	1.800 - 1.810	1.289	–0.629 - –0.625

3.3.3. The polycondensation reaction with the Lewis acid mechanism

The activation energies of the reaction with the Lewis acid mechanism (mechanism L) are reported in Table 3.3. Activation energies shown in Table 3.3 are nearly identical to that for non catalyzed reaction; in this mechanism, metal ethoxides seem to have only a little effect on the reaction. PCM correction have only a little effect on activation energies.

The optimized geometries of the reactant and TS complexes shown in Figure 3.4 exhibit the distance between the metal center and the carbonyl oxygen atom of DET (R(M-O)) in each model is too long to have strong interaction. The values of R(M-O) in the reactant structures are written in Table 3.4. Table 3.4 also shows the Mulliken charge densities of carbonyl carbon ($q^{\text{carbonyl C}}$) in each model. Although Lewis acid withdraws electron density from the carbonyl group and activate the carbon atom to nucleophilic attack, $q^{\text{carbonyl C}}$ values in our models are almost identical to that of isolated DET molecule. We did not found significant change in the negative frequencies of TSs either.

These results suggest that the Lewis acid mechanism is not applicable to antimony, germanium and titanium alkoxides. However, Parshall and Ittel indicate that divalent metal ions, such as calcium dication, are said to act as Lewis acids in the catalysis of transesterification. [5]

Table 3.3. Activation energies (kcal/mol) of the transesterification reaction in the Lewis-acid mechanism (mechanism L).

Environment		In vacuo	Methanol	Ethanol
Activation energies	Antimony	46.8	47.1	47.1
	Germanium	43.6	44.9	44.8
	Titanium(IV)	45.0	45.1	45.1

Table 3.4. The distance between the metal center and the carbonyl oxygen atom of DET (R(M-O)), the Mulliken charge densities of carbonyl carbon ($q^{\text{carbonyl C}}$), and the negative frequencies of TSs for the mechanism L.

	R (M-O) / Å	$q^{\text{carbonyl C}}$	Negative frequencies of TSs / cm^{-1}
Uncatalyzed	-	0.610	–1131.59
Antimony	2.923	0.638	–1193.00
Germanium	4.858	0.615	–1178.31
Titanium(IV)	2.766	0.636	–1165.03

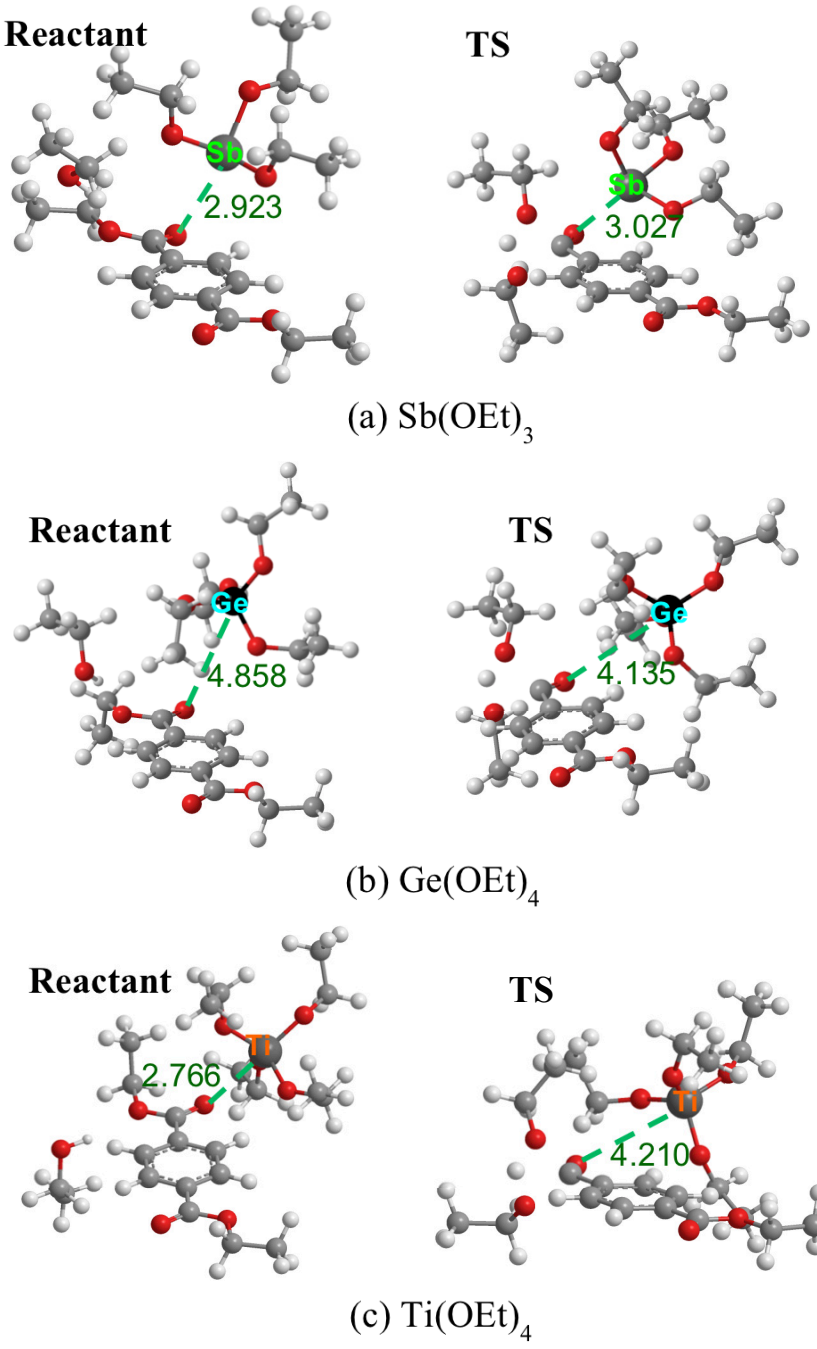

Figure 3.4. Optimized geometries of the reactants (left) and TSs (right) complexes in the Lewis-acid catalyzed transesterification reaction of DET with ethanol. Metal-carbonyl oxygen bond lengths are shown in angstroms.

3.3.4. Coordination of the ester or carbonyl oxygen atom mechanisms

Figure 3.5 shows the optimized geometries of the reactant and TS complexes in the coordination of ester oxygen atom mechanism (mechanism E). In this mechanism, the alkoxy oxygen atom of ethoxy ligands of antimony or titanium alkoxides attacks to the carbonyl carbon atom of the ester to form four-centered TSs. Our calculations failed to locate the TS for germanium alkoxide; it seems that the tetrahedral structure of $Ge(OEt)_4$ is bulky and the interaction between germanium center and ester alkoxy oxygen atom is too weak to activate this type of reaction. Activation energies and the negative frequencies of TSs of the TSs are reported in Table 3.5. Activation barriers are much lower than that of uncatalyzed reaction, but our result of 31.9 kcal/mol for antimony is higher than 18.5 kcal/mol for antimony catalyzed PET polycondensation according to Yokoyama. [18] For titanium, we obtained 26.9 kcal/mol but it is much higher than 11.2 kcal/mol for tetrabutoxy titanium catalyzed poly(butylene terephthalate) reported by Pilati *et al.* [21]

Finally, another mechanism, coordination of the carbonyl oxygen atom (mechanism C), was investigated and activation energies are summarized in Table 3.6. Although this mechanism includes multiple steps as illustrated in Figure 3.1, we studied only the first half of the reaction because the TS of the second half is identical to the first one in our model system. Because we could not find the exact structure of the TS for antimony, figures for antimony are calculated for the quasi TS structure and written in parenthesis to differentiate them from those for other catalysts, whose TSs are examined carefully. The case for antimony will be discussed later in detail. Reactant and TS structures are illustrated in Figure 3.6, while shown TS for antimony is the quasi TS written above.

Table 3.6 shows the lowest activation barrier heights among all three mechanisms. The activation energy for tetraethoxy titanium in vacuo is 15.5 kcal/mol; this is slightly higher than 11.2 kcal/mol for PBT/$Ti(OBu)_4$ reported by Pilati *et al.* [21], but approximately equivalent to the experimental result. Although 22.6 kcal/mol for antimony is a tentative value, it is also comparable to the experimental result of 18.5 kcal/mol reported by Yokoyama. [18]

These results suggest that the coordination of the carbonyl oxygen atom is the most convincing mechanism of PET polycondensation catalysis by antimony, germanium and titanium alkoxides. Our conclusion is consistent with the consideration by Bradley

and Mehrotra. [6]

In addition, Table 3.4 and 3.5 show that PCM correction has only a little effect in these two mechanisms, as same as the mechanism L shown in Table 3.3.

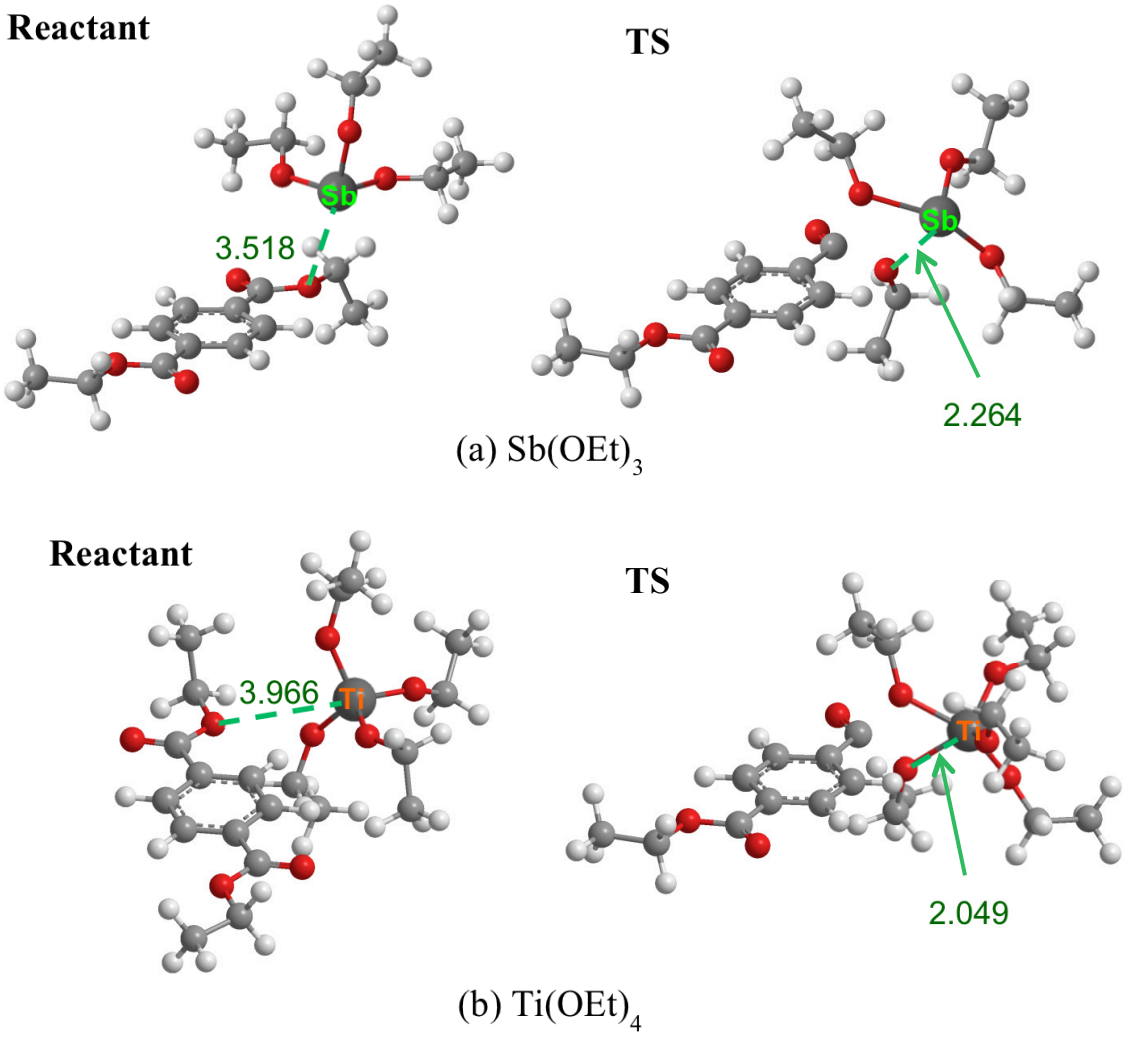

Figure 3.5. Optimized geometries of the reactants (left) and TSs (right) complexes in the coordination of ester oxygen atom mechanism (mechanism E). Metal-ester oxygen bond lengths are shown in angstroms. The TS for $Ge(OEt)_4$ catalyst was not found in this mechanism.

Table 3.5. Activation energies (kcal/mol) and the negative frequencies of TSs (cm^{-1}) of the transesterification reaction in the ester oxygen atom mechanism (mechanism E).

	Activation energies			Negative frequencies of
	In vacuo	Methanol	Ethanol	TSs (In vacuo)
Antimony	31.87	32.43	32.46	–167.37
Germanium		TS not found		
Titanium(IV)	26.91	26.58	26.61	–142.91

Table 3.6. Activation energies (kcal/mol) and the negative frequencies of TSs of the transesterification reaction in the carbonyl oxygen atom mechanism (mechanism C).

	Activation energies			Negative frequencies of
	In vacuo	Methanol	Ethanol	TSs (In vacuo)
Antimony	(22.6)	(22.1)	(22.2)	(–198.3)
Germanium	21.60	23.12	23.10	–119.55
Titanium(IV)	15.47	15.73	15.63	–225.21

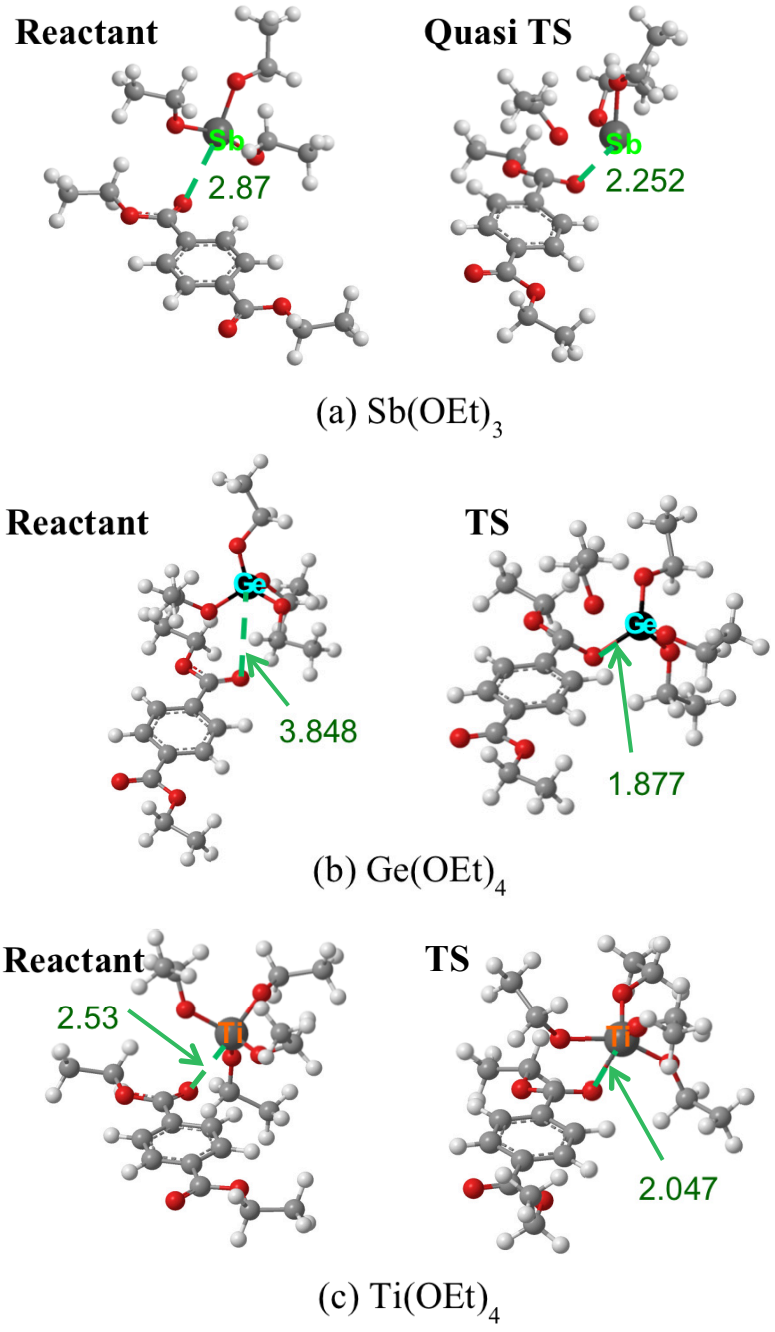

Figure 3.6. Optimized geometries of the reactants (left) and TSs (right) complexes in the coordination of carbonyl oxygen atom mechanism (mechanism C). Metal-carbonyl oxygen bond lengths are shown in angstroms. The quasi TS is illustrated for $Sb(OEt)_3$ catalyst (see Section 3.3.5 for detailed discussion).

3.3.5. The potential energy surface for the antimony catalyzed reaction in the coordination of carbonyl oxygen atom mechanism

Because the TS structure for the antimony-catalyzed reaction in the coordination of carbonyl oxygen atom mechanism was not obtained by standard procedure, we carried out a two dimensional potential energy surface (PES) scan for that reaction. The first coordinate was taken to be the distance between the carbonyl carbon atom and the oxygen atom of ethoxy ligand (R(C-O)), and the second coordinate was the distance between the antimony atom and the ethoxy oxygen (R(M-O)). These coordinates and the PES contour plot are illustrated in Figure 3.7.

In the PES plot, the reactant structure is located at the lower right corner and the intermediate is at the upper left. While the TS should exist between these two points, any efforts to optimize the TS structure around R(C-O) = 1.8 Å and R(M-O) = 2.2 Å failed to give false TS which corresponds to the torsional motion of the ligand ethoxy group. This implies that any potential energy wells and the saddle points on the surface around the real TS must be shallow. We therefore picked up the point (R(C-O), R(M-O)) = (1.75 Å, 2.2 Å) as the quasi TS structure and performed normal mode analysis to examine that the structure has only one negative sign frequency and the negative mode oscillates in the right direction which connects the reactant and the intermediate.

The coordinates of the TSs for germanium and titanium are also indicated in Figure 3.7. In comparison with germanium and titanium, the TS for antimony has longer R(M-O). That reflects the ion radius of antimony(III) is larger than those of germanium(IV) or titanium(IV); the antimony-oxygen distances in an alkoxide, $Sb(OEt)_3$, is 1.96 Å, which is longer than 1.75 Å in $Ge(OEt)_4$ or 1.80 Å in $Ti(OEt)_4$.

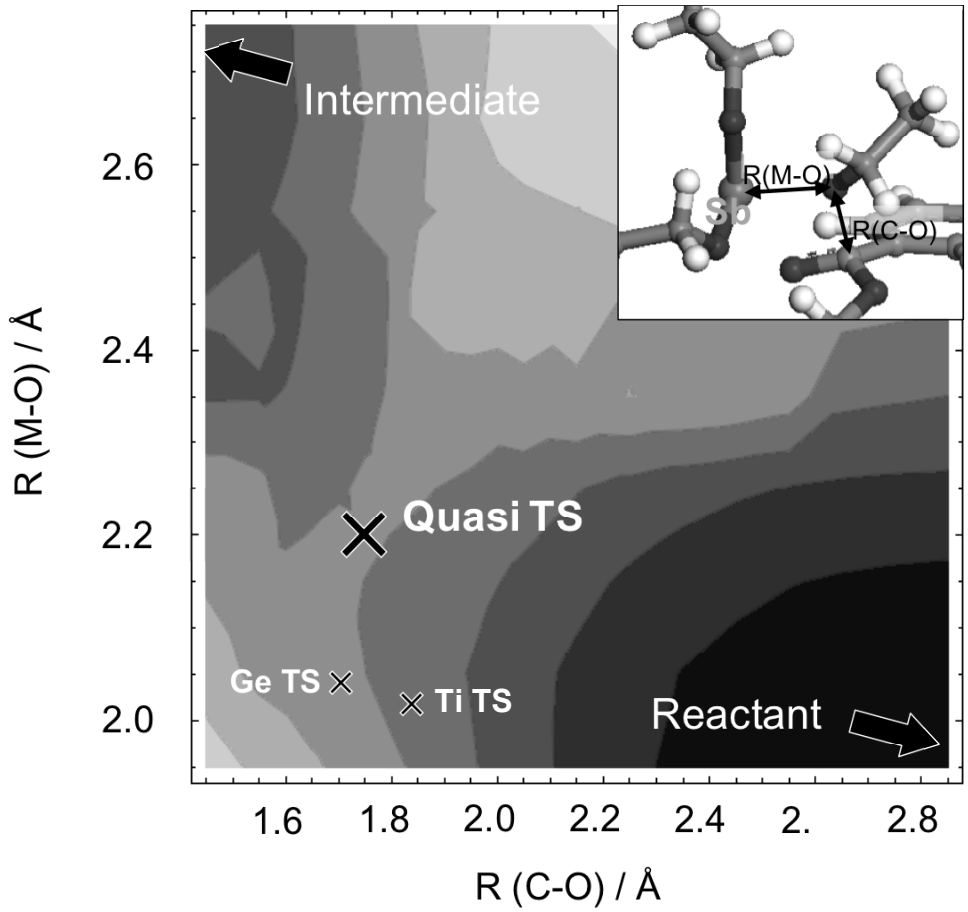

Figure 3.7. Contour plot of the potential energy surface of the $Sb(OEt)_3$ catalyzed reaction in the coordination of carbonyl oxygen atom mechanism. TS geometries for $Ge(OEt)_4$ and $Ti(OEt)_4$ catalysts are also indicated.

3.4. Concluding remarks

In order to investigate the mechanism of catalysis in the PET polycondensation reaction, B3LYP studies on Diethylterephthalate model molecule and $Sb(OEt)_3$, $Ge(OEt)_4$ and $Ti(OEt)_4$ model catalysts were carried out. We found that the most convincing mechanism of PET polycondensation reaction catalyzed by antimony, germanium and titanium alkoxides is the coordination of the carbonyl oxygen atom mechanism; the metal center of metal alkoxides coordinates to the carbonyl oxygen atom of the ester, and the alkoxy oxygen atom of an alkoxy ligand attacks to the carbonyl carbon atom of the ester to form the four-centered transition state. The activation energies in this mechanism are comparable to the experimental results for both antimony and titanium. Other mechanism gave much higher activation energies.

3.5. References

[1] MacDonald WA. New advances in poly(ethylene terephthalate) polymerization and degradation. Polym. Int. 2002; 51: 923-930.

[2] Pilati F. In: Allen G, Bevington JC, Eastmond GC, Ledwith A, Russo S, Sigwalt P, editors. Comprehensive Polymer Science, vol. 5. Chapter 17. Polyesters. Oxford: Pergamon Press, 1989. Chapter 17.

[3] Ravindranath K, Mashelkar RA. In: Whelan A, Craft JL, editors. Developments in Plastic Technology, vol. 2. London: Elsevier Applied Science Publishers, 1985. Chapter 1.

[4] Tomita K. Studies on the formation of poly(ethylene terephthalate): 6. Catalytic activity of metal compounds in polycondensation of bis(2-hydroxyethyl) terephthalate. Polymer 1976; 17: 221-224.

[5] Parshall GW, Ittel S. Homogeneous Catalysis, 2nd ed. New York: Wiley-Interscience, 1992. Chapter 11.

[6] Bradley DC, Mehrotra RC, Gaur DP. Metal Alkoxides. London: Academic Press, 1978. Chapter 2.

[7] Becke AD. Density-functional exchange-energy approximation with correct asymptotic behavior. Phys. Rev. A 1988; 38: 3098–3100.

[8] Becke AD. Density-functional thermochemistry. III. The role of exact exchange. J. Chem. Phys. 1993; 98: 5648-5652.

[9] Lee C, Yang W, Parr RG. Development of the Colle-Salvetti correlation-energy formula into a functional of the electron density . Phys. Rev. B 1988; 37: 785-789.

[10] Hay PJ, Wadt WR. Ab initio effective core potentials for molecular calculations. Potentials for the transition metal atoms Sc to Hg. J. Chem. Phys. 1985; 82: 270-283.

[11] Hay PJ, Wadt WR. Ab initio effective core potentials for molecular calculations. Potentials for main group elements Na to Bi. J. Chem. Phys. 1985; 82: 284-298.

[12] Hay PJ, Wadt WR. Ab initio effective core potentials for molecular calculations. Potentials for K to Au including the outermost core orbitals. J. Chem. Phys. 1985; 82: 299-310.

[13] Gonzalez C, Schlegel HB. An improved algorithm for reaction path following. J. Chem.

Phys. 1989; 90: 2154-2161.

[14] Gonzalez C, Schlegel HB. Reaction Path Following in Mass-Weighted Internal Coordinates. J. Phys. Chem. 1990; 94: 5523-5527.

[15] Mennucci B, Tomasi J. Continuum solvation models: A new approach to the problem of solute's charge distribution and cavity boundaries. J. Chem. Phys. 1997; 106: 5151-5158.

[16] Cossi M, Barone V, Mennucci B, Tomasi J. Ab initio study of ionic solutions by a polarizable continuum dielectric model. Chem. Phys. Lett. 1998; 286: 253-260.

[17] Gaussian 03, Revision E.01. Frisch MJ, Trucks GW, Schlegel HB, Scuseria GE, Robb MA, Cheeseman JR, Montgomery Jr. JA, Vreven T, Kudin KN, Burant JC, Millam JM, Iyengar SS, Tomasi J, Barone V, Mennucci B, Cossi M, Scalmani G, Rega N, Petersson GA, Nakatsuji H, Hada M, Ehara M, Toyota K, Fukuda R, Hasegawa J, Ishida M, Nakajima T, Honda Y, Kitao O, Nakai H, Klene M, Li X, Knox JE, Hratchian HP, Cross JB, Adamo C, Jaramillo J, Gomperts R, Stratmann RE, Yazyev O, Austin AJ, Cammi R, Pomelli C, Ochterski JW, Ayala PY, Morokuma K, Voth GA, Salvador P, Dannenberg JJ, Zakrzewski VG, Dapprich S, Daniels AD, Strain MC, Farkas O, Malick DK, Rabuck AD, Raghavachari K, Foresman JB, Ortiz JV, Cui Q, Baboul AG, Clifford S, Cioslowski J, Stefanov BB, Liu G, Liashenko A, Piskorz P, Komaromi I, Martin RL, Fox DJ, Keith T, Al-Laham MA, Peng CY, Nanayakkara A, Challacombe M, Gill PMW, Johnson B, Chen W, Wong MW, Gonzalez C, Pople JA. Gaussian, Inc., Wallingford CT, 2004.

[18] Yokoyama H, Sano T, Chijiiwa T, Kajiya R. Influence of Catalyst, Stabilizer and Temperature on the Ethylene Glycol Terephthalate Polycondensation Process. J. Japan. Petrol. Inst. 1978; 21(3): 208-210.

[19] Challa G. The Formation of Polyethylene Terephthalate by Ester Interchange. II. The Kinetics of Reversible Melt-Polycondensation. Makromol. Chem. 1968; 38: 123-137.

[20] Hovenkamp SG. Kinetic Aspects of Catalyzed Reactions in the Formation of Poly(ethylene terephthalate). J. Polym. Sci. A-1 1971; 9: 3617-3625.

[21] Pilati F, Manaresi P, Fortunato B, Munari A, Passalacqua V. Formation of poly(butylene terephthalate): growing reactions studied by model molecules. Polymer 1981; 22: 799-803.

Chapter 4.

The Mechanism of Thermal Degradation Reaction of Polyesters

Chapter 4.

The Mechanism of Thermal Degradation Reaction of Polyesters

4.1. Introduction

It is generally known that thermal degradation of the PET chain accompanies the spinning, extrusion or molding process. It may cause the reduction of molecular weight, also lead to the discoloration of PET resin. The published view for color formation in PET caused by thermal degradation is that PET undergoes a β scission reaction resulting in the formation of a vinyl ester and a carboxylic acid end-groups. [1-11] The reaction scheme of β elimination reaction at ester linkage in Ei (elimination internal) mechanism is shown in Figure 4.1. Buxbaum studied the reaction mechanism in detail using model compounds. He concluded that PET breaks down by a molecular mechanism with β chain scission at the ester link, and there was no evidence for a radical mechanism. [5] Pohl proposed that the principal point of weakness in the polyester chain is the β-methylene group, and replacement of the β-hydrogens with methyl groups improves thermal stability. [8] Trischler and Hollander replaced β-hydrogens by fluorine and also indicated that blocking of β elimination path is effective in improving thermal stability of ester linkage. [9] Tomita reported that the rate of thermal degradation of ethylene dibenzoate (EDB), a model compound of PET, is found to obey first order kinetics and the activation energy E_a = 53.4 kcal/mol. [10] Hergenrother measured degradation rate of PET by IR-spectroscopy and derived E_a = 47.3 kcal/mol. [11]

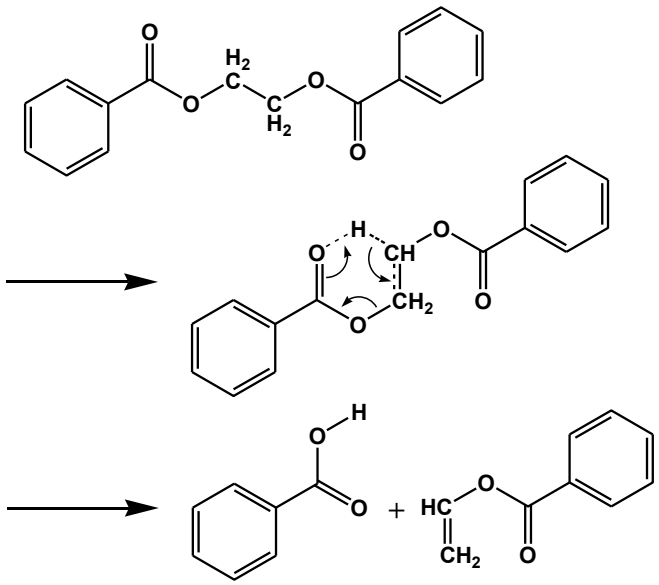

Figure 4.1. Reaction scheme of β elimination reaction at ester linkage.

Furthermore, these vinyl ester end-groups generated by β scission can undergo further reactions, one of which leads to polymerization of the vinyl group ultimately to yield polyenes, which may cause discoloration of PET resin. [1,2,5,6] Buxbaum [5] and Yoda [6] reported that they confirmed the presence of polyene by IR spectroscopy. MacDonald argued, however, that quinone structure is the cause of discoloration and classical polyenes are not responsible for the color formation in PET. [1] The mechanism of discoloration in PET accompanied by thermal degradation has not been clarified yet.

In addition to the β elimination reaction itself, the interaction of catalyst with PET must be considered in the study of PET degradation reaction. The most common polycondensation catalyst in commercial production of PET is antimony trioxide. [1,2] Although antimony has a good balance of catalytic activity, color and cost, more active catalyst is demanded to improve plant efficiencies. The most promising candidate as an alternative to antimony is titanium. [1] Although titanium-based catalysts are very active relative to antimony, the first generation of titanium based catalysts, which were either alkoxides or simple chelates, were prone to hydrolysis to reduce activity and yielded polymers of poor color. Latest catalysts are designed to be stable and have been formulated to give a balance of good activity and good color, however, more efficient and better color catalyst system is still demanded. [1]

There are several reports that the reaction rate of thermal degradation of PET depends on the catalyst included in the resin. [4,12,14,15] Tomita investigated the catalytic activity of metal compounds in the thermal degradation of EDB. [12] He showed a kind of volcano plot, similar to the activity in polycondensation reaction [13], and found that titanium is the most active degradation catalyst. Zimmerman *et al.* studied the activity of zinc acetate on thermal scission of EDB and found that the activation energy of E_a = 40.9 kcal/mol, whereas it is reduced to 29.5 kcal/mol without Zn. [14,15] They considered that the transition state is activated by Zn ion; by intermediary coordinative bonding of metal ion, the ester group is polarized, thus favoring the scission of the proton and the formation of vinyl structures.

Focusing on the structure of polyester, it is known that catalyst has only a little effect on the rate of thermal degradation reaction of poly(butylene terephthalate) (PBT), in contrast to PET. [2] Several studies on thermal degradation of PBT are reported; [14-18] Zimmerman *et al.* found that the activation energy of thermal scission of butylene-1,4-dibenzoate (BDB), a model of PBT, is 41.5 kcal/mol and addition of cobalt acetate has no effect on it. [14,15] Pilati *et al.* also investigated thermal degradation of BDB and reported that titanium(IV) butoxide has no significant effect on the initial rate of formation of benzoic acid. [16] Recently, ^{1}H NMR study on thermal stability of poly(trimethylene terephthalate) (PPT) is carried out by Kelsey *et al.* [19] They indicated that neither titanium catalyst nor cobalt acetate, which is added as toner, affect on the kinetics of thermal degradation reaction of PPT.

As mentioned above, our concern about the thermal degradation reaction of polyesters can be reduced to two points; (i) reaction mechanism of β chain scission, (ii) effect of catalyst on thermal degradation reaction. To clarify these two aspects of the reaction and design a new catalyst which have a good balance of catalytic activity and polymer color, we carried out a theoretical study on the reaction mechanism and determined the structures and energetics of the species involved in the reaction, using the hybrid density functional theory (DFT) method at the B3LYP level of theory. Furthermore, the polarizable continuum model was utilized to account for the effect of the solvent. Methanol and ethanol were used as solvents to mimic polar environments in the polycondensation reactor.

4.2. Model molecules and computational procedure

To reduce computational cost, ethylene dibenzoate (EDB), propylene-1,3-dibenzoate (PDB) and butylene-1,4-dibenzoate (BDB) were employed as model molecules for PET, PPT and PBT, respectively. Antimony, germanium, titanium(IV) and zinc catalysts were modeled as ethoxides or acetates, with the formulae being $Sb(OEt)_3$, $Ge(OEt)_4$, $Ti(OEt)_4$ and $Zn(OAc)_2$, respectively. Methanol and ethanol were chosen as solvents to represent polar environments, with the dielectric constants being 32.63 and 24.55, respectively.

We employed the same computational method as our previous work on polycondensation reaction described in Chapter 3.

4.3. Results and discussion

4.3.1. The β elimination reaction without a catalyst

First of all, we had studied the β elimination reaction of EDB as a model system of a thermal degradation reaction of PET without a catalyst. In this reaction, the carbonyl oxygen atom of ester linkage acts as a nucleophile and attacks to the β hydrogen atom of glycol unit, then six-center cyclic TS is formed. The geometries of reactant, TS and product are illustrated in Figure 4.2. The electronic activation energy in vacuo, which is the difference between total energies of the reactant and the TS isolated in vacuum, was calculated to be 51.1 kcal/mol; PCM corrected results were 50.8 kcal/mol for both methanol and ethanol solvents. PCM correction has only a little effect on activation energies. These values are comparable to the activation energy of thermal degradation of EDB E_a = 53.4 kcal/mol reported by Tomita. [10]

The transition states of β elimination reaction of PDB and BDB were calculated in same way. Those structures were similar to that of EDB, but the activation energies were about 3 kcal/mol lower than EDB. As in EDB, PCM calculation had no substantial effect on the activation energies. Calculated activation energies are summarized in Table 4.1.

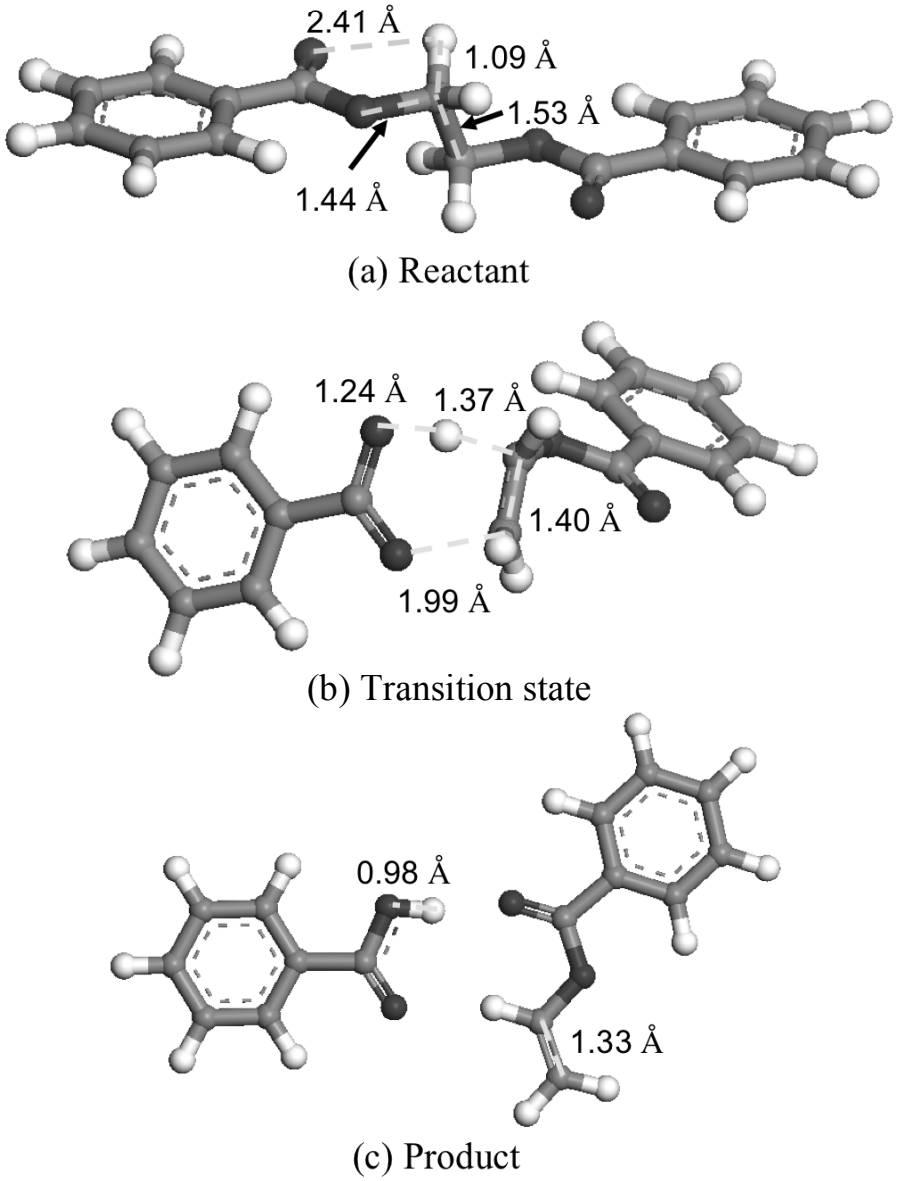

Figure 4.2. Optimized structures for the reactant, TS complex, and product of β elimination reaction of EDB. Reaction path with six-center TS was assumed.

Table 4.1. Activation energies of the β elimination reactions (in kcal/mol).

Environment	In vacuo	PCM	
		Methanol	Ethanol
EDB	51.1	50.8	50.8
PDB	48.4	48.6	48.6
BDB	48.0	47.2	47.2

4.3.2. The β elimination reaction in the Lewis acid mechanism

The activation energies of the β elimination reaction of EDB, PDB and BDB in the Lewis acid mechanism are reported in Table 4.2. Activation energies shown in Table 4.2 are nearly identical to that for non-catalyzed reaction; in this mechanism, metal catalysts seem to have no substantial effect on the reaction. PCM correction has only a little effect on activation energies, as same as in case of the reaction without catalyst.

The optimized geometries of the reactants and TS complexes for $Ti(OEt)_4$ and $Zn(OAc)_2$ catalyzed β elimination reaction of EDB are shown in Figure 4.3 and 4.4, respectively. These Figures also exhibit the distance between the metal center and the carbonyl oxygen atom of EDB (R(M-O)), and the distance of breaking C-O bond (R(C-O)) in the TS structure. The values of R(M-O) and R(C-O) in the TS structures calculated for a series of model molecules and catalysts are summarized in Table 4.3. Because the nature of M-O interaction is electron donation from the lone pair of carbonyl oxygen to the unoccupied orbital of the metal center, R(M-O)'s should reflect not only the ionic radii but also the LUMO level of the metal complexes. The energies of the lowest unoccupied Kohn-Sham orbitals of Ge, Sb, Ti and Zn complexes are 0.0288, -0.0199, -0.0325 and -0.0651 Hartrees, respectively, and the order of orbital energies agrees to the order of R(M-O)'s. The negative frequencies of TSs are also shown in Table 4.3, but we found no significant change in frequencies as well as activation energies.

In this mechanism, a metal catalyst is thought to withdraw electron density from the carbonyl group and activate the carbon atom to nucleophilic attack, [14,15,19] therefore the Mulliken charge densities of carbonyl carbon ($q^{\text{carbonyl C}}$) in metal catalyzed reaction should be more positive than that in non-catalyzed reaction. Table 4.3 includes $q^{\text{carbonyl C}}$ in each model. Zinc gave the shortest R(M-O) and the most positive $q^{\text{carbonyl C}}$ among our model catalysts, so zinc has the strongest interaction with the carbonyl group.

In order to investigate the effect of M-O interaction on reaction and TS structures, E_a, R(C-O), $q^{\text{carbonyl C}}$, and several bond lengths in the TSs are shown in Figure 4.5. In case of zinc, C=O bond (1) is stretched and C-O bond (2) is compressed compared to non-catalyzed reaction. Although these structure changes reflect stronger interaction between Zn and carbonyl O atoms, the difference in length is only 0.03 or 0.04 angstroms and E_a reduction is 1.2 kcal/mol, which is not thought to be significant

difference in B3LYP level of theory. There are no substantial length changes in bond (3), (4) and (5), either. Since titanium has weaker interaction than zinc, changes in structure are smaller than Zn and E_a diminution from non-catalyzed reaction is less than 1 kcal/mol. These results suggest that the Lewis acid mechanism is not applicable to zinc and titanium catalysts in β elimination reaction of EDB. In addition, antimony and germanium showed no significant effect on TS structure because of poor interaction and long coordination distance of these two metals. As interaction between BDB and zinc or titanium catalyst exhibited similar character to EDB, C=O bond (1) stretching and C-O bond (2) compression were also observed. The difference in the C-H bond length (5) between Zn and Ti for BDB, however, is smaller than that for EDB. This is because that insulating methylene groups in butylene glycol unit in BDB prevent electron delocalization between the metal coordinated carbonyl group and the reaction center, and avoid electron-withdrawing effect of the complexed metal catalysts. [14,19]

Table 4.2. Activation energies of the β elimination reaction in the Lewis-acid mechanism (in kcal/mol).

Environment		In vacuo	Methanol	Ethanol
EDB	Uncatalyzed	51.1	50.8	50.8
	Antimony	50.2	49.7	49.7
	Germanium	49.8	49.4	49.4
	Titanium	50.5	49.7	49.9
	Zinc	49.8	49.7	49.6
PDB	Uncatalyzed	48.4	48.6	48.6
	Titanium	48.2	48.7	48.6
BDB	Uncatalyzed	48.0	47.2	47.2
	Titanium	47.6	46.5	46.5
	Zinc	46.3	46.6	46.4

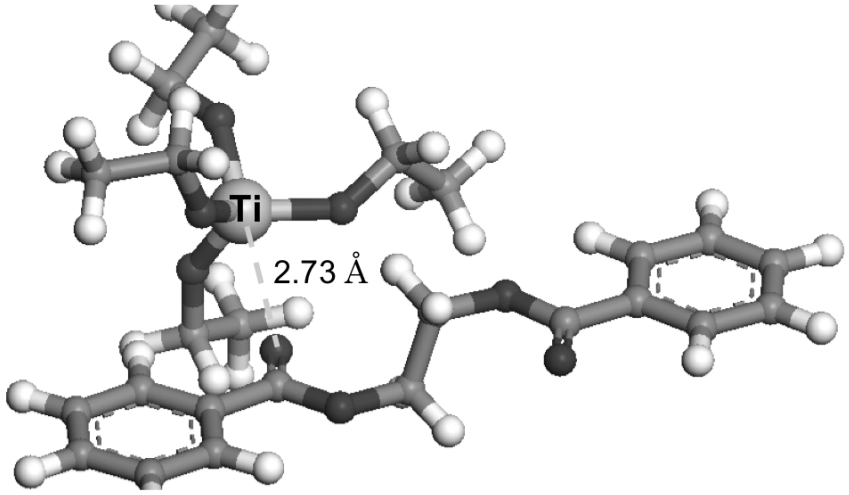

(a) Reactant

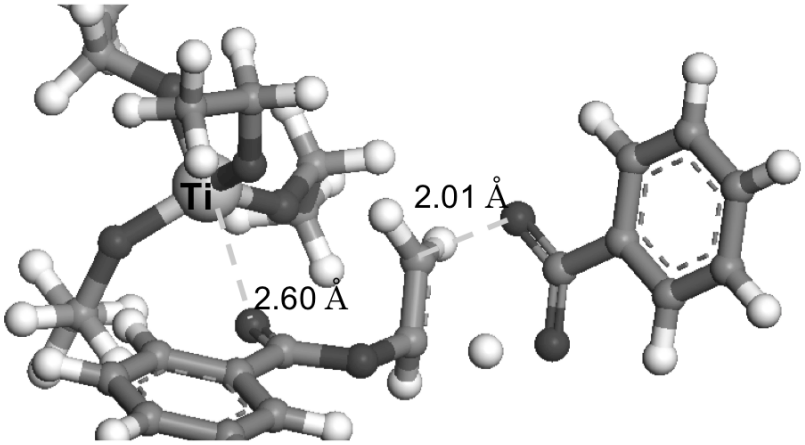

(b) Transition state

Figure 4.3. Optimized structures for the reactant and TS complex of β elimination reaction of EDB with titanium catalyst. Lewis acid mechanism was assumed.

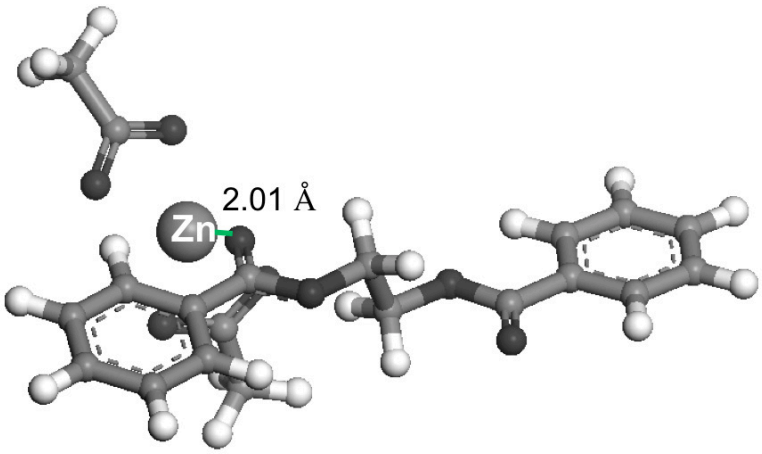

(a) Reactant

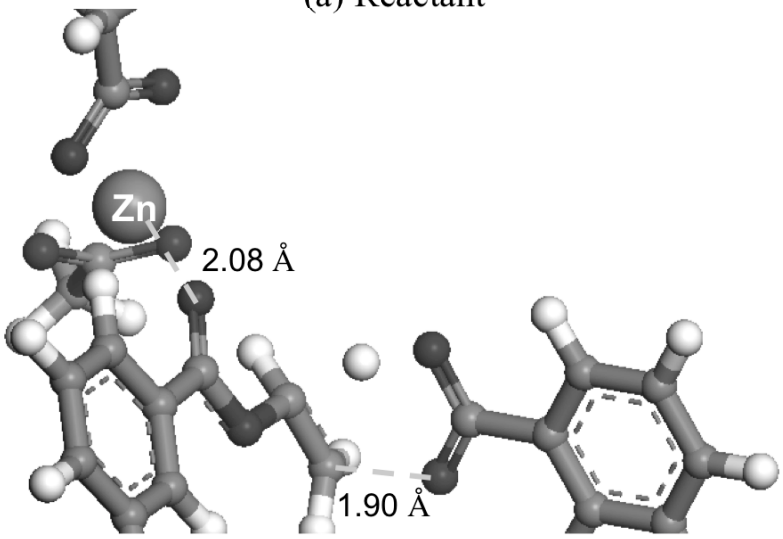

(b) Transition state

Figure 4.4. Optimized structures for the reactant and TS complex of β elimination reaction of EDB with zinc catalyst. Lewis acid mechanism was assumed.

Table 4.3. The distance between the metal center and the carbonyl oxygen atom of model molecules (R(M-O)), the distance of breaking C-O bond (R(C-O)), the Mulliken charge densities of carbonyl carbon ($q^{\text{carbonyl C}}$), and the negative frequencies of TSs for the β elimination reaction.

Properties		R (M-O) / Å	R (C-O) / Å	$q^{\text{carbonyl C}}$	Negative frequencies / cm^{-1}
EDB	Uncatalyzed	-	1.99	0.597	–1470.15
	Antimony	2.98	2.01	0.619	–1458.21
	Germanium	4.10	2.02	0.616	–1447.19
	Titanium	2.60	2.01	0.635	–1453.23
	Zinc	2.08	1.90	0.651	–1488.12
PDB	Uncatalyzed	-	1.95	0.602	–1449.97
	Titanium	2.47	1.95	0.642	–1457.91
BDB	Uncatalyzed	-	1.99	0.602	–1405.05
	Titanium	2.48	1.99	0.640	–1399.86
	Zinc	2.09	2.01	0.644	–1363.61

		E_a / kcal mol^{-1}	R(M-O) / Å	q^C	(1) C=O	(2) C-O	(3) O-C	(4) C-C	(5) C-H
	No cat.	51.07	-	0.597	1.21	1.36	1.43	1.40	1.37
	Zn	49.85	2.01	0.654	1.24	1.32	1.44	1.40	1.40
EDB	Ti	50.46	2.60	0.635	1.22	1.35	1.43	1.40	1.37
	Sb	50.20	2.98	0.619	1.22	1.35	1.43	1.40	1.36
	Ge	49.76	4.10	0.616	1.22	1.35	1.43	1.40	1.36
	No cat.	48.00	-	0.602	1.22	1.35	1.44	1.41	1.32
BDB	Zn	46.32	2.02	0.645	1.24	1.33	1.46	1.41	1.32
	Ti	47.61	2.48	0.640	1.22	1.34	1.45	1.41	1.33

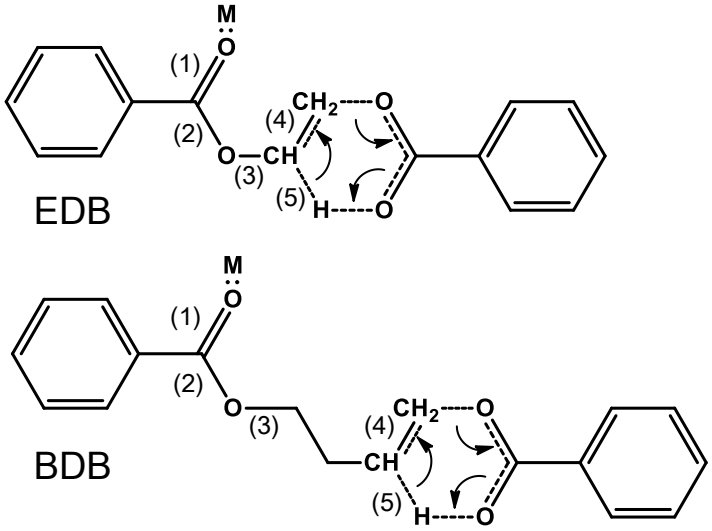

Figure 4.5. Activation energies, metal-carbonyl oxygen distances, Mulliken charges on carbonyl carbon, and bond lengths in the TS structures. Lewis acid mechanism was assumed for catalyzed reactions.

4.3.3. The β elimination reaction in the alkoxy ligand mechanism

As discussed above, we cannot elucidate the catalytic mechanism of thermal degradation reaction of polyesters assuming Lewis acid hypothesis. Our previous quantum chemical study on polycondensation reaction exhibited that Lewis acid also failed to describe catalytic activity of titanium alkoxide (see Chapter 3). In the previous work, we obtained reasonable picture of polycondensation catalysis by

assuming that the nucleophilic attack of the alkoxy end group, which coordinates to the metal center of catalyst, on carbonyl carbon atom. We therefore suppose another mechanism of β elimination reaction in which the alkoxy ligand of catalyst directly abstracts β hydrogen atom. Figure 4.6 illustrates our hypothetical scheme of the reaction. We refer this scheme as alkoxy ligand mechanism because the alkoxy ligand of catalyst acts as a nucleophile in the reaction, in contrast to the carbonyl oxygen in Ei elimination mechanism.

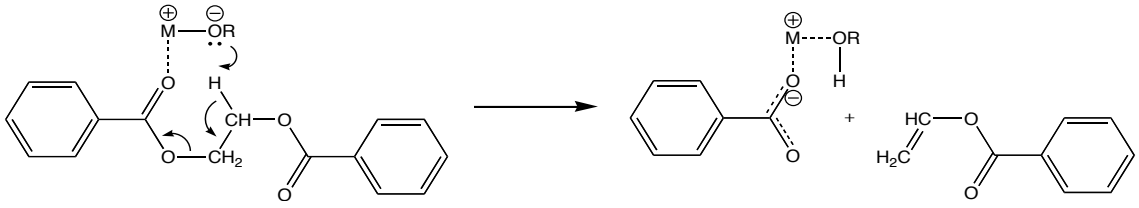

Figure 4.6. Reaction scheme of the β elimination reaction in alkoxy ligand mechanism.

The optimized reactant and TS structures for the $Ti(OEt)_4$ catalyzed β elimination reaction of EDB in this mechanism is depicted in Figure 4.7. Figure 4.8 shows those structures of BDB. As illustrated in these Figures, we successfully found the TS structures in which the alkoxy ligand separates from titanium center with abstracting β-hydrogen atom and generating carboxylic acid group coordinates to titanium center. However, an antimony catalyst gave the TS whose *E*a is higher than that for non-catalyzed Ei reaction, and we could not find the TS which connects the reactant and product for germanium catalyst in this mechanism.

Activation energies are summarized in Table 4.4. The energy of E_a = 43.8 kcal/mol for titanium catalyzed elimination reaction of EDB is 7.3 kcal/mol lower than non-catalyzed reaction. Absolute value of negative frequency is also decreased by 340 cm^{-1}. That means the curvature of potential energy surface around TS becomes soft. Reduction of E_a by titanium catalyst for PDB and BDB are 4.2 kcal/mol, which is less than that for EDB. These results are consistent with well-known observations; catalyst has less effect on the rate of thermal degradation reaction of PPT or PBT, compared to

PET. [2,19] PCM correction has no substantial effect on activation energies, as same as in case of the calculation on Lewis acid mechanism.

Let us investigate the difference between catalytic effect of $Ti(OEt)_4$ for EDB and BDB. The TS structures of EDB and BDB, shown in Figures 4.7 and 4.8 respectively, are very similar and there is no significant difference, except that the ester O - α C and alkoxy O - β H distances are slightly longer in BDB.

We then surveyed Mulliken charge distribution in reactants and TSs, shown in Figure 4.9, to clarify charge transfer in the reaction. Focusing on titanium center (1) and carbonyl oxygen (4), both absolute charge values and differences between reactants and TSs are almost same, because the interactions of titanium with carbonyl oxygen are common in both molecules. β hydrogen (3) showed no significant difference, either. On the other hand, charge on β carbon (8) of EDB is around zero, whereas that of BDB has substantially negative value; nevertheless reactant/TS differences are very similar. Other atoms showed no significant change between EDB and BDB in reactant/TS difference. These results suggest that there is no substantial difference between EDB and BDB concerning about charge transfer in reaction.

Finally, we compared the stability of the products. The reaction energies calculated from total energies are +14.2 kcal/mol for EDB and +16.8 kcal/mol for BDB; the product for EDB is 2.6 kcal/mol more stable than that for BDB. This is because that vinyl group and carboxyl group in vinyl benzoate, which is the product of elimination reaction of EDB, compose resonant structure, whereas insulating methylene groups in BDB prevents resonance between the vinyl group and the carbonyl group in the product. This energy difference can be comparable to the difference in activation energy, 3.1 kcal/mol.

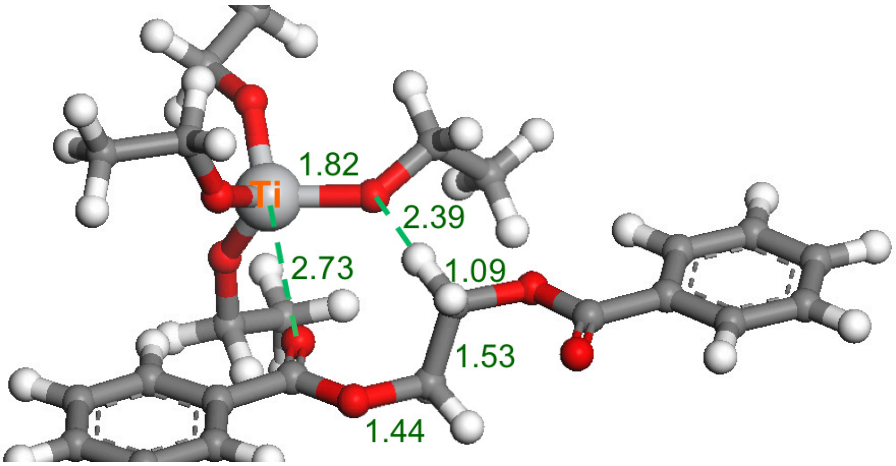

(a) Reactant

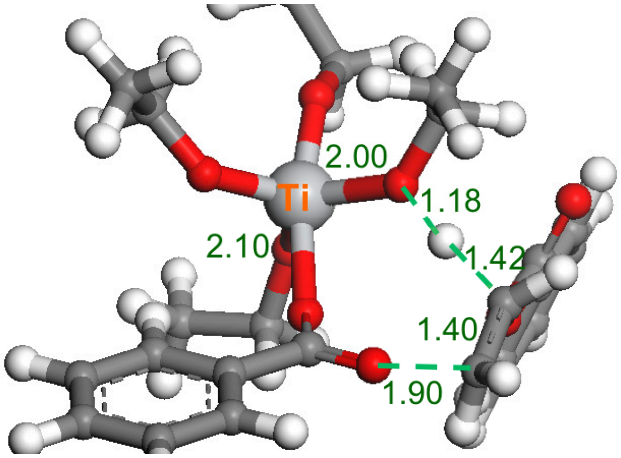

(b) Transition state

Figure 4.7. Optimized structures for the reactant and TS complex of β elimination reaction of EDB with titanium catalyst. Alkoxy ligand mechanism was assumed. Atom-atom distances are written in angstroms.

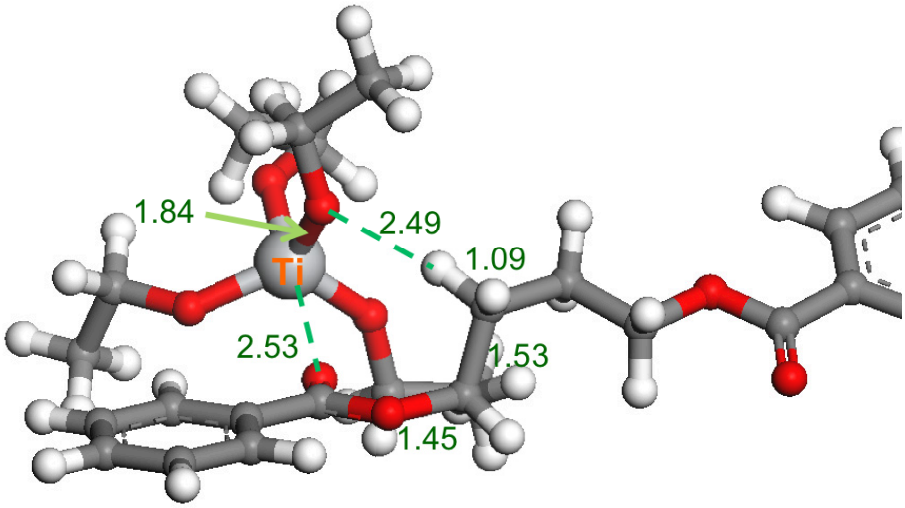

(a) Reactant

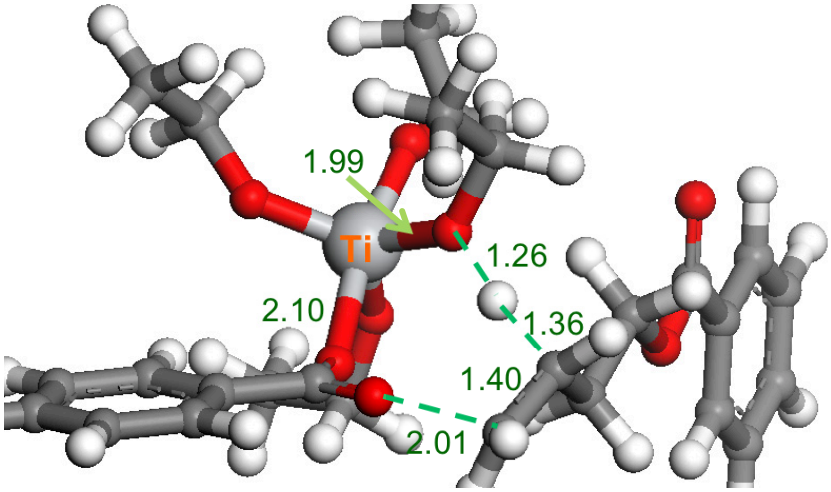

(b) Transition state

Figure 4.8. Optimized structures for the reactant and TS complex of β elimination reaction of BDB with titanium catalyst. Alkoxy ligand mechanism was assumed. Atom-atom distances are written in angstroms.

Table 4.4. Activation energies (kcal/mol) of the β elimination reaction in the alkoxy ligand mechanism. The negative frequencies of TSs (cm^{-1}) are described in parenthesis.

Environment		In vacuo	Methanol	Ethanol
EDB	Uncatalyzed	51.1 (-1470.15)	50.8	50.8
	Antimony	55.2 (–971.92)	54.1	54.2
	Germanium	TS not found		
	Titanium	43.8 (–1129.59)	44.0	44.2
PDB	Uncatalyzed	48.4 (–1449.97)	48.6	48.6
	Titanium	44.2 (–1117.88)	44.1	44.0
BDB	Uncatalyzed	48.0 (–1405.05)	47.2	47.2
	Titanium	43.8 (–1145.40)	44.3	44.2

	Atom	(1) Ti	(2) OEt	(3) Hβ	(4) O=C	(5) C=O	(6) O	(7) CH2	(8) CH2	(9) O	(10) C=O	(11) O=C
EDB	Reactant	1.331	-0.665	0.191	-0.478	0.623	-0.489	0.010	0.026	-0.501	0.615	-0.491
	TS	1.408	-0.691	0.386	-0.633	0.646	-0.521	-0.057	-0.085	-0.480	0.625	-0.510
	Δq	0.077	-0.026	0.195	-0.155	0.023	-0.032	-0.067	-0.111	0.021	0.010	-0.019
	Atom	(1) Ti	(2) OEt	(3) Hβ	(4) O=C	(5) C=O	(6) O	(7) CH2	(8) CH2	(12) CH2	(13) CH2	(14) O
BDB	Reactant	1.341	-0.661	0.173	-0.496	0.631	-0.486	0.033	-0.230	-0.229	0.068	-0.498
	TS	1.406	-0.706	0.389	-0.647	0.642	-0.525	-0.029	-0.333	-0.213	0.051	-0.498
	Δq	0.065	-0.045	0.216	-0.151	0.011	-0.039	-0.062	-0.103	0.016	-0.017	0.000

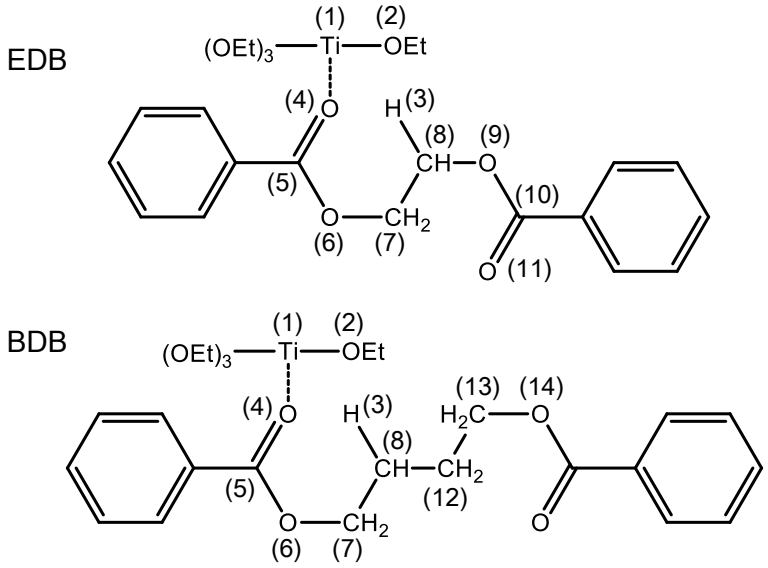

Figure 4.9. Mulliken charge distribution in the reactant and TS structures in alkoxy ligand mechanism. Δq indicates the difference between these two values.

4.4. Concluding remarks

In order to investigate the mechanism of thermal degradation reaction of PET, PPT and PBT, we carried out B3LYP studies on β elimination reaction of EDB, PDB and BDB model molecules. The activation energy for non-catalyzed reaction in vacuo is 51.1 kcal/mol; this is comparable to the experimental result of 53.4 kcal/mol by Tomita. [10] We also studied the catalysis mechanism of $Sb(OEt)_3$, $Ge(OEt)_4$, $Ti(OEt)_4$ and $Zn(OAc)_2$ in that reaction. Although the catalysis mechanism in β elimination reaction is generally thought to be electron-withdrawing effect of Lewis acidity of metal center, the activation energies in this mechanism were very similar to those in non-catalyzed reactions and no catalytic effect was observed. We found that β hydrogen abstraction by the alkoxy ligand of catalyst is more favorable reaction path; the activation energy in alkoxy ligand mechanism is 43.8 kcal/mol, which is 7.3 kcal/mol lower than that for non-catalyzed reaction.

4.5. References

[1] MacDonald WA. New advances in poly(ethylene terephthalate) polymerization and degradation. Polym. Int. 2002; 51: 923-930.

[2] Pilati F. In: Allen G, Bevington JC, Eastmond GC, Ledwith A, Russo S, Sigwalt P, editors. Comprehensive Polymer Science, vol. 5. Chapter 17. Polyesters. Oxford: Pergamon Press, 1989. Chapter 17.

[3] Jabarin SA. In: Salamone JC, editor-in-chief. Polymeric Materials Encyclopedia vol. 8. POLY(ETHYLENE TEREPHTHALATE) DEGRADATION (CHEMISTRY AND KINETICS). Boca Raton: CRC Press, 1996. p. 6114.

[4] Grassie N. Chemistry of High Polymer Degradation Processes. London: Butterworths, 1956. p.285-294.

[5] Buxbaum LH. The Degradation of Poly(ethylene terephthalate). Angew. Chem. Int. Ed. 1968; 7: 182-190.

[6] Yoda K, Tsuboi A, Wada M, Yamadera R. Network Formation in Poly(ethylene Terephthalate) by Thermooxidative Degradation. J. Appl. Polym. Sci. 1970; 14: 2357-2376.

[7] Goodman I. In: Mark HF, Bikales NM, Overberger CG, Menges G, editors. Encyclopedia of Polymer Science and Engineering, Vol. 12. POLYESTERS. New York: Wiley, 1986. p. 25.

[8] Pohl HA. The Thermal Degradation of Polyesters. J. Am. Chem. Soc. 1951; 73: 5660-5661.

[9] Trischler FD, Hollander J. Thermally Stable Polyesters. J. Polym. Sci. A-1 1969; 7: 971-975.

[10] Tomita K. Studies on the formation of poly(ethylene terephthalate): 9. Thermal decomposition of ethylene dibenzoate as a model compound of poly(ethylene terephthalate). Polymer 18 (1977) 295-297.

[11] Hergenrother WL. Influence of copolymeric poly(diethylene glycol) terephthalate on the thermal stability of poly(ethylene terephthalate). J. Polym. Sci. Chem. Ed. 12 (1974)

875-883.

[12] Tomita K. Catalytic activity of metal compounds in the thermal decomposition of ethylene dibenzoate. Polymer 1977; 18: 1295.

[13] Tomita K. Studies on the formation of poly(ethylene terephthalate): 6. Catalytic activity of metal compounds in polycondensation of bis(2-hydroxyethyl) terephthalate. Polymer 1976; 17: 221-224.

[14] Zimmerman H, Kim NT. Investigations on Thermal and Hydrolytic Degradation of Poly(Ethylene Terephthalate). Polym. Eng. Sci. 1980; 20: 680-683.

[15] Zimmermann H, Lohmann P. Kinetik und Mechanismus der durch Metallderivate katalysierten thermischen Spaltung von Polyethyleneterephthalat. Acta Polymerica 1980; 31: 686-693.

[16] Pilati F, Manaresi P, Fortunato B, Munari A, Passalacqua V. Formation of poly(butylene terephthalate): Secondary reactions studied by model molecules. Polymer 1981; 22: 1566-1570.

[17] Passalacqua V, Pilati F, Zamboni V, Fortunato B, Manaresi P. Thermal degradation of poly(butylene terephthalate). Polymer 1976; 17: 1044-1048.

[18] Lum RM. Thermal Decomposition of Poly(butylene Terephthalate). J. Polym. Sci. Polym. Chem. Ed. 1979; 17: 203-213.

[19] Kelsey DR, Kiibler KS, Tutunjian PN. Thermal stability of poly(trimethylene terephthalate). Polymer 2005; 46: 8937-8946.

Chapter 5.

Catalytic Performance of Chelated Complex of Titanium

Chapter 5.
Catalytic Performance of
Chelated Complex of Titanium

5.1. Introduction

Among a large number of main group and transition metals that have been shown to have catalytic activity for the polycondensation of PET, [1-5] antimony trioxide is the most common polycondensation catalyst in commercial production. Although antimony has a good balance of catalytic activity, color and cost, more active catalyst is demanded to improve plant efficiencies. Furthermore, using antimony in the preparation of PET has come under increasing scrutiny in Europe and Asia. [1,6,7] This has led to PET manufacturers researching non-antimony catalyst (NAC). [1,6,7]

There are several scientific hurdles in research and development of NAC. First, the homogeneous catalysis where the catalyst substance remains in the polymer matrix has in general the drawback that the catalyst and all its side or conversion products will occur and alter in correlation to process conditions. More severe are chemical and technical circumstances of esterification and polycondensation where always side- and exchange products are generated. Another hurdle is that the new catalyst must be active comparable to antimony in melt phase and solid-state polycondensation as well.

The most promising candidate of NAC is a titanium complex. [1,6-8] Although titanium-based catalysts are very active relative to antimony, the first generation of titanium based catalysts, which were either alkoxides or simple chelates, were prone to hydrolysis to reduce activity and yielded polymers of poor color. Now several companies are developing titanium-based catalysts and have patented in this area. [7] These latest catalysts are designed to be stable and have been formulated to give a balance of good activity and good color, however, more efficient and better color

catalyst system is still demanded.

Despite the importance of catalysis to PET manufacture and a number of patents on this subject, the mechanism of catalysis in the polycondensation reaction is poorly understood; yet an increased understanding of how the metal center interacts with the polymerizing PET chain is important for facilitating further developments in catalyst design.

For the purpose of understanding the mechanism of PET catalysis clearly, we carried out a quantum chemical study on PET polycondensation reaction at B3LYP level of theory and found the coordination-activation mechanism (Scheme 5.1) is the most reasonable catalysis model for antimony, germanium and titanium complexes. [9] In this mechanism, carbonyl oxygen atom coordinates to the metal center, like the Lewis acid mechanism, and the carbonyl carbon atom have an attack by the alkoxy oxygen atom of one of the ligand oligomers (see Chapter 3 for detail).

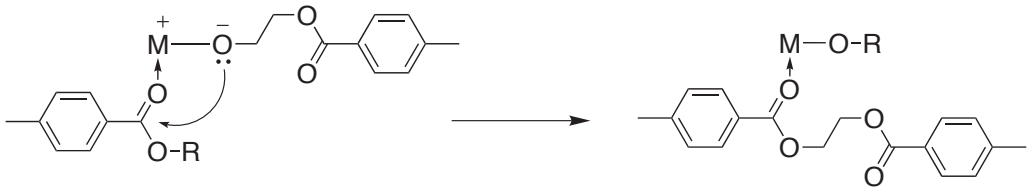

Scheme 5.1. Coordination-activation mechanism of polycondensation reaction.

Our next quantum chemical study is performed on thermal degradation reaction of polyesters. [10] It is generally known that thermal degradation of the PET chain accompanies the spinning, extrusion or molding process. To prevent degradation reaction is very important matter in PET industry because it may cause the reduction of molecular weight, also lead to the discoloration of PET resin. The published view for color formation in PET caused by thermal degradation is that PET undergoes a β scission reaction resulting in the formation of a vinyl ester end-group and a carbonyl end-group. [2,10-16] The reaction scheme of β elimination reaction at ester linkage is shown in Scheme 5.2.

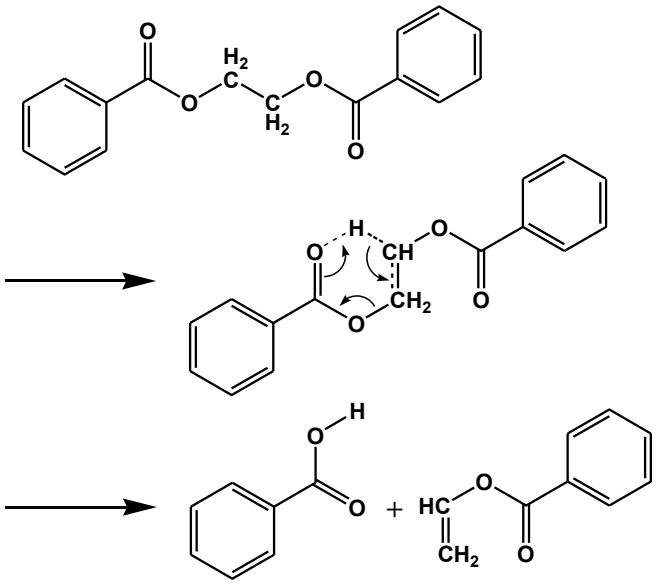

Scheme 5.2. β hydrogen elimination in PET thermal degradation reaction. [10]

It is known that catalyst has only a little effect on the rate of thermal degradation reaction of poly(butylene terephthalate) (PBT), in contrast to PET. [2] Recently, ^{1}H NMR study on thermal stability of poly(trimethylene terephthalate) (PPT) is carried out by Kelsey *et al*. [16] They indicated that neither titanium catalyst nor cobalt acetate, added as toner, affect on the kinetics of thermal degradation reaction of PPT. They considered the Lewis acid mechanism, in which a metal catalyst withdraws electron density from the carbonyl group and activate the carbon atom to nucleophilic attack (Scheme 5.3). Less catalytic effect for PBT and PPT is attributed to 'insulating' methylene groups in butylene or propylene glycol unit, which prevents electron delocalization between the metal coordinated carbonyl group and the reaction center, and avoid electron-withdrawing effect of the complexed metal catalysts. However, our DFT study described in Chapter 4 indicated that the Lewis acid mechanism could not describe high catalytic activity of titanium. [10]

In contrast to Lewis mechanism, we proposed new catalysis mechanism shown in Scheme 5.4. In this reaction model, β hydrogen is directly abstracted by the alkoxy ligand of catalyst. Our DFT calculation at B3LYP level showed that the activation energy for this mechanism is 7 kcal/mol lower than the Lewis acid mechanism (See Chapter 4 for detail).

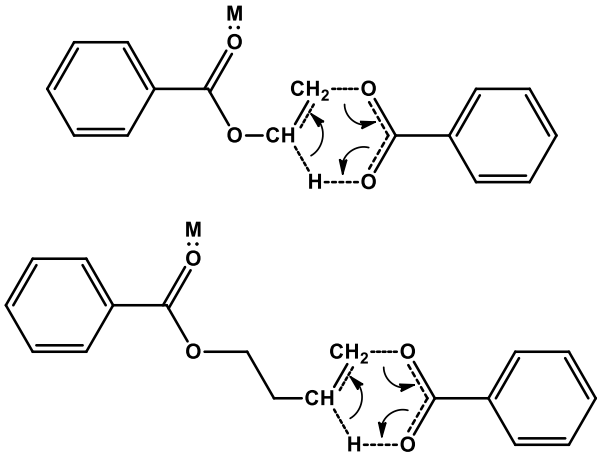

Scheme 5.3. Lewis acid mechanism of thermal degradation reaction.

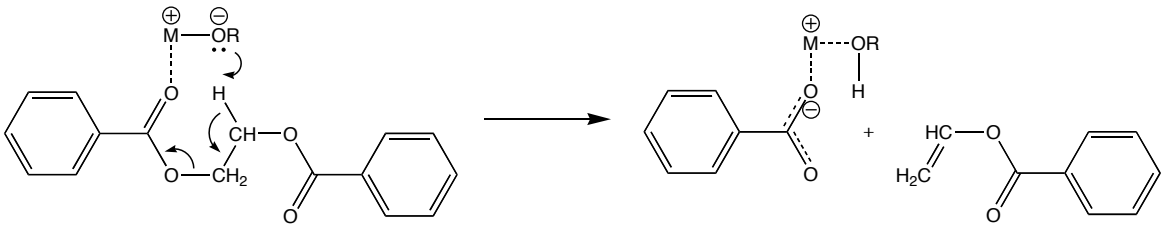

Scheme 5.4. Catalytic mechanism of PET thermal degradation reaction. [10]

As mentioned above, we clarified the catalysis mechanisms of polycondensation and thermal degradation reactions in previous studies. By using these knowledge, we performed B3LYP level of calculations on the electronic state, steric structure, polycondensation and thermal degradation catalytic activities of titanium(IV) model catalysts with multidentate ligands in this study. Regarding the activity of different chelated and non-chelated titanium catalysts, Ahmadnian *et al*. reported that the activity of chelated catalysts depend strongly on the structure of the ligand, whereas the nature of monodentate ligands has no strong effect on the catalytic activity in PET synthesis because of their poor thermal stability. [8] From the point of view of activity controllability and thermal stability of the catalyst complex, we focused on chelated titanium(IV) derivatives with bidentate ligands.

5.2. Model molecules and computational procedure

Model catalysts with bidentate ligands are shown in Scheme 5.5. The first category (No. 1 to 3) involves aromatic ligands and the second (No. 4 to 6) has aliphatic ligands, which have hydroxyl or carboxyl groups as coordination sites. In order to investigate how electron-withdrawing and -donating groups affect on catalytic activity, we prepared more 7 model catalysts illustrated in Scheme 5.6. The third category (No. 7 to 10) possesses electron-withdrawing fluorine atoms, whereas the fourth (No. 11 and 12) has electron-donating groups. To reduce computational cost, diethyl terephthalate (DET) and ethylene dibenzoate (EDB) were employed as PET model molecules for polycondensation and thermal degradation reactions, respectively.

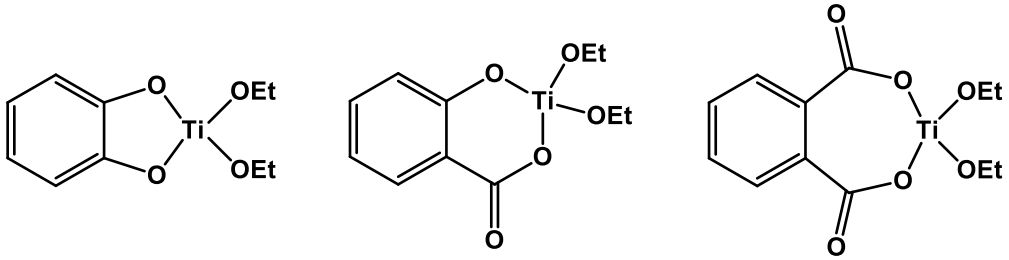

Scheme 5.5. Ti model catalysts with bidentate ligands.

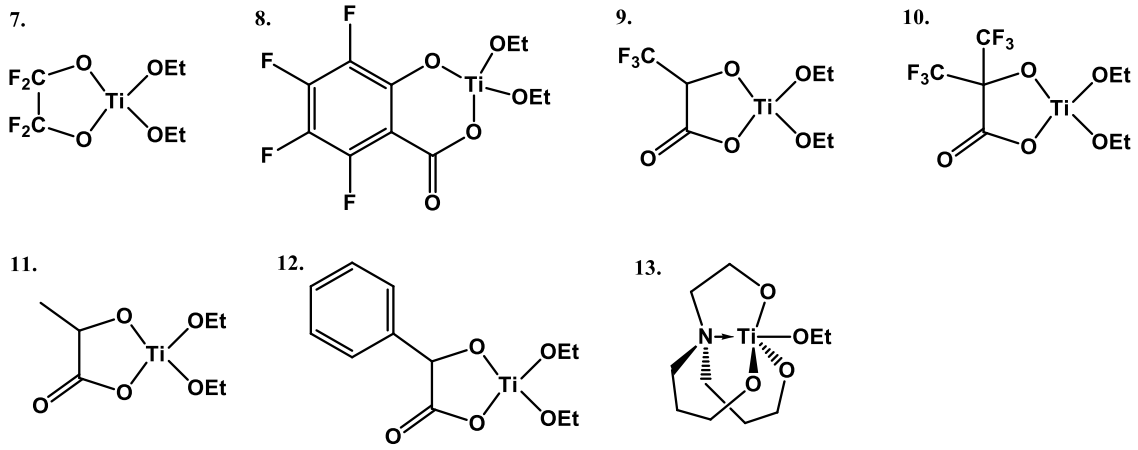

Scheme 5.6. Ti model catalysts with electron-withdrawing and -donating groups.

All geometry optimization, harmonic vibrational frequency, and intrinsic reaction coordinates analysis were performed with same level of theory as Chapter 3 and 4. Since our previous work on polycondensation [9] and thermal degradation [10] reactions revealed that solvent effect correction by using polarizable continuum model was negligible, all of the geometry optimizations and electronic structure analysis were carried out in gas phase. In addition to reaction analysis, we performed UV/vis spectra calculations on model catalysts by using time-dependent DFT (TDDFT) method [17-19] for the purpose of investigating coloration of the complex itself.

5.3. Results and discussion

5.3.1. The molecular structures and electronic states of model catalysts

Optimized structures for titanium(IV) model catalysts illustrated in Scheme 5.5 and 5.6 are shown in Figure 5.1 and 5.2 respectively. Figure 5.2 also contains the optimized structure of $Ti(OEt)_4$ as a comparison non-chelated complex. Except for triethanolamine (No. 13), coordination structures around titanium(IV) ions are all 4-coordinated tetrahedral structures. On the other hand, No. 13 is a 5-coordinate complex, in which the nitrogen atom is considered to be coordinated to the titanium(IV) ion since the distance between nitrogen and titanium is 2.4Å.

In order to investigate the electronic structures of model catalysts, we estimated 4 parameters listed below. Results are given in Table 5.1.

1) q(Ti) Mulliken charges of titanium(IV) ion.
2) q(O) Mulliken charges of the O atoms of ethoxy ligands (averaged if multiple ethoxy ligands are coordinated.)
3) q(OEt) Summed up Mulliken charges of the atoms involved in the ethoxy ligands (averaged if multiple ethoxy ligands are coordinated.).
4) LUMO The orbital energies of the lowest unoccupied Kohn-Sham orbitals.

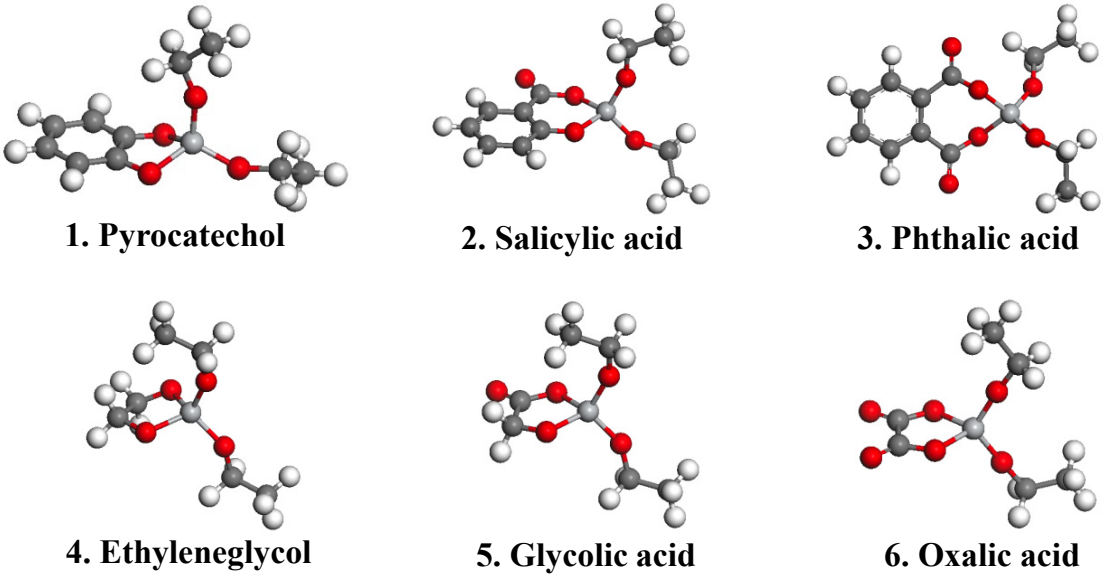

Figure 5.1. Optimized structures for Ti model catalysts with bidentate ligands.

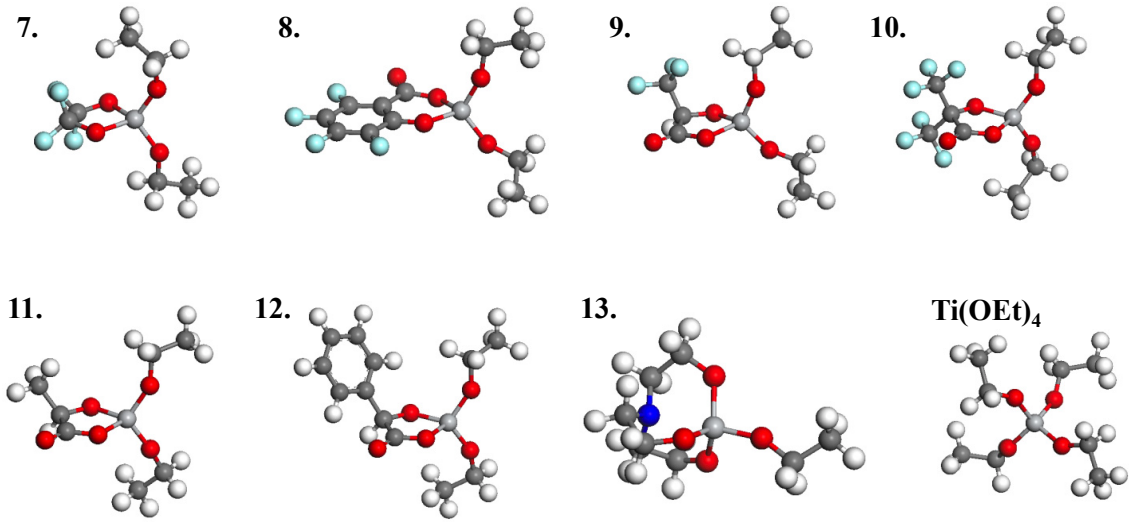

Figure 5.2. Optimized structure for Ti model catalysts with electron-withdrawing and -donating groups.

Table 5.1. Electronic structure parameters of model catalysts.

Model No.	q(Ti)	q(O)	q(OEt)	LUMO / eV
1	1.353	–0.626	–0.287	–1.94
2	1.385	–0.624	–0.280	–2.13
3	1.363	–0.616	–0.257	–2.19
4	1.364	–0.640	–0.322	–1.84
5	1.381	–0.631	–0.291	–2.41
6	1.395	–0.620	–0.258	–2.87
7	1.388	–0.620	–0.259	–2.96
8	1.397	–0.620	–0.266	–2.51
9	1.374	–0.623	–0.272	–2.64
10	1.379	–0.622	–0.265	–3.00
11	1.369	–0.633	–0.295	–2.32
12	1.378	–0.631	–0.289	–2.44
13	1.392	–0.643	–0.333	–0.85
14($Ti(OEt)_4$)	1.289	–0.626	–0.322	–0.89

To analyze correlation between these parameters, we employed principal component analysis (PCA) by using the R statistical package. [20] PCA is a mathematical procedure that uses an orthogonal transformation to convert a set of observations of possibly correlated variables into a set of values of linearly uncorrelated variables called principal components. This transformation is defined in such a way that the first principal component has the largest possible variance (that is, accounts for as much of the variability in the data as possible), and each succeeding component in turn has the highest variance possible under the constraint that it be orthogonal to the preceding components. PCA results for electronic structure parameters of model catalysts are summarized in Table 5.2. The principal component scores of model catalysts are shown in Figure 5.3, in which principal component (PC) 1 is plotted on x-axis and PC2 is plotted on y-axis. Figure 5.3 also gives PC loadings for PC1 and PC2 as arrows from the origin. These arrows indicate the relation between PC1, PC2 and each electronic structure parameters.

Table 5.2. PCA results for electronic structure parameters of model catalysts.

	q(Ti)	q(O)	q(OEt)	LUMO / eV
Average	1.3720	–0.6268	–0.2854	–2.2127
Standard deviation	0.0272	0.0078	0.0253	0.6695

Principal component loading

	1st component	2nd component	3rd component	4th component
q(Ti)	0.3333	–0.8033	0.4542	0.1933
q(O)	0.4856	0.5549	0.3903	0.5513
q(OEt)	0.5893	0.1466	0.1581	–0.7786
LUMO	–0.5529	0.1594	0.7851	–0.2291
Eigenvalue	1.6691	1.0031	0.4452	0.0985
Contribution	0.6965	0.2516	0.0496	0.0024
Cumulative contribution	0.6965	0.9480	0.9976	1.0000

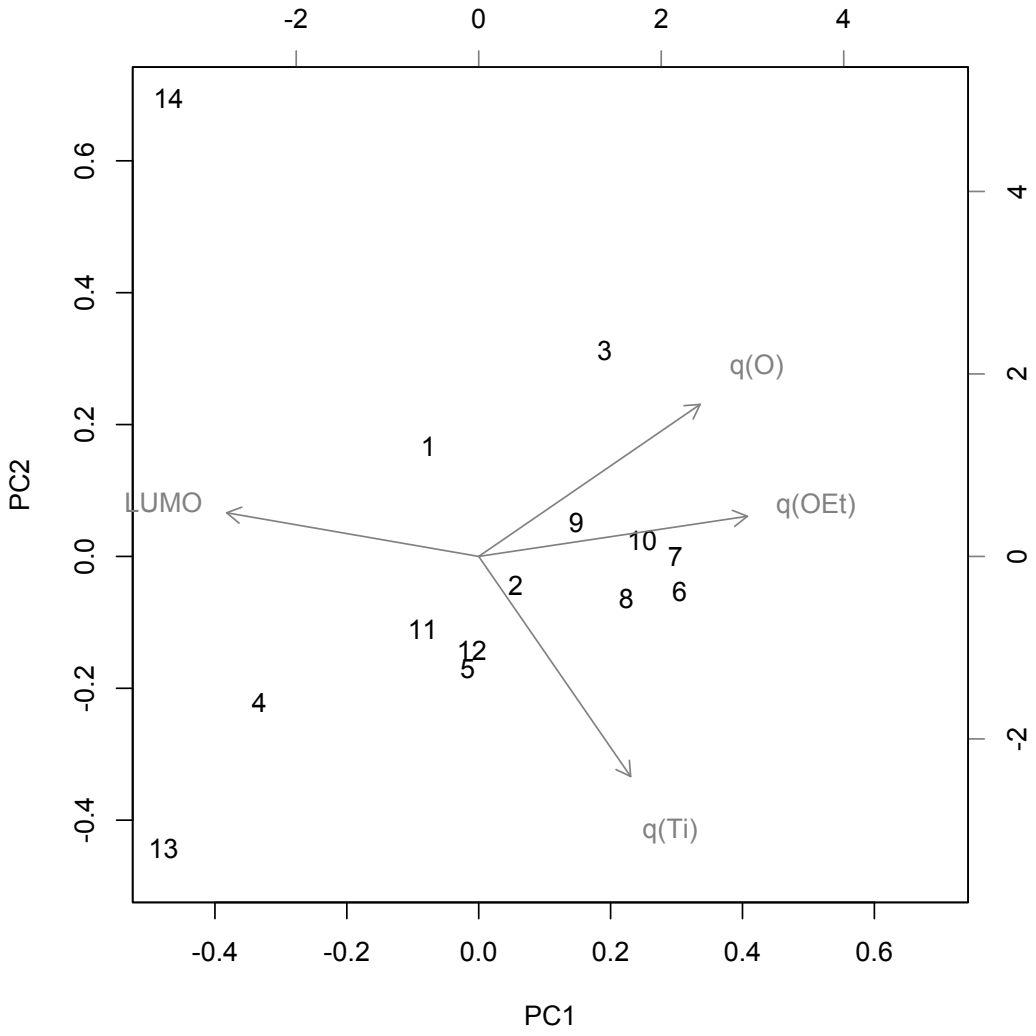

Figure 5.3. Principal component scores are plotted in PC1 (x-axis) - PC2 (y-axis) plane. PC loadings for PC1 and PC2 are also displayed as arrows from the origin.

From the point of view of PC loading shown in Table 5.2 and Figure 5.3, PC1 is in strongly positive correlation with q(OEt) and negative correlation with LUMO. In other words, q(OEt) is in opposite correlation with LUMO. On the other hand, q(O) has weaker correlation with PC1 than q(OEt), and correlation with q(Ti) is even weaker. In contrast, PC2 has strong negative correlation with q(Ti), weak correlation with q(O). LUMO and q(OEt) have are in very little correlation with PC2.

Figure 5.3 shows that model catalysts (No. 1 to 13) is distributed upward to the right

in PC1-PC2 plane, whereas $Ti(OEt)_4$ (No. 14) is distant from other data. Regarding the effect of substituted groups, comparison of No. 4 and 7, No. 2 and 8, No. 5 and 9 or 10 (in each case, the latter corresponds to F or CF_3 substituted model of the former) indicate that electron-withdrawing groups make positive shift in PC1. It can be seen that since F atom or CF_3 group withdraw electron density from the titanium(IV) center, LUMO levels fall and electron densities of OEt groups are positively shifted. In contrast, comparing No. 5 and 11, 12, substitutions with electron-donating groups make imperceptible change in PC scores.

5.3.2. UV/vis spectra of model catalysts

We applied TDDFT (B3LYP, 6-31G** for C, N, O, H, LanL2DZ for Ti, Nstates=20) method for UV/vis spectra calculations in order to evaluate the possibility that the model catalyst itself causes coloration of the polymer. Figure 5.4 and 5.5 show evaluated UV/vis spectra of model catalyst No. 1 to 6 (Figure 5.1) and 7 to 14 (Figure 5.2), respectively. These results indicate that titanium(IV) complexes with aromatic (No. 1, 2, 3 and 8) or highly planar (No. 6) ligands have absorbance in the visible region. Analysis of excited states indicates that low-energy (long wavelength) absorption bands correspond to the excitation from the occupied orbital of the ligands to the unoccupied orbital of titanium for every model catalyst. It is thought that since p-conjugation in aromatic or planar ligands raise the HOMO energy level and narrow the HOMO-LUMO gap, excitation energies are reduced, i.e., absorption wave length become longer. From the point of view of prevention of coloration of the polymer, these ligands are undesirable for PET polymerization catalyst.

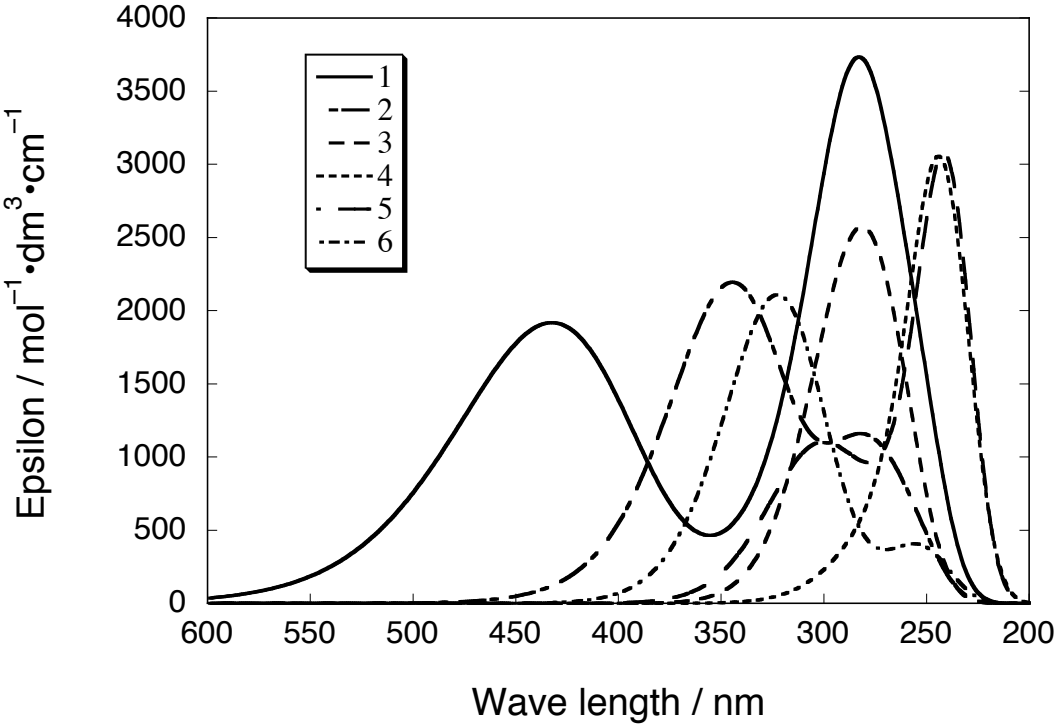

Figure 5.4. UV/vis spectra for Ti model catalysts with bidentate ligands calculated by TDDFT (B3LYP, 6-31G** for C, N, O, H, LanL2DZ for Ti, Nstates=20).

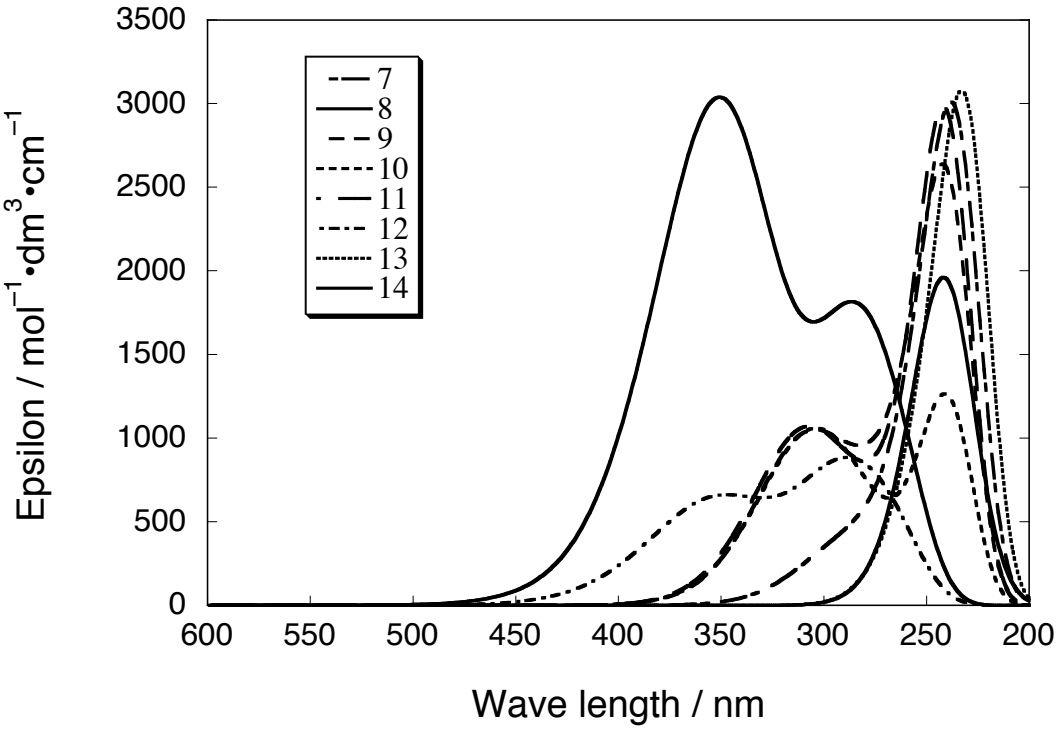

Figure 5.5. UV/vis spectra for Ti model catalysts with electron-withdrawing and -donating groups calculated by TDDFT (B3LYP, 6-31G** for C, N, O, H, LanL2DZ for Ti, Nstates=20).

5.3.3. Activation energies of polycondensation and thermal degradation reactions

Table 5.3 shows the activation energies (Ea's) for polymerization and thermal degradation reactions catalyzed by the model catalysts. PC scores of electronic structure parameters of the model catalysts are also summarized in the table. In addition, the correlation between Ea's for polycondensation and thermal degradation is given in Figure 5.6, in which Ea for polycondensation is plotted on x-axis while Ea for thermal degradation is plotted on y-axis.

Table 5.3. Activation energies (Ea's) for polymerization, thermal degradation reactions and PC scores.

Model No.	Ea(polymerization) /(kcal/mol)	Ea(thermal degradaition) /(kcal/mol)	PC1	PC2
1	19.2	42.9	–0.4787	0.6261
2	18.5	45.7	0.3490	–0.1636
3	19.8	46.8	1.1934	1.1742
4	18.0	43.4	–2.0784	–0.8315
5	18.2	43.6	–0.1056	–0.6404
6	21.0	46.8	1.9032	–0.2005
7	20.3	44.7	1.8617	0.0008
8	21.3	45.2	1.3992	–0.2418
9	19.7	43.9	0.9249	0.1920
10	20.6	46.5	1.5477	0.0901
11	18.0	43.7	–0.5307	–0.4159
12	16.4	44.3	–0.0653	–0.5344
13	23.9	55.6	–2.9843	–1.6646
$Ti(OEt)_4$	15.5	43.8	–2.9361	2.6095

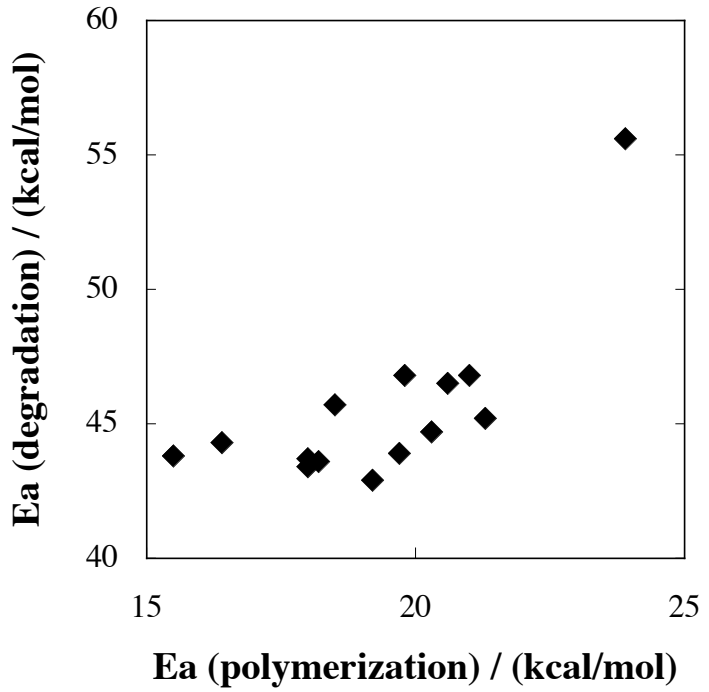

Figure 5.6. Correlation between activation energies (Ea's) for polycondensation and thermal degradation.

Although an ideal polycondensation catalyst should exhibit both small Ea for polycondensation and large Ea for thermal degradation, a positive correlation exists between polycondensation and degradation about model catalysts in this study, i.e., high polymerization activity and low degradation activity are incompatible. On the other hand, No. 13 (TEA) ligand gave a very low-polymerization/low-degradation catalyst. To consider the reason of low catalytic activity of the TEA ligand, we picked up high-activity mandelic acid (No. 12) and $Ti(OEt)_4$ (No. 14), whose PC1 is almost same as TEA but much more active, and compared O-Ti-O angles of these models. The results are displayed in Figure 5.7.

In the mandelic acid complex, the ligand and titanium atom forms 5-membered ring whose O-Ti-O angle is narrow as 83.8 degrees. In contrast, the remaining O-Ti-O angles such as EtO-Ti-OEt are wide as 112 to 116 degrees, which are wider than the tetrahedral bonding angle of 109 degrees. Since this spacial configuration makes the steric hindrance around the central titanium small, the carbonyl oxygen atom of PET is considered to easily coordinate to the titanium ion. In $Ti(OEt)_4$, although the titanium

center and the coordinated oxygen atoms compose almost tetrahedral structure and O-Ti-O angles are about 110 degrees, ethoxy ligands can flexibly bend to let titanium easily coordinated by PET because $Ti(OEt)_4$ does not contain any rigid ring structure.

In contrast to above two models, the TEA complex consists 5-coordinated structure in which three 5-membered rings are composed by Ti-O-C-C-N. Since O-C-O angles involved in the three rings are wide as 113 to 115 degrees, the space around the titanium center is limited and the steric hindrance for PET coordination becomes greater than other two models. Moreover, TEA ligand cannot bend flexibly to promote the coordination of PET because its ring structure. These structural characteristics of the TEA complex make Ea's for polycondensation and thermal degradation higher than other model catalysts.

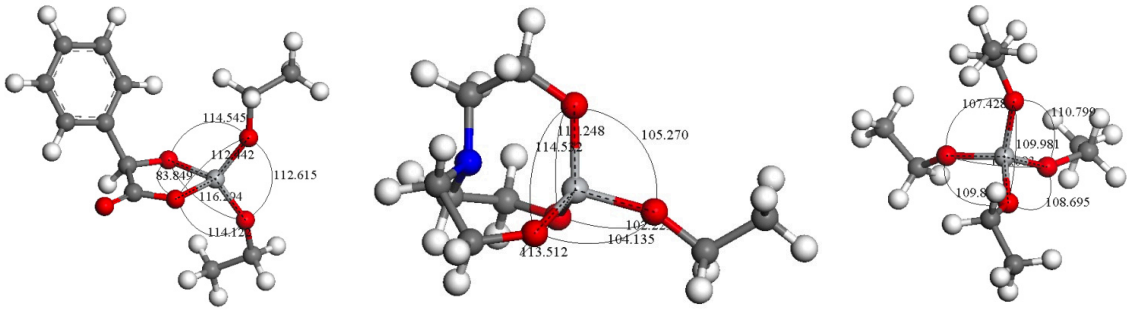

12. Mandelic acid **13. Triethanol amine** **14. $Ti(OEt)_4$**

Figure 5.7. Spacial configurations of mandelic acid, TEA and ethoxy complexes.

In order to analyze the relationship between the electronic structure and the catalytic activity of the model catalysts, correlation between PC1 and Ea's of reaction are plotted in Figure 5.8. In this figure, PC1 evaluated in Section 5.3.1 is plotted on x-axis, while Ea for polycondensation (left) and thermal degradation (right) are plotted on y-axis.

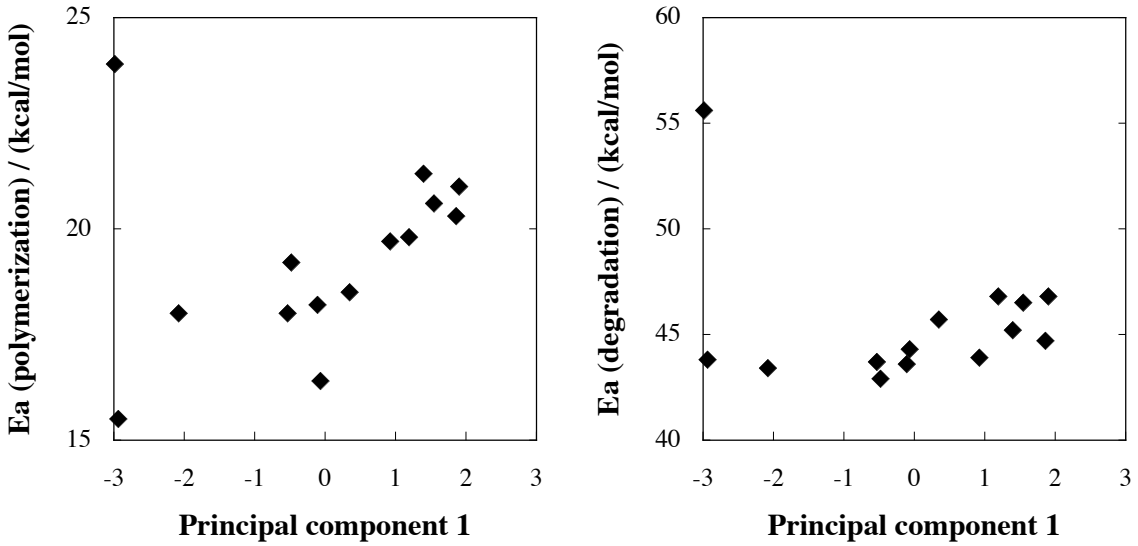

Figure 5.8. (Left) Correlation between PC1 and Ea of polycondensation reaction. (Right) Correlation between PC1 and Ea of thermal degradation.

Figure 5.8 indicates that there is a positive correlation between PC1 and Ea for polycondensation reaction, whereas the correlation between PC1 and Ea for degradation is weaker than that for polycondensation. Accordingly, a titanium(IV) complex with negative PC1 value is expected to strongly activate polycondensation and weakly catalyze degradation, i.e., to achieve an ideal NAC which gives a good balance of high polymerization and low degradation activities. In addition, the data points isolated in upper left are both TEA complex. The TEA ligand is thought to prevent PET from coordinating to titanium because of its steric hindrance, as discussed above. Poor catalytic activity of the TEA complex indicates that we need to consider not only the electronic state but also the steric structure of the candidate complex in order to design an effective catalyst.

5.4. Concluding remarks

In this study, we performed quantum chemical calculations on the electronic state, steric structure, polycondensation and thermal degradation catalytic activities of titanium(IV) model catalysts with multidentate ligands. First of all, principal component analysis on electronic structure parameters of model catalysts showed that the 1st principal component (PC1) had 70% of contribution, so that the description of electronic structure of model catalysts was successfully reduced to single parameter. We then performed TDDFT calculations on the model complexes. Ligands with aromatic rings might cause visible light absorbance and coloration of the complex itself because of the electron excitation from occupied orbitals of the ligand to unoccupied orbitals of titanium center. Estimation of the activation energies (Ea's) for polycondensation and thermal degradation reactions indicated that no model catalyst showed significant balance of polycondensation and degradation activities, since Ea's for both reactions were in positive correlation. Nevertheless, a titanium(IV) complex with negative PC1 should be a good-balanced catalyst, because the positive correlation between PC1 and Ea for polycondensation is stronger than that between PC1 and Ea for degradation.

5.5. References

[1] MacDonald WA. New advances in poly(ethylene terephthalate) polymerization and degradation. Polym. Int. 2002; 51(10): 923-930.

[2] Pilati F. In: Allen G, Bevington JC, Eastmond GC, Ledwith A, Russo S, Sigwalt P, editors. Comprehensive Polymer Science, vol. 5. Oxford: Pergamon Press, 1989. Chapter 17.

[3] Ravindranath K, Mashelkar RA. In: Whelan A, Craft JL, editors. Developments in Plastic Technology, vol. 2. London: Elsevier Applied Science Publishers, 1985. Chapter 1.

[4] Tomita K. Polymer 1976; 17(3): 221-224.

[5] Parshall GW, Ittel S. Homogeneous Catalysis, 2nd ed. New York: Wiley-Interscience, 1992. Chapter 11.

[6] Thiele UK. Inter. J. Polym. Mater. 2001; 50(3-4): 387-394.

[7] Thiele UK. Chem. Fiber. Inter. 2004; 54: 162-163.

[8] Ahmadnian F, Velasquez F, Reichert KH. Macromol. React. Eng. 2008; 2(6): 513-521.

[9] Shigemoto I, Kawakami T, Taiko H, Okumura M. A quantum chemical study on the polycondensation reaction of polyesters: The mechanism of catalysis in the polycondensation reaction. Polymer 2011; 52: 3443-3450.

[10] Shigemoto I, Kawakami T, Taiko H, Okumura M. A quantum chemical study on the thermal degradation reaction of polyesters. Polymer Degradation and Stability 2012; 97: 941-947.

[11] Jabarin SA. In: Salamone JC, editor-in-chief. Polymeric Materials Encyclopedia vol. 8. POLY(ETHYLENE TEREPHTHALATE) DEGRADATION (CHEMISTRY AND KINETICS). Boca Raton: CRC Press, 1996. p. 6114.

[12] Grassie N. Chemistry of High Polymer Degradation Processes. London: Butterworths, 1956. p.285-294.

[13] Buxbaum LH. The Degradation of Poly(ethylene terephthalate). Angew. Chem. Int. Ed. 1968; 7: 182-190.

[14] Tomita K. Studies on the formation of poly(ethylene terephthalate): 9. Thermal decomposition of ethylene dibenzoate as a model compound of poly(ethylene

terephthalate). Polymer 1977; 18: 295-297.

[15] Hergenrother WL. Influence of copolymeric poly(diethylene glycol) terephthalate on the thermal stability of poly(ethylene terephthalate). J. Polym. Sci. Chem. Ed. 1974; 12: 875-883.

[16] Kelsey DR, Kiibler KS, Tutunjian PN. Thermal stability of poly(trimethylene terephthalate). Polymer 2005; 46: 8937-8946.

[17] Runge E, Gross EKU. Density-Functional Theory for Time-Dependent Systems. Phys. Rev. Lett. 1984; 52: 997-1000.

[18] Bauernschmitt R, Ahlrichs R. Treatment of electronic excitations within the adiabatic approximation of time dependent density functional theory. Chem. Phys. Lett. 1996; 256: 454-464.

[19] Stratmann RE, Scuseria GE, Frisch MJ. An efficient implementation of time-dependent density-functional theory for the calculation of excitation energies of large molecules. J. Chem. Phys. 1998; 109: 8218-8224.

[20] R Development Core Team (2005). R: A language and environment for statistical computing. R Foundation for Statistical Computing, Vienna, Austria. ISBN 3-900051 -07-0, URL http://www.R-project.org.

Chapter 6.

Candidate of Non-Antimony Catalyst: Sugar-Alcohol Complex of Titanium

Chapter 6.

Candidate of Non-Antimony Catalyst: Sugar-Alcohol Complex of Titanium

6.1. Introduction

Based on the previous study described in Chapter 5, let us enumerate the conditions for our new non-antimony catalyst (NAC) as listed below:

a. Having multidentate ligands for thermal stability of the complex.
b. No aromatic rings coordinating to the titanium center to prevent the complex from being the cause of discoloration.
c. Principal component 1 defined in Section 5.3.1 is negative.

Sugar alcohols such as sorbitol or mannitol meet the conditions a and b. In addition, because these compounds are used as food additives or medicines, there is no concern about environmental regulation or toxicity problem. Chemical structures of D-sorbitol and D-mannitol are depicted in Scheme 6.1.

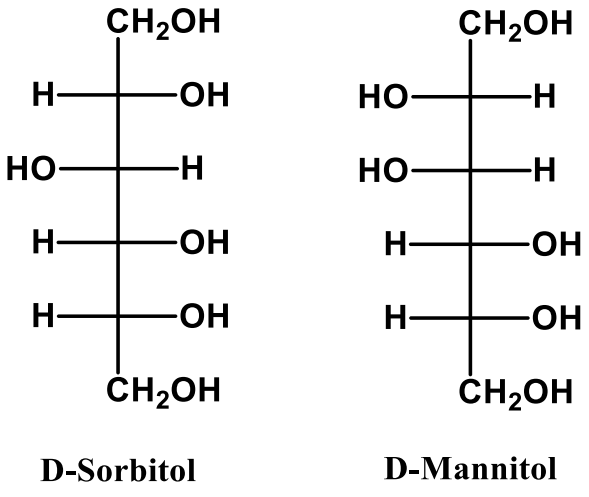

Scheme 6.1. Chemical structures of D-sorbitol (left) and D-mannitol (right).

6.2. Model molecules

Titanium(IV) complex of sugar alcohols are thought to have several variations in steric structures since these ligands have 6 hydroxyl groups and soft backbones. In this study, we made 3 model complexes for sorbitol, and 2 models for mannitol. Figure 6.1 shows B3LYP optimized structures of these complexes. Computational procedure is same as described in Section 5.2.

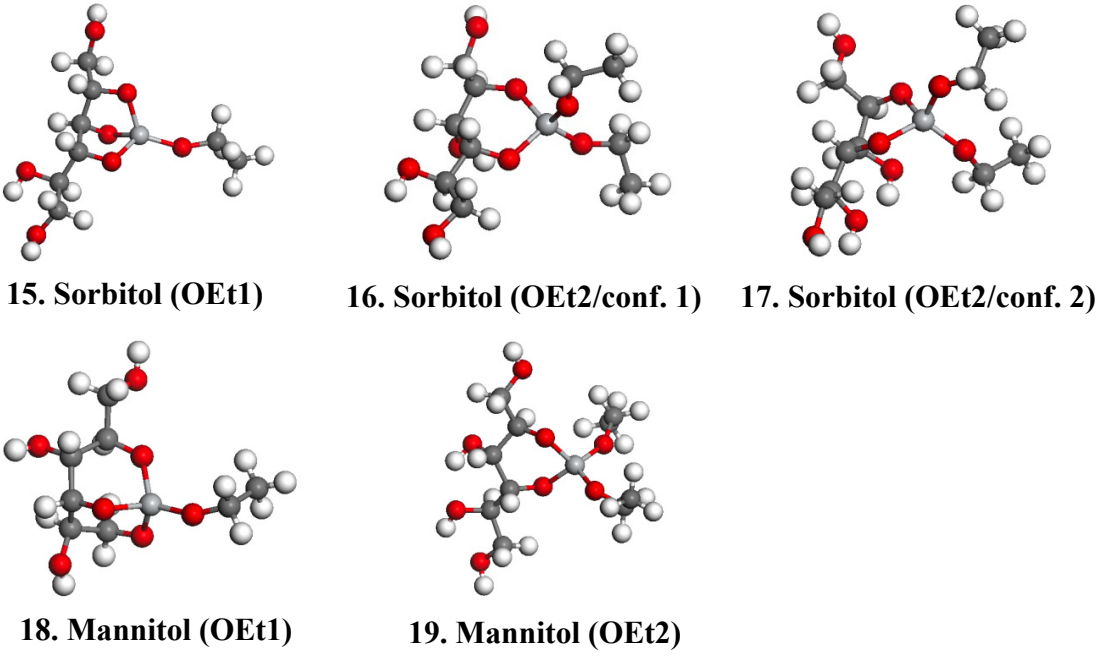

Figure 6.1. Optimized structures for Ti model catalysts with sorbitol and mannitol ligands. No. 15: 3 hydroxyl groups of sorbitol and 1 ethoxy group are coordinated to Ti. No. 16 and 17: 2 hydroxyl groups of sorbitol and 2 ethoxy groups are coordinated to Ti. No. 18: 3 hydroxyl groups of mannitol and 1 ethoxy group are coordinated to Ti. No. 19: 2 hydroxyl groups of mannitol and 2 ethoxy groups are coordinated to Ti.

6.3. Computational Results and discussion

To analyze the electronic structure of the model catalysts, we estimated 4 parameters defined in Section 5.4.1 and executed PCA together with the data summarized in Table 5.1. The results are given in Table 6.1. Comparing Table 5.2 and 6.1, no significant difference is found except for a little increment of the contribution of PC1. Figure 6.2 shows the distribution of PC scores, and we can confirm that all of the PC1's of our new model catalysts (No. 15 to 19) are negative as we expected.

We then calculated the UV/vis spectra of these model catalysts by using TDDFT. The evaluated spectra depicted in Figure 6.3 shows no sugar-alcohol complex has significant absorbance in visible region.

Table 6.1. PCA results for electronic structure parameters of Ti-sugar alcohol complexes.

	q(Ti)	q(O)	q(OEt)	LUMO / eV
Average	1.3650	–0.6312	–0.2951	–1.9730
Standard deviation	0.0304	0.0109	0.0275	0.7081

Principal component loading

	1st component	2nd component	3rd component	4th component
q(Ti)	0.3444	–0.8222	–0.4387	–0.1133
q(O)	0.4872	0.5381	–0.5056	–0.4664
q(OEt)	0.5762	0.1466	–0.0299	0.8035
LUMO	–0.5585	0.1136	–0.7423	0.3523
Eigenvalue	1.6987	0.9638	0.3896	0.1835
Contribution	0.7214	0.2322	0.0380	0.0084
Cumulative contribution	0.7214	0.9536	0.9916	1.0000

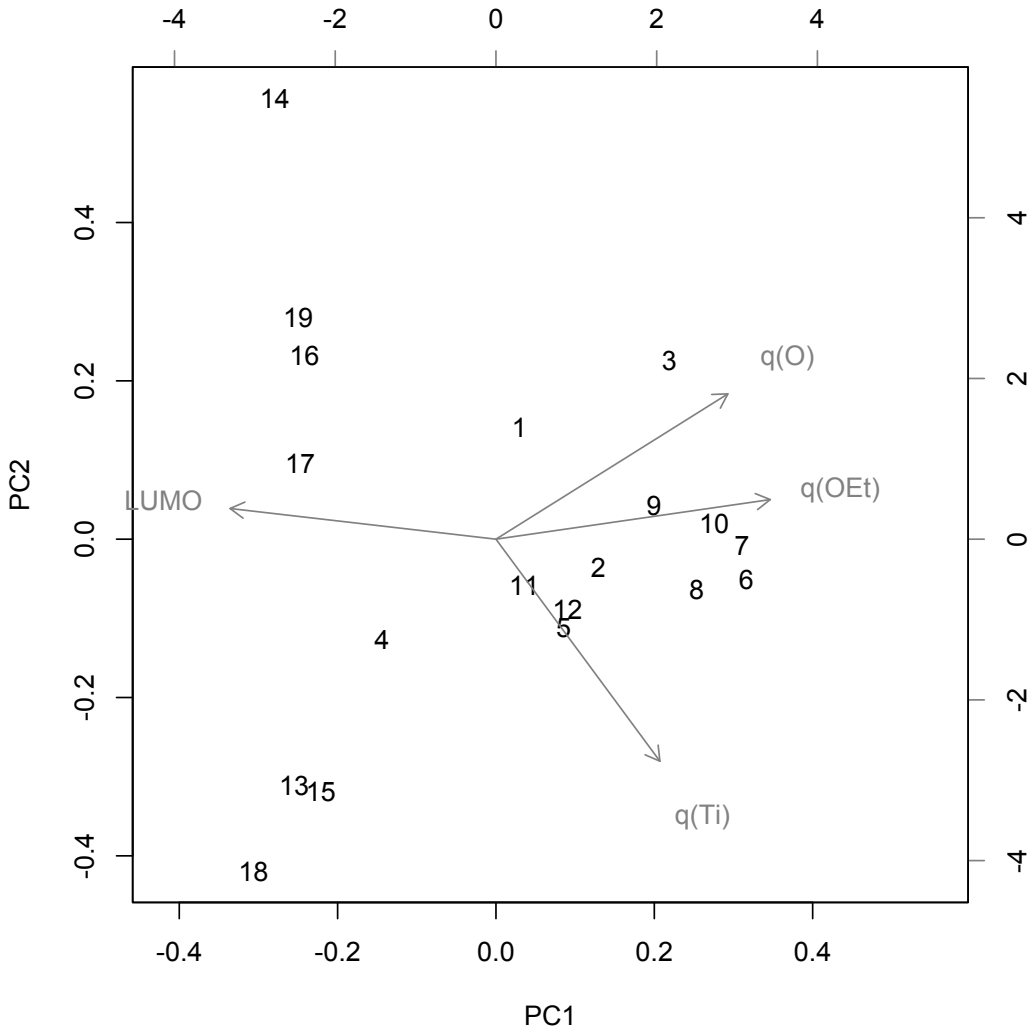

Figure 6.2. Principal component scores including Ti-sugar alcohol complexes are plotted in PC1 (x-axis) - PC2 (y-axis) plane. PC loadings for PC1 and PC2 are also displayed as arrows from the origin.

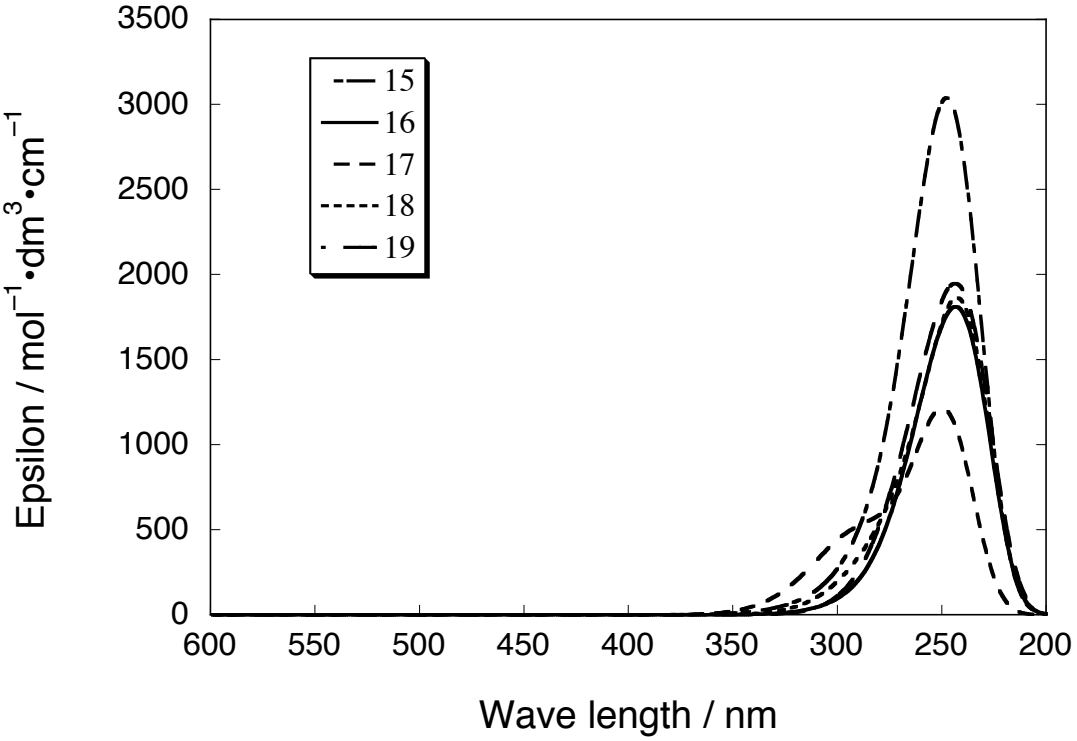

Figure 6.3. UV/vis spectra for Ti-sugar alcohol complexes calculated by TDDFT (B3LYP, 6-31G** for C, N, O, H, LanL2DZ for Ti, Nstates=20).

Finally, we calculated the activation energies for polycondensation and thermal degradation reactions catalyzed by the titanium(IV)-sugar alcohol catalysts. Ea's and PC1, PC2 are summarized in Table 6.2. Correlation between PC1 and Ea's of reaction including sugar-alcohol catalysts are shown in Figure 6.4, in which PC1 is plotted on x-axis and Ea for polycondensation (left) and thermal degradation (right) are plotted on y-axis.

The left graph in Figure 6.4 exhibits that sugar-alcohol model catalysts give relatively good polycondensation activity, especially No. 17 of and 18 show high activity comparable to $Ti(OEt)_4$. In addition, thermal degradation activities of sugar-alcohol catalysts are not worse than others. These results indicate that the titanium(IV)-sugar alcohol catalysts, in toto, present moderate polycondensation and thermal degradation activities, while few steric structures of them exhibit high polycondensation catalytic activity. Accordingly, titanium(IV)-sugar alcohol catalysts are thought to be potential candidate for NAC with a good balance of catalytic activity and polymer color.

Table 6.2. Activation energies (Ea's) for polymerization, thermal degradation reactions and PC scores for sugar-alcohol model catalyts.

Model No.	Ea(polymerization) /(kcal/mol)	Ea(thermal degradation) /(kcal/mol)	PC1	PC2
15	20.4	44.2	–1.6382	–1.3409
16	19.0	47.6	–1.7904	0.9727
17	15.9	45.9	–1.8306	0.4005
18	15.8	43.9	–2.2673	–1.7635
19	18.2	47.2	–1.8507	1.1776

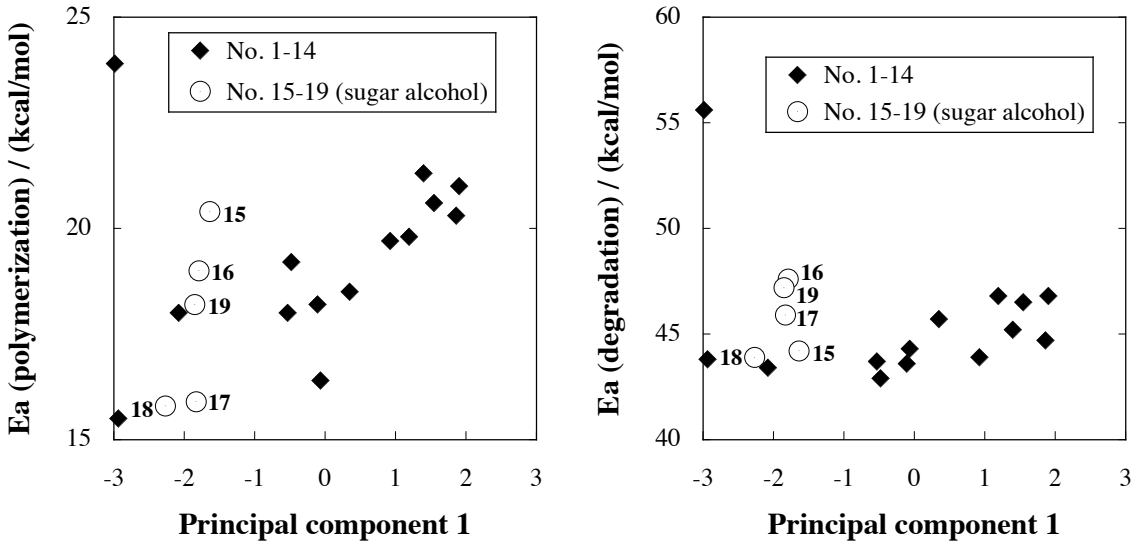

Figure 6.4. (Left) Correlation between PC1 and Ea of polycondensation reaction. (Right) Correlation between PC1 and Ea of thermal degradation. In both graphs, sugar-alcohol model catalysts are designated with open circles and figures indicate model number.

6.4. Experimental results and discussion

In order to assess the catalytic performance of sugar-alcohol complex of titanium, polymerization experiments and measurement of physical properties of the obtained polyesters were carried out. [2]

6.4.1. Preparation of catalysts

TM-1 To a 3-L, three-necked flask, which had been filled with nitrogen, were added 1000 mL of dehydrated ethylene glycol as a reaction solvent and 5.7 g (31.3 mmol) of mannitol, which were then stirred while being heated on an oil bath so that the internal temperature would become 80°C. Since the mannitol dissolved in about one hour, the oil bath was removed and cooling was conducted until the internal temperature became 40°C, which was a reaction temperature. When the internal temperature reached 40°C, 2.69 g (15.7 mmol) of titanium tetramethoxide ($Ti(OMe)_4$) was added as a titanium compound, followed by stirring at a reaction temperature of 40°C over a reaction time of 24 hours. In this way, a colorless, transparent catalyst solution TM-1 (titanium content: 0.75 g/L) was obtained.

TM-2 A colorless, transparent catalyst solution TM-2 (titanium content: 0.75 g/L) was obtained in the same manner as in TM-1 except for changing the titanium compound into titanium tetraethoxide ($Ti(OEt)_4$), the reaction temperature into 0°C, and the reaction time into 0.1 hour.

TM-3 A colorless, transparent catalyst solution TM-3 (titanium content: 0.75 g/L) was obtained in the same manner as in TM-1 except for changing the titanium compound into titanium tetraisopropoxide ($Ti(OiPr)_4$), the molar ratio mannitol/Ti into 1/1, the reaction temperature into 40°C, and the reaction time into 0.5 hour.

6.4.2. Polymerization of PET

TM-1 To an esterification reaction vessel in which about 100 kg of bis(hydroxyethyl) terephthalate (BHET) had been charged and which had been held at a temperature of 250°C and a pressure of 1.2×10^5 Pa was feed a slurry of 82.5 kg of high purity terephthalic acid and 35.4 kg of EG slowly over 4 hours, and an esterification reaction was performed over an additional one hour also after the completion of the feeding, and

then 101.5 kg of the resulting esterification reaction product was transferred to a polycondensation vessel.

An ethylene glycol solution of magnesium acetate in an amount corresponding to 5 ppm in terms of magnesium atom relative to the polymer to be obtained, an ethylene glycol solution of cobalt acetate in an amount corresponding to 30 ppm in terms of cobalt atom relative to the polymer to be obtained, and tetrakis(2,4-di-tert-butyl-5-methylphenyl)[1,1-biphenyl]-4,4'-diylbisphosphonite in an amount corresponding to 10 ppm in terms of phosphorus atom relative to the polymer to be obtained were mixed in advance in another mixing vessel 30 minutes before being added to the esterification reaction product and were stirred at normal temperature for 30 minutes, and the resulting mixture was added to the esterification reaction product. Five minutes thereafter, catalyst TM-1 in an amount corresponding to 5 ppm in terms of titanium atom relative to the polymer to be obtained was added and further 5 minutes later, an ethylene glycol slurry of titanium oxide particles in an amount of 0.3% by weight in terms of titanium oxide particles relative to the polymer to be obtained was added. And further 5 minutes later, the pressure of the reaction system was reduced, so that the reaction was started. The temperature in the reactor was increased from 250°C to 290°C slowly and the pressure was reduced to 40 Pa. Both a time to be required for reaching the final temperature and that to be required for reaching the final pressure were adjusted to 60 minutes. When a prescribed stirring torque was achieved, the reaction system was returned to normal pressure by nitrogen purge, so that the polycondensation reaction was stopped. Then, the product was discharged into a strand form and cut immediately, affording pellets of a polymer. The time taken from the start of the pressure reduction to the arrival at the prescribed stirring torque was 2 hours and 18 minutes.

TM-2 Polyesters were polymerized in the same manner as in TM-1 except for changing the catalyst as TM-2. The polymerization time was 2 hours and 21 minutes.

TM-3 Polyesters were polymerized in the same manner as in TM-1 except for changing the catalyst as TM-3 and the added amount of the catalyst as shown in Table 6.3. The polymerization time was 2 hours and 16 minutes.

TPT Polyesters were polymerized in the same manner as in TM-1 except for changing the catalyst as EG solution of $Ti(OiPr)_4$ without mannitol. The polymerization time was 2 hours and 15 minutes. In contrast to the polymers obtained by using TM-1, the polymer was rich yellow in color tone.

TM-4 Polyesters were polymerized in the same manner as in TM-1 except for changing the catalyst as EG solution of $Ti(OiPr)_4$ and adding mannitol aside from the catalyst to the polymerization system so that the molar ratio mannitol/Ti would become 2. The polymerization time was 2 hours and 19 minutes. Similarly to TPT, the polymer was colored in rich yellow.

Sb_2O_3 A polyester was polymerized and melt-spun in the same manner as in TM-1 except for adding antimony oxide (Sb_2O_3) instead of the titanium compound and increasing the added amount of a phosphorus compound. A little long time, 2 hours and 38 minutes, was taken until reaching a prescribed stirring torque. It was a polymer satisfactory in color tone.

6.4.3. Measurement of physical properties

Physical property values of obtained polymers were measured by the methods described below.

IV Intrinsic viscosity (IV) is good index for the degree of polymerization. Measurement was conducted at 25°C by using orthochlorophenol as a solvent.

Carboxyl terminal group content of polymer Carboxyl (COOH) terminal group content of polymer reflects the degree of thermal degradation of polyester. Measurement was done by performing titration with an automatic titrator using orthocresol as a solvent and a 0.02-N aqueous NaOH solution at 25°C.

b value Measurement was done as hunter values (L, a, b) by using a color difference meter. Large b value means the polymer is colored deeply yellow.

Δb value@290°C A polyester chip was dried under reduced pressure at 150°C for 12

hours, and then heated to melt at 290°C under nitrogen atmosphere for 60 minutes. Subsequently, color tone was measured by color difference meter and the difference between before and after the heat melting was measured as a Δb value@290°C. Large Δb value @290°C indicates poor thermal stability of the polymer.

6.4.4. Discussion

Measurement results are summarized in Table 6.3. First of all, all catalysts in the present experiment gave IV of 0.66. That means all catalysts have enough polycondensation activity to increase the molecular weight. Especially, titanium based catalysts gave short polymerization time and showed better activity than antimony. Regarding the color tone and thermal stability of obtained polymers, TM-1, 2 and 3 exhibited much smaller amounts of COOH terminals, b values and Δb values@290°C than primitive TPT catalyst. On the other hand, the thermal stability of these polymers is poorer than the polymer obtained by antimony catalyst, because Δb values@290°C of TM-1, 2 and 3 are a little larger than Sb_2O_3. Comparing physical properties of TM-3, 4 and TPT, TM-3 gave much better color tone and thermal stability than TM-4, whereas TPT and TM-4 showed similar properties. The former observation implies that Ti/mannitol complex persists stably throughout the polymerization process, and the latter result indicates that Ti/mannitol complex must be prepared before being fed into polymerization system in order to obtain stable catalyst complex.

These results mean that sugar-alcohol complexes of titanium are promising candidates of non-antimony polyester polycondensation catalysts, whereas they cannot completely replace antimony catalysts.

Table 6.3. Results of polymerization experiments and physical properties measurement. [2]

Catalyst	Titanium compound[*1]	Ti content in PET (in terms of atom) [ppm]	Mannitol content in PET [ppm]	Molar ratio of mannitol/Ti	Phosphorus stabilizer[*2] content (in terms of P atom) [ppm]	$Mg(OAc)_2$ content (in terms of Mg atom) [ppm]	$Co(OAc)_2$ content (in terms of Co atom) [ppm]	Polymeri-zation time [min]	IV[*3]	Amounts of carboxyl terminals [Eq/ton]	Color tone (b value)	Thermal stability of polymer (Δb value@290°C)
TM-1	TMT	5	38	2	10	5	30	138	0.66	29.9	-1.4	1.8
TM-2	TET	5	38	2	10	5	30	141	0.66	28.6	-1.5	1.6
TM-3	TPT	5	19	1	10	5	30	136	0.66	28.8	-1.8	1.6
TPT	TPT	5	0	0	10	5	30	135	0.66	41.2	8.1	7.1
TM-4	TPT	5	38[*4]	2	10	5	30	139	0.66	39.1	7.9	6.3
Sb_2O_3		250	0	0	15	5	30	158	0.66	35.1	0.8	1.1

*1 TMT: tetramethyl titanate, TET: tetraethyl titanate, TPT: tetra(isopropyl) titanate

*2 Phosphorus stabilizer: Tetrakis(2,4-di-tert-butyl-5-methylphenyl)[1,1-biphenyl]-4,4'-diylbisphosphonite

*3 IV: intrinsic viscosity

*4 Mannitol was added aside from a catalyst.

6.5. General conclusions

By using theoretical calculation, we investigated catalytic mechanisms of polyester polycondensation and thermal degradation reactions, which had not been clarified yet from the point of view of molecular theory. We proposed some new catalytic mechanisms based on the observations: coordination of the carbonyl oxygen atom mechanism for polycondensation, and β hydrogen abstraction by the alkoxy ligand mechanism for thermal degradation reactions.

Our mechanism gave us a guiding principle for designing new titanium based non-antimony catalyst. From the point of view of thermal stability of complex, we chose chelated titanium complexes with multidentate ligands as candidates of new catalyst. Then we analyzed the electronic structure of titanium complexes by using principal component analysis (PCA) and showed that PCA is useful for screening catalysts.

From the investigation mentioned above, sugar-alcohol complex of titanium is selected as potential candidate of non-antimony catalyst. Polymerization experiments and physical properties measurement revealed that mannitol complex of titanium is much better catalyst than conventional titanium alkoxides regarding polymer color tone and thermal stability.

6.6. References

[1] Shigemoto I, Kawakami T, Okumura M. A Quantum Chemical Study on the Polymerization Catalyst for Polyesters: Catalytic Performance of Chelated Complex of Titanium. Polymer; submitted.

[2] Tanaka Y, Hatano E, Honda K. POLYESTER POLYMERIZATION CATALYST AND METHOD FOR PRODUCING POLYESTER USING SAME. WO/2010/035591 (2010/4/1).

Publication List

Main Publication

1) **I. Shigemoto**, T. Kawakami, H. Taiko, M. Okumura, A quantum chemical study on the polycondensation reaction of polyesters: The mechanism of catalysis in the polycondensation reaction, *Polymer*, **52**, 3443-3450, 2011.

2) **I. Shigemoto**, T. Kawakami, H. Taiko, M. Okumura, A quantum chemical study on the thermal degradation reaction of polyesters, *Polymer Degradation and Stability*, **97**, 941-947, 2012.

3) **I. Shigemoto**, T. Kawakami, M. Okumura, A Quantum Chemical Study on the Polymerization Catalyst for Polyesters: Catalytic Performance of Chelated Complex of Titanium, *Polymer*, submitted.

Others

4) **I. Shigemoto**, M. Nakano, S. Yamada, S. Kiribayashi and K. Yamaguchi, Theoretical studies on nonlinear optical properties of organometallic conjugated systems I: Static Third-order hyperpolarizabilities of first-transition-metal and metal-methylene cations, *Mol. Cryst. Liq. Cryst.*, **286**, 159-164, 1996.

5) **I. Shigemoto**, M.Nakano, S. Yamada, S. Kiribayashi and K. Yamaguchi, Theoretical studies on nonlinear optical properties of organometallic conjugated systems III: second hyperpolarizabilities of Mn(I)-carbene systems, *Synthetic Metals*, **85**, 2241-2242, 1997.

6) **I. Shigemoto**, M.Nakano, S. Yamada, and K. Yamaguchi, Theoretical study on second hyperpolarizability of copper dimer, *Synthetic Metals*, **102**, 1562, 1999.

7) M. Nakano, **I. Shigemoto**, S. Yamada and K. Yamaguchi, Size-consistent approach and density analysis of hyperpolarizability: Second hyperpolarizabilities of

polymeric systems with and without defects, *J. Chem. Phys.*, **103**, 4175-4191, 1995.

8) M. Nakano, S. Yamada, **I. Shigemoto**, and K. Yamaguchi, Dynamic (hyper)polarizability density analysis based on virtual excitation processes: Visualization of dynamic electron fluctuatability of systems under time-dependent, *Chem. Phys. Lett.*, **250**, 247-254, 1996.

9) M. Nakano, S. Yamada, **I. Shigemoto**, and K. Yamaguchi, Theoretical study on the geometry dependence of the second hyperpolarizability of allyl cation based on a numerical Liouville three-type analysis, *Chem. Phys. Lett.*, **251**, 381-396, 1996.

10) S. Yamada, M. Nakano, **I. Shigemoto**, and K. Yamaguchi, Static second hyperpolarizabilities γ of nitroxide radical and formaldehyde: evaluation of spatial contributions to g by a hyperpolarizability density analysis, *Chem. Phys. Lett.*, **254**, 158-164, 1996.

11) M. Nakano, Y. Matsuzaki, H. Nagao, S. Yamada, **I. Shigemoto**, and K. Yamaguchi, Damping wave packets approach: a calculation method of intensity-dependent nonlinear optical susceptibilities including effects of nuclear motions at finite temperatures, *Chem. Phys. Lett.*, **258**, 307-315, 1996.

12) M. Nakano, S. Kiribayachi, S. Yamada, **I. Shigemoto**, and K. Yamaguchi, Theoretical study of the second hyperpolarizabilities of three charged states of pentalene. A consideration of the structure-property correlation for the sensitive second hyperpolarizability, *Chem. Phys. Lett.*, **262**, 66-73, 1996.

13) H. Nagao, M. Nakano, S. Yamanaka, Y. Shigeta, S. Yamada, D. Yamaki, **I. Shigemoto**, S. Kiribayashi and K. Yamaguchi, Many-Electron-Wavepackets Method, *I. J. Quantum. Chem.*, **60**, 79-80, 1996.

14) S. Yamada, M. Nakano, S. Kiribayashi, **I. Shigemoto** and K. Yamaguchi, Theoretical studies on hyperpolarizabilities of nitroxide species. III. Effects of

intermolecular interactions of p-NPNN on the γ, *Synthetic Metals*, **85**, 1081-1082, 1997.

15) M.Nakano, S. Kiribayashi, **I. Shigemoto**, and K. Yamaguchi, Hyperpolarizabilities of one-dimensional systems I, *Synthetic Metals*, **85**, 1147-1148, 1997.

16) S. Kiribayashi, M.Nakano, S. Yamada, **I. Shigemoto**, H. Nagao and K. Yamaguchi, Theoretical studies for second hyperpolarizabilities of alternant and condensed ring conjugated systems II, *Synthetic Metals*, **85**, 1163-1164, 1997.

17) S. Yamada, M. Nakano, **I. Shigemoto**, S. Kiribayashi, K. Yamaguchi, Theoretical study on the third-order nonlinear optical susceptibilities for β-phase crystal of p-NPNN, *Chem. Phys. Lett.*, **267**, 438-444, 1997.

18) M. Nakano, S. Yamada, **I. Shigemoto**, S. Kiribayashi, and K. Yamaguchi, Theoretical studies on hyperpolarizabilities of nitroxide species II. Second hyperpolarizability of p-NPNN, *Mol. Cryst. Liq. Cryst.*, **294**, 251-254, 1997.

19) S. Yamada, M. Nakano, **I. Shigemoto**, S. Kiribayashi, and K. Yamaguchi, Intense electron correlation dependencies of first hyperpolarizabilities for nitroxide radical and formaldehyde, *Chem. Phys. Lett.*, **267**, 445-451, 1997.

20) T. Kawakami, **I. Shigemoto**, Molecular-Dynamics Studies on the Structures of Polymer Electrolyte Membranes and the Diffusion Mechanism of Protons and Small Molecules, *Proceedings of the 14th International Conference on the Properties of Water and Steam*, pp. 415-420, MARUZEN Co. Ltd., 2004.

21) 川上智教, **茂本 勇**, 電荷ゆらぎ分子動力学法による高分子電解質のナノ構造形成, *高分子論文集*, **67**, 28-38, 2010.

22) T. Kawakami, **I. Shigemoto**, N. Matubayasi, Free-energy analysis of water affinity in polymer studied by atomistic molecular simulation combined with the theory of solutions in the energy representation, *J. Chem. Phys.*, **137**, 234903, 2012.